

Summer 2013

The measurement of the dielectric constant of concrete pipes and clay pipes

David McGraw

Follow this and additional works at: <https://digitalcommons.latech.edu/dissertations>

 Part of the [Condensed Matter Physics Commons](#)

**THE MEASUREMENT OF THE DIELECTRIC
CONSTANT OF CONCRETE PIPES
AND CLAY PIPES**

by

David McGraw, Jr. B.A., M.S., M.A.

A Dissertation Presented in Partial Fulfillment
of the Requirements for the Degree
Doctor of Philosophy

COLLEGE OF ENGINEERING & SCIENCE
LOUISIANA TECH UNIVERSITY

August 2013

UMI Number: 3577724

All rights reserved

INFORMATION TO ALL USERS

The quality of this reproduction is dependent upon the quality of the copy submitted.

In the unlikely event that the author did not send a complete manuscript and there are missing pages, these will be noted. Also, if material had to be removed, a note will indicate the deletion.

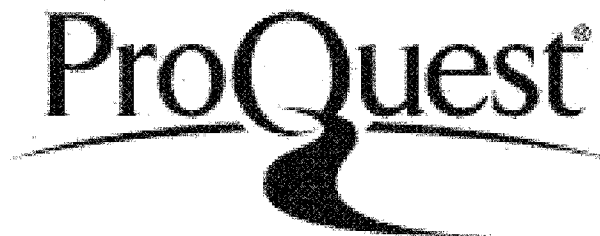


UMI 3577724

Published by ProQuest LLC 2014. Copyright in the Dissertation held by the Author.

Microform Edition © ProQuest LLC.

All rights reserved. This work is protected against unauthorized copying under Title 17, United States Code.



ProQuest LLC
789 East Eisenhower Parkway
P.O. Box 1346
Ann Arbor, MI 48106-1346

LOUISIANA TECH UNIVERSITY

THE GRADUATE SCHOOL

March 15, 2013

Date

We hereby recommend that the dissertation prepared under our supervision
by David McGraw, Jr.

entitled The Measurement of the Dielectric Constant of Concrete Pipes and
Clay Pipes

be accepted in partial fulfillment of the requirements for the Degree of
Doctor of Philosophy

Ward
Supervisor of Dissertation Research
Lee Sawyer
Head of Department
Department of Physics
Department

Recommendation concurred in:

Grumpraborsky
Sandra Zivanovic

Lee Sawyer
Stan P. Wolf

Advisory Committee

Approved: Pritha Punahauchan
Director of Graduate Studies

Approved: Werryn McSorley
Dean of the Graduate School

Stan Nigam
Dean of the College

ABSTRACT

To optimize the effectiveness of the rehabilitation of underground utilities, taking in consideration limitation of available resources, there is a need for a cost effective and efficient sensing systems capable of providing effective, in real time and in situ, measurement of infrastructural characteristics. To carry out accurate non-destructive condition assessment of buried and above ground infrastructure such as sewers, bridges, pavements and dams, an advanced ultra-wideband (UWB) based radar was developed at Trenchless Technology Centre (TTC) and Centre for Applied Physics Studies (CAPS) at Louisiana Tech University (LTU). One of the major issues in designing the FCC compliant UWB radar was the contribution of the pipe wall, presence of complex soil types and moderate-to-high moisture levels on penetration depth of the electromagnetic (EM) energy.

The electrical properties of the materials involved in designing the UWB radar exhibit a significant variation as a result of the moisture content, mineral content, bulk density, temperature and frequency of the electromagnetic signal propagating through it. Since no measurements of frequency dependence of the dielectric permittivity and conductivities of the pipe wall material in the FCC approved frequency range exist, in this thesis, the dielectric constant of concrete and clay pipes are measured over a microwave frequency range from 1 Ghz to 10 Ghz including the effects of moisture and chloride content.

A high performance software package called MU-EPSLNTM was used for the calculations. Data reduction routines to calculate the complex permeability and permittivity of materials as well as other parameters are also provided. The results obtained in this work will be used to improve the accuracy of the numerical simulations and the performances of the UWB radar system.

APPROVAL FOR SCHOLARLY DISSEMINATION

The author grants to the Prescott Memorial Library of Louisiana Tech University the right to reproduce, by appropriate methods, upon request, any or all portions of this Dissertation. It is understood that "proper request" consists of the agreement, on the part of the requesting party, that said reproduction is for his personal use and that subsequent reproduction will not occur without written approval of the author of this Dissertation. Further, any portions of the Dissertation used in books, papers, and other works must be appropriately referenced to this Dissertation.

Finally, the author of this Dissertation reserves the right to publish freely, in the literature, at any time, any or all portions of this Dissertation.

Author *Guilford M. Williams, Jr.*
Date 3-15-2013

TABLE OF CONTENTS

ABSTRACT.....	iii
LIST OF TABLES.....	viii
LIST OF FIGURES	x
ACKNOWLEDGMENTS	xiii
CHAPTER 1 LITERATURE REVIEW	1
1.1 Introduction.....	1
1.2 Measurement Techniques	14
1.3 Transmission/Reflection Line Technique	15
1.4 Open-ended Coaxial Probe Technique	17
1.5 Free Space Technique.....	19
1.6 Resonant Technique.....	20
1.7 Measurement Procedure	21
1.8 Nicholson-Ross-Weir (NRW).....	22
1.9 NIST Iterative	23
1.10 New Non-Iterative Technique	24
1.11 Short Circuit Line (SCL)	25
CHAPTER 2 THEORY OF THE DIELECTRIC PROPERTIES	27
2.1 Definition and Physics of Dielectric Properties.....	27
2.2 Section II.....	38

2.2.1	Coaxial Transmission Line Theory.....	38
2.2.2	Coaxial Line TEM Modes	41
2.2.3	Coaxial Line TE Modes.....	42
2.2.4	Coaxial Line TM Modes.....	45
CHAPTER 3 SAMPLE PREPARATION.....		53
3.1	Sample Preparation.....	53
3.2	Drill Press	54
CHAPTER 4 PROPERTIES OF CONCRETE, CONCRETE PIPES, AND CLAY PIPES		63
4.1	Concrete Pipes	79
4.2	Clay Pipes	93
CHAPTER 5 MEASUREMENT TECHNIQUES.....		100
5.1	Fundamentals of a Vector Network Analyzer	113
5.2	Vector Network Analyzer Measurements.....	115
5.3	Network Analyzer Architectures	117
5.3.1	Calibration	119
5.3.2	Process Requirements	120
CHAPTER 6 RESULTS.....		122
6.1	Data Correction for Graphs.....	123
CHAPTER 7 SUMMARY AND CONCLUSIONS.....		134
7.1	Summary.....	134
7.2	Conclusions.....	137
7.3	Recommendations for Future Work.....	138

REFERENCES139

APPENDIX A TIME DOMAIN TESTS.....145

APPENDIX B GENERAL APPROACHES TO DETERMINE DIELECTRIC
PROPERTIES161

LIST OF TABLES

Table 1-1: Some comparison between the measurement techniques.....	15
Table 1-2: The difference between the conversion techniques.....	22
Table 2-1: Types of magnetic materials.....	33
Table 2-2: Types of dielectric materials	36
Table 2-3: Summaries of various materials by conductivity	38
Table 4-1: Five types of standard specifications for Portland cement from the American Society for Testing and Materials	66
Table 4-2: Maximum w/c ratio for various exposure conditions for concrete.....	67
Table 4-3: Maximum permissible w/c ratios for concrete when strength data is need for a specified job	68
Table 4-4: Minimum concrete requirement for concrete that can be used in slabs, of flatwork, aggregate size in inches and cement in lb/cy	69
Table 4-5: Approximate mixing water and air content requirements for different slumps and sizes of aggregate.....	70
Table 4-6: Approximate mixing water and air content requirements for different slumps and maximum sizes of aggregates	70
Table 4-7: Recommended slumps for various types of construction.....	71
Table 4-8: Standards for clay pipe	95
Table 6-1: Percentage of moisture content, m [%]	123
Table A-1: List of sample types used during Experiment 2	151

LIST OF FIGURES

Figure 2-1: Coaxial line.	41
Figure 3-1: Drill press used to cut samples.....	55
Figure 3-2: Cutting with drill press.	56
Figure 3-3: Drill bit used to cut samples.	57
Figure 3-4: Samples of clay and concrete.....	58
Figure 3-5: Machine used to sand off samples.	59
Figure 3-6: Samples placed in freshwater and saltwater.	60
Figure 3-7: PVC sample.	61
Figure 3-8: Samples of the different materials used in research.	62
Figure 4-1: Concrete pipe.	72
Figure 4-2: Concrete building.....	73
Figure 4-3: Concrete pavement.....	74
Figure 4-4: Concrete wall.	75
Figure 4-5: Concrete sidewalk.....	76
Figure 4-6: Concrete spillway.	77
Figure 4-7: Concrete bridge.....	78
Figure 5-1: System connections one port.	102
Figure 5-2: System connections two port.	103
Figure 5-3: Vector network analyzer.	106

Figure 5-4: Sample holder.	107
Figure 5-5: Look at a VNA and oscilloscope.	108
Figure 5-6: Sample holders and some samples.....	108
Figure 5-7: PVC sample with computer.	109
Figure 5-8: All three components: Computer, VNA, and holder ready to take data.	110
Figure 5-9: Equipment and computer needed for data collecting.....	111
Figure 5-10: Computer graphing.	112
Figure 5-11: Starting data collection process.	113
Figure 5-12: Transmission (T) and reflection (Γ) coefficients.	114
Figure 6-1: Permittivity of dry clay (frequency in Ghz).....	125
Figure 6-2: Permittivity of PVC pipe (frequency in Ghz).....	126
Figure 6-3: Permittivity of wet clay pipe and air (frequency in Ghz).	126
Figure 6-4: Permittivity of wet concrete pipe and air (frequency in Ghz).	127
Figure 6-5: Permittivity of wet clay (frequency in Ghz).	127
Figure 6-6: Permittivity of soil (directly from the program).	128
Figure 6-7: Loss factor of saltwater clay pipe and air (frequency in Ghz).....	128
Figure 6-8: Loss factor of saltwater concrete pipe and air (frequency in Ghz).	129
Figure 6-9: Conductivity of concrete. Red dots represent dry concrete, green dots represent wet concrete, and blue dots represent saltwater concrete (conductivity is in S/m).....	130
Figure 6-10: Conductivity of clay. Red dots represent dry clay, green dots represent wet clay, and blue dots represent saltwater clay (conductivity is in S/m).....	131
Figure 6-11: Dielectric constant for concrete- red dots represent dry concrete, green dots represent wet concrete, and blue dots represent saltwater concrete.....	132

Figure 6-12: Dielectric constant of clay. red dots represent dry concrete, green dots represent wet concrete, and blue dots represent saltwater clay.	133
Figure A-1: Experiment one setup.....	146
Figure A-2: Moisture measurement instrument manufactured by general tools.	147
Figure A-3: Time domain plots obtained during experiment 1.	148
Figure A-4: Magnitude spectrum of data collected during experiment 1.....	149
Figure A-5: Experiment 2.....	150
Figure A-6: Time domain plots.	151
Figure A-7: Magnitude spectrum of the transmitted signal between two horns with different samples placed in between the antennas.	152
Figure A-8: Transmission loss measurements.	153
Figure A-9: Magnitude of dry concrete and concrete + metal.....	158
Figure A-10: Magnitude of concrete plate + metal, metal plate, and outer metal.....	159
Figure A-11: Magnitude of dry concrete pipe, wet concrete pipe, and flat dry concrete.....	159
Figure A-12: Concrete pipe.	160
Figure A-13: Oscilloscope.....	161
Figure A-14: Impulse generator.....	162

ACKNOWLEDGMENTS

I would like to thank my adviser Dr. Neven Simicevic for his generous assistance and support in making this work rewarding and possible. Though work places great demands on his time, he has always had the time to answer my many questions. I would also like to thank my co-adviser Dr. Arun Jaganathan; his constant guidance and support helped me to overcome various challenges during this research. I also want to thank Bryan Cody for his technical help on the project and for making the drill bit. I want to thank Dr. Youssef Dib for his help with MatLab programs, and Dr. John Anderson for his technical advice. I would like to express my gratitude to those who have made my progress to this point possible. My parents, Mr. and Mrs. David McGraw, whose love and support have guided me through my life and through my two masters' degrees, I thank you for everything. Also, I would like to thank my wife Heather and my two kids, Lindsey and Austin, for supporting me through my research. Finally, I would like to thank God Almighty, for without his support nothing is possible.

CHAPTER 1

LITERATURE REVIEW

1.1 Introduction

Of the approximately 11 million miles of underground utilities in the U.S, potable, storm and wastewater distribution and collection systems make nearly 6.2 million miles [1]. Efficient operation of such a system is essential in maintaining basic societal needs which includes public health and environmental protection. Still, due to the costs associated with their maintenance, underground utilities are suffering from increasing rates of failure. Report released by Battelle Memorial Institute [2] estimated annual expenditures on water work rehabilitation in the U.S. at 4.5 billion dollars, with an annual projected grow of 8% to 10%.

To optimize the effectiveness of the rehabilitation of underground utilities, taking in consideration limitation of available resources, there is a need for a cost effective and efficient sensing systems capable of providing effective, in real time and in situ, measurement of infrastructural characteristics. As an example, development of advanced technologies for condition assessment of civil infrastructure systems was considered by the National Institute for Standards and Technology (NIST) a “critical national need” [3].

One of the factors contributing to the structural deterioration of buried pipes is the formation of soil voids. As reported by Tan and Moore [4], the voids contribute to the formation of cracks, fractures and the loss of the pipe-wall thickness. They can facilitate a sudden surface collapse resulting in disruption of transportation routes, economic losses and in some cases injuries or even deaths [5]. This can be prevented if there is ability to quantify parameters such as pipe wall thickness, presence and dimensions of voids surrounding the pipe, and presence and dimensions of cracks in the pipe wall. The direct or indirect methods available to carry out the condition assessments in a non-destructive manner utilize electromagnetic waves, acoustic/seismic waves, electric and magnetic fields, temperature field, nuclear methods, biosensor and gas detection methods, but full condition assessment techniques of a buried infrastructure are not yet commercially available [6].

To carry out accurate non-destructive condition assessment of buried and above ground infrastructure such as sewers, bridges, pavements and dams, an advanced ultra-wideband (UWB) based radar was developed at Trenchless Technology Centre (TTC) and Centre for Applied Physics Studies (CAPS) at Louisiana Tech University (LTU). The primary objective of the radar is to access the structural integrity of the cementitious walls of pipes and tunnels (approx. 96% of the US civil infrastructure by volume) and detect the presence of soil voids immediately outside such buried structures. The sensor module is designed to be mounted on commercially available robotic transporters, to collect data and transmit it back to the operator in real-time. This particular application has been licensed to a robotic equipment manufacturer specializing in sewer inspection technologies.

A significant contribution in the process of designing such an ultra-wideband (UWB) based radar system came from a two- and three-dimensional numerical modeling of the propagation of electromagnetic pulses inside and outside buried non-metallic pipes using the finite difference time domain (FDTD) technique [7]. To satisfy the Federal Communication Commission (FCC) imposed limits on the electromagnetic emissions for UWB imaging systems the condition assessment radar was designed at Louisiana Tech University to operate in the bandwidth of 3.1 to 10.6 GHz.

Three of the major issues in designing the FCC compliant UWB radar has been the contribution of the pipe wall, presence of complex soil types and moderate-to-high moisture levels on penetration depth of the electromagnetic (EM) energy. Also, the effect of the specific pipe geometry on electromagnetic clutter created inside a pipe was a contributing factor to the quality of the signal. Since the objects in the (FDTD) simulation are represented as discontinuities resulting from sudden changes in electrical properties of the material, in our case the accuracy of the numerical simulation and therefore the viability of the final product depended on the knowledge of the dielectric properties and conductivities of the pipe wall and a surrounding soil.

The electrical properties of the materials involved in designing the UWB radar exhibit a significant variation as a result of the moisture content, mineral content, bulk density, temperature and frequency of the electromagnetic signal propagating through it. No measurement of frequency dependence of the dielectric permittivity and conductivities of the pipe wall material in the FCC approved frequency range exists. At the beginning of the numerical simulations, the pipe material was treated as dielectric material with relative permittivity of three which correspond to the dielectric value of dry

clay [8]. The electromagnetic properties of the surrounding soil were also taken from [8]. To improve the accuracy of the numerical simulations, the dielectric properties and conductivity of the clay and concrete pipes were measured for the first time in the frequency range approved by the FCC for UWB imaging radar system. The measurements were performed for dry and moisture saturated pipe walls.

The measurement of the complex dielectric is important in many areas of research. Dielectric measurements are important in this research, because it can provide the electric or magnetic characteristics of materials. There is a growing industrial demand for dielectric characterization of materials for design, manufacturing, and quality control purposes in industries [9]. This research measures the dielectric properties of materials using a coaxial line fixture. A method for determining the dielectric constant of concrete pipe, clay pipe, and soil will be described in this research. A high performance software package called MU-EP SLNTM has been used to do the calculations. The MU-EP SLNTM is a complete software package for making S-parameter measurements using one and two port coax or waveguide fixtures. Data reduction routines to calculate the complex permeability and permittivity of materials as well as other parameters are provided. The user has access to all raw and processed data, so that it can be studied at any time. The user can select bands to be swept; many frequencies can be swept depending on the VNA. All the capabilities of the VNA are available to the user either through the external controller or the front panel [10]. The complex μ and ϵ are normalized relative to free space parameters μ_0 and ϵ_0 .

The complex μ and ϵ are written as

$$\mu = \mu' - i \mu'' \quad (1.1)$$

$$\epsilon = \epsilon' - i \epsilon'' \quad (1.2)$$

where μ'' and ϵ'' are nonnegative real numbers and $i = \sqrt{-1}$. The complex time dependence in the relevant field equations is of the form $e^{j\omega t}$. The MU-EPSLNTM program calculates the free space and short backed reflection and transmission coefficients for a material. The sample thickness is input by the user. This implementation is based upon a direct analogy of TEM propagation in a coaxial line, and a normally incident plane wave propagation in a coaxial line, and a normally incident plane wave propagating in free space [11]. A measurement that uses the Transmission/Reflection line technique involves putting a sample in a section of a coaxial line, and measuring the two ports complex scattering parameters with a vector network analyzer (VNA). The VNA must be calibrated before a measurement can be made.

The Transmission/Reflection line technique involves the need to measure both reflected (S11) and transmitted (S21). The relevant scattering parameters relate closely to the complex permittivity and permeability of the material by equations. The conversion of s-parameter to complex dielectric parameter is computed by solving the equations using a computer program. The different samples were machined to fit into the sample holder [12]. Calibrations in transmission line measurements use different terminations that produce various resonant behaviors in the transmission line.

For good dielectric measurement, a high electric field is required. This measurement technique allows for the measurement of permittivity and permeability of the dielectric material. The VNA can be calibrated and the samples are then placed in the

sample holder. The better that the sample fits the less the measurement uncertainty will be. The measurement accuracy is limited by the numerical uncertainty and by the air gaps [13]. Cylindrical samples specimens were made using a drill press. The specimens were drilled from different types of materials: clay, clay pipe, concrete, concrete pipe, and soil. Dimensions of the specimens varied from two to three cm in diameter to four to five cm in height.

A number of different conditions of the specimens were used for the measurements: (1) saturated specimens with moisture on the inside for one month or more, (2) air dried specimens exposed to just room temperature and humidity, and finally (3) specimens were placed into saltwater for one month or more. Concrete is a dielectric, nonmagnetic material. Dielectric materials are usually made up of atoms whose valence electron shells are nearly full, resulting in low conductivity. Using a coaxial transmission line, a particular material's dielectric properties can be tested as amounts of certain substances within it are varied. For concrete, there have been studies to ascertain the effects of different admixtures, the type of aggregate, water content, and curing time on dielectric properties [14].

In general, the real part of the dielectric constant is larger when it is easier for the material to polarize, meaning that the ions are mobile and there is little crystallization. The addition of chlorides increases the dielectric constant, as does the amount of water. The dielectric constant decreases over curing time, because the amount of water decreases during this time. Also, the dielectric constant of concrete is dependent on the constant of its aggregate: mixes containing limestone have a higher constant than those

containing granite, this correlates with the fact that limestone itself has a higher constant than granite does [15].

There are certain concrete properties that influence the performance of concrete pipes. These properties include concrete compressive strength, density, absorption, water cement ratio, cement content and type, and aggregates. All of these factors would have an influence on the dielectric properties of concrete pipes. For example, the dielectric constant for concrete with coarse aggregates is higher than concrete with fine aggregates. Compressive strengths for concrete pipes normally range from 4000 psi to 6000 psi. Concrete strength is a function of many factors including, aggregates, cement material, manufacturing, curing process, and mix design. These factors must also play a role in the dielectric constant of concrete pipes, since concrete pipe strength is a function of these same factors. Concrete pipe design strengths refer to 28 days concrete strengths, but in actuality, the design strengths are obtained much earlier than 28 days. Quality concrete pipe densities typically range from 145-155 pounds per cubic foot. In general, the higher the density of concrete pipe, the greater the durability of the concrete, which leads us to believe that the dielectric constant could be affected by, changes in density.

Absorption is primarily used to check the density of the concrete. As with compressive strength, the absorption can be greatly influenced by the aggregates and the manufacturing process that is used for each concrete pipe. For example, ASTM C 76 specifies a maximum allowable absorption of 8.5% or 9%, for concrete pipe. Low water-cement (W/C) ratios are one of the trademarks of quality concrete pipe. Typical precast concrete pipe have W/C ratios that range from 0.33 to 0.45, with 0.53 being the

maximum allowed by ASTM C 76. The cement content has always been a topic of concern with concrete pipe.

The key to proper cement content is proper design of the mix, with consideration of all material properties, manufacturing, and curing processes. Materials used to manufacture concrete pipe consist of aggregates and manufactured products, such as Portland cement and reinforcing steel. Each of the components has a standard specifying its properties and methods of testing. Portland cement is a closely controlled chemical combination of calcium, silicon, aluminum, iron, and small amounts of other compounds. Gypsum, which regulates the setting time of the concrete, is added during the final process of grinding [16].

Calculating the dielectric constant of a mult-phased heterogeneous composite like concrete is a challenging task. Chemical admixtures are also used in practice as a processing addition to aid in manufacturing and handling of concrete or as a functional addition to modify the properties of concrete. In this research, because of the difficulties in making the samples, the problems of chemical admixtures or the microscopic structure in calculating the dielectric constant of clay, clay pipe, concrete, and concrete pipe are not considered [17]. This research is justified because the dielectric properties of concrete pipes and clay pipes have not been studied in the past. In the last 10 to 20 years, it has become apparent that a growing percentage of waste conveyance systems are approaching their design life.

There is an increasing chance that in the future the failure rate will accelerate. These conditions lead us to the need to understand the dielectric properties of pipes. The goal of my research is to: first, to examine the methods that would best help us in

calculating the properties that we are looking for, second, discuss the theory behind my research and sample preparation that is needed before data can be examine, and finally the calculation of the dielectric properties of concrete pipes and clay pipes.

The rest of Chapter 1 is the literature review, and the discussion of different measurement techniques used in the calculation of the dielectric constant. Chapter 2 discusses the theory and the physics behind dielectric properties. Chapter 3 talks about the methods and the problems of sample preparation. Chapter 4 is an overview about the general properties of concrete, concrete pipes, and clay pipes. The measurement techniques that have been used in the dissertation are discussed in Chapter 5. The final results (including graphs) are presented in Chapter 6. Finally, the summary and conclusion follow in Chapter 7, which includes a section about recommendation for future work.

Concrete is made by adding water to a mixture of cement, sand, and coarse aggregate. Hydration takes place between the water and cement producing a matrix of compounds known as cement paste. This matrix locks together the coarse and fine aggregate particles to form a material with considerable compressive strength. A concrete mix is normally defined by the mass ratios of its constituents, i.e.: the water/cement ratio, the cement/sand/aggregate ratio and the cement/total-aggregate ratio. The real and imaginary parts of the complex permittivity of different concrete mixes have been investigated by a number of different authors [4][18]. Data presented by Hasted and Moore refer mostly to the real and imaginary parts of the complex permittivity of hardened concrete. These data characterize the complex permittivity for different water-

cement ratios, for conditions of different water volume absorption. Results were recorded at 3 GHz, 9 GHz, and 24 GHz.

For the interesting case where concrete can be considered dry or having a small amount of water content, the real part of the complex permittivity was found to vary between 5.0-7.0 while the imaginary part between 0.1-0.7. Data was also recorded for aerated concrete at 3.0 GHz and 9.0 GHz [19]. Aerated concrete consists of a cement paste to which a small proportion of aluminum powder is added. During the heating process the aluminum is oxidized producing sufficient hydrogen to aerate the mix into a strong light material. In this case and for small water contents, the real part of the complex permittivity was found to vary between 2.0-2.5, while the imaginary part was between 0.12-0.50. All the constitutive parameters presented up to now for different concrete types, do not vary significantly from data recorded by other sources. In the latter case for the range of frequencies 1- 95.9 GHz the real part of the complex permittivity was found to vary from 6.0-7.0 and the imaginary part was found to vary from 0.34 to 0.85 for hardened concrete. In [18], aerated concrete measured at 1GHz was found to have a value of $\epsilon_{\text{complex}} = 2 - i0.5$ which is close to the values reported at 3.0 GHz and 9.0 GHz. Similar measurements between 0.5-0.7 GHz suggest a value for the relative permittivity between 2.5-3 and a conductivity range between 0.0138-0.025 (S/m) [18].

An open-ended coaxial probe method was used by Buyukozturk and Rhim to measure real and imaginary parts of the complex permittivity of hardened concrete [15]. They looked at the frequency range of 0.1 to 20 GHz at 0.4 GHz steps. Also, they used different moisture content to examine the effects of moisture on the electromagnetic properties of concrete. They used cylindrical concrete samples that were casted with a

water/cement/sand/coarse aggregate mix. Portland cement of Type 1 was used. It appears that at dry conditions, the dielectric constant does not vary much over the measured frequency range. This is not true when the moisture level increases. The dielectric constant of the saturated sample is almost double that of the oven dried sample. This is possible due to the high value of the dielectric constant of water [15]. So then, the increases of water content in concrete must greatly affect the change in the dielectric constant of the concrete.

A co-axial transmission line test rig was used to measure the dielectric properties of concrete. Measurements were made on nineteen samples at various levels of water volume as a percentage of concrete. All samples were made using ordinary Portland cement and the concrete mixes were made with ten mm gravel aggregate with Hope Quarry sand. They provided measurements data showing the variation of permittivity and conductivity with frequency and moisture content. The values that they measured were in the range of previous studies with the dielectric constant of dry concrete between 3.5 and 5.0. In 2006, Rohde and Schwarz performed a similar measurement on five samples of concrete, but they used the maximum size of 30 mm gravel aggregate [20]. The data showing the influence of moisture content and the effects of chloride on the permittivity were presented [20].

Five material models with frequency-dependent permittivity were compared to the experimental data. Kaatz, compared two models, the Cole-Cole model and the Debye's model; he thought the Cole-Cole model worked the best in fitting the measurement values [21]. In the literature, several techniques have been used to extract permittivity and permeability of materials. For example, the rectangular waveguide

technique is one of a class of two ports measurement which includes transmission and reflection. It has been used as an easy way for studying properties of materials in the microwave frequency. The results of these studies obtain results which are very similar [15][22]. They measured the complex permittivity for concrete, based on measuring the scattering parameters.

Belrhiti, Nakheli, Haddad, and Mamouni presented their results of studying the dielectric constant of concrete using Ku band [23]. They measured the dielectric constant using a Vector Network Analyzer using a thru-reflect-line calibration. The Newton-Raphson method was used as a numerical tool to estimate the value of relative complex permittivity. The results that they obtained were compared with the Nicholson-Ross technique. The two methods were in good agreement [23]. The researchers who have studied the dielectric constant of concrete have stated that the complex permittivity of concrete samples does not vary significantly due to frequency changes, even over a wide frequency range. It does not change significantly for different mixing ratios of similar materials. It seems that the biggest difference observed is between hardened and lightweight, aerated concrete samples. The concrete parameters presented up to now referred to non-reinforced concrete samples.

In the case of reinforced concrete, it has been shown that other parameters that can influence the transmission characteristics of a concrete wall include the square grid side length and the steel diameter used in the reinforced concrete. Even in these cases, the value of the complex permittivity used to describe the concrete was equal to $\epsilon_{\text{complex}} = 7 - i0.3$ for 900 MHz and 1800 MHz [10].

The measurement of complex dielectric properties of materials at microwave frequency has gained increase importance in many areas of research. In recent years, the dielectric properties of materials have received increasing attention along with the use of electromagnetic waves in the investigations of material and structural assessment.

Dielectric properties of a material correlate with other material characteristics may be used to determine properties such as moisture content, bulk density, biocontent, chemical concentration, and stress-strain relationship. Generally, the integration of material in an application system requires the exact knowledge of its dielectric parameters. Many techniques have been developed to measure these complex properties. This research will look at such techniques in time domain or frequency domain with one or two ports. Each technique has some limitation based on specific frequencies, materials and applications.

With all the new advances in technologies, the techniques can be employed with a software program that measures the complex reflection and transmission coefficients with a vector network analyzer and converts the data into the complex dielectric property parameter. The last part of Chapter 1, will describe the general procedures on dielectric measurements using a network analyzer and show the methods to convert from s-parameter to dielectric properties. Chapter 1 will discuss ideas about the four conversion techniques: the Nicolson-Ross-Weir technique, NIST iterative technique, new non-iterative technique, and short circuit line technique. This study will discuss conversion techniques that are applicable to most non-liquid materials. To convert the s-parameter obtained from a liquid measurement, a different conversion technique is needed which will be discussed only briefly [21].

1.2 Measurement Techniques

Measurement of dielectric properties involves measurements of complex relative permittivity (ϵ_r) and complex relative permeability (μ_r) of the materials. A complex dielectric permittivity consists of a real part and an imaginary part. The real part of the complex permittivity is a measure of the amount of energy from external electric field stored in the material. The imaginary part is zero for lossless materials and is also called the loss factor. It is a measure of the amount of energy loss from the material due to an external field. The term $\tan \delta$ which is also called the loss tangent represents the ratio of the imaginary part to the real part of the complex permittivity. The loss tangent is also called the tangent loss or the dissipation factor. The complex permeability consists of a real part which represents the amount of energy from an external magnetic field stored in the material. The imaginary part of the complex permeability represents the amount of energy dissipated due to the magnetic field [24]. Measurement on the complex permeability is only applicable to magnetic materials. Most materials are non-magnetic which leads to a permeability value that is very near to the permeability of free space. There are many techniques that have been developed for measuring the complex permittivity and permeability [25] [26] [27]. Each of these many techniques is limited to specific frequencies, materials, etc. this study will be discussing the following four techniques: transmission/reflection line technique, open ended coaxial probe technique, frees space technique, and resonant technique. The measurement techniques are outlined in Table 1-1.

Table 1-1: Some comparison between the measurement techniques.

Measurement techniques	Materials	S-parameters	Dielectric properties
Transmission/Reflection Line	Coaxial line waveguides	S11, S21	ϵ_r and μ_r
Open-ended coaxial probe	Liquids and semi-solids	S11	ϵ_r
Free space	High Temperature material	S11, S21	ϵ_r and μ_r
Resonant Technique	Rod shaped solid materials, waveguides, liquids	Frequencies, Q-factors	ϵ_r and μ_r

1.3 Transmission/Reflection Line Technique

A measurement using the Transmission/Reflection line technique involves placing a sample in a section of waveguide and measuring the two ports complex scattering parameters with a vector network analyzer. Calibration is very important and must be carried out before making the measurement. The technique involves measurement of the reflected (S11) and transmitted signal (S21). The relevant scattering parameters relate closely to the complex permittivity and permeability of the material by equations. The conversion of s-parameters to complex dielectric parameters is computed by solving the equations using a computer program. In many cases, this technique requires that the person match the sample, which requires that the sample fit tightly into the waveguide or coaxial line [9]. Calibrations in transmission line measurements use various terminations that produce different resonant behavior in the transmission line. For good dielectric measurement, maximum electric field is required, which one can accomplish by open circuited or other termination. In coaxial measurements, calibration can be made using one of several methods like short circuited, open circuited, or load termination. The measurement technique allows the measurement of permittivity and permeability of the dielectric constant. When one has everything connected for the experiment, the VNA can

be calibrated and the material which is being tested can be placed in the sample holder. The material must fit tightly in the sample holder so that it will reduce the measurement uncertainty caused by air gaps. The calibration plane can be extended to the sample surface by two different methods [11]. The first method is to manually feed the phase factor which is equivalent to the distance between the sample surface and the connector calibration plane. The phase factor can be easily included into the measurement with the features in the VNA. The VNA will shift the calibration plane from the connector to the material surface. The second method involves the de-embedding function of the VNA. The method requires measuring the s-parameters of an empty sample holder after calibration was done. The measured s-parameter of the empty holder is then inputted into the network analyzer. Using the de-embedding function in the VNA, the influence of the sample holder on the actual material measurement can be cancelled out. Both methods will end in the same results. The measured s-parameters are then post processed to determine the complex dielectric properties using a program. There are various techniques to calculate the dielectric parameters from the measured s-parameters. A discussion of these conversion techniques are included later on. The advantages of this technique are: coaxial lines and waveguides are commonly used to measure samples with medium to high loss, and it can be used to determine both the permittivity and permeability of the material under test. The disadvantages of this technique are: measurement accuracy is limited by the air-gap effects, and it is limited to low accuracy when the sample length is the multiple of one-half wavelength in the material [10] [13].

1.4 Open-ended Coaxial Probe Technique

Open-ended coaxial probe has been used for years as a non-destructive testing method. In this technique the permittivity is determined by using a probe and it is pressed against a specimen or it is used by immersing it in a liquid. Also, for some measurements, it may not be possible to cut out the sample of a material for measurement. An example is the case of biological specimens, it is necessary to perform in-vivo measurements because the material characteristics may change. It is therefore possible with this technique to place the sample in close contact with the probe without causing any changes in the material characteristics. By using a vector network analyzer one can measure the reflection coefficient. One starts by calibrating the VNA with a probe system so that the reflection coefficient measurements are referenced to the probe aperture plane. There are two methods that can be used. The first method uses reference liquids for direct calibration at the open end of the probe. This method is simple, but the uncertainties in the measurement are due to the uncertainties in the characterization of the reference liquids. In this method, all measurements are performed by placing the standards at the end of the probe. The referenced liquid must be a liquid with known dielectric properties. Water is an example of a liquid selected as the reference liquid. The standard one port full calibration is then applied. The s-parameters can then be measured and processed to obtain the dielectric properties [28].

The second method uses a combination of standard calibration to calibrate at the connector plane and a simulated model of the probe to translate the connector calibration plane to probe aperture. One can then calculate the permittivity from the reflection coefficient at the probe aperture. The measurement accuracy is related closely to the

precision of the physical characteristics of the probe's aperture. The calibration process involves calibrating the VNA at the connector plane using a calibration standard. The probe is then connected at the connector plane. On the VNA we use the gating function of the time domain feature to minimize the reflection from the connector. The complex coefficient data referenced to the connector plane can then be recorded and processed in two ways.

The first way involves a de-embedding model used to compensate the propagation characteristics of the probe. One can then translate the measurement reference from the connector plane to the probe aperture plane. The model will derive the embedded reflection coefficient, then using the de-embedding model; the probe is treated as a two port microwave network. In this model the s-parameters are used to relate the reflection coefficient at the connector to the reflection coefficient at the aperture plane by an equation. To measure the unknown s-parameters, the measured data, and simulated data are used. For the measured data, the reflection coefficients of three reference liquids are measured. If one immersed each of the reference liquids, one can then compute the embedded reflection coefficient using a simulation model of an ideal probe [29].

From the combinations of the data, the s-parameter can be determined. By determining the s-parameters, the de-embedding model can determine the unknown reflection coefficient. Then by using a rational function model one can calculate the permittivity of the sample. The advantages of open ended coaxial probe technique are: requires no matching of the sample, easy sample preparation, after calibration, the dielectric properties of a large number of samples can be measured in a short time, and the measurement can be performed in a temperature controlled environment. The

disadvantages of open ended coaxial probe technique are: only reflection measurement are available, and affected by air gaps are important for measurement on specimen [28] [12].

1.5 Free Space Technique

Free space measurement allows measurements on the material under test under high temperatures and generally operates in wide band frequencies. The material under test needs to be large and flat for the measurement. For the measurement two antennas are placed facing each other and the antennas are connected to a network analyzer. Before starting the measurement, the VNA must first be calibrated. There are a number of calibration techniques that can be used, but the LRL line-reflect-line calibration technique produces the highest calibration quality. The line standard can be achieved by separating the focal plane of the two antennas to around a quarter of wavelength [30]. The reflect standard can be obtained by placing a metal plate on the sample holder in between the antennas. Once calibrated, the s-parameters of an empty sample holder are measured by placing the sample holder midway between the two antennas. The material under test is then placed on the sample holder between the antennas, and the s-parameter measurement is performed again. Using the de-embedding function of the VNA, one can cancel out the influence of the sample holder. After that only the s-parameter of the material under test can be determined. The s-parameter for both the reflection and transmission coefficients can be determined. To ensure there are no multiple reflections in a sample, the time domain gating should be applied. If the material under test has the appropriate thickness one should be able to avoid the problem.

The dielectric properties can be determined by post processing the measured reflection and transmission coefficient using a program. The advantages of the free space technique are: the technique can be used for high frequency measurement, the technique allows non-destructive measurement, the technique allows the material under test to be in a hostile environment, and the technique allows one to evaluate both the magnetic and electric properties. The disadvantages of the free space technique are: the technique needs large and flat materials, the technique allows multiple reflections between antenna and surface of the sample, and the technique allows diffraction effects at the edge of the sample [31].

1.6 Resonant Technique

The last method to discuss is the most accurate method to calculate permittivity and permeability. However, there are limitations on what can be measured with the technique, like frequencies and loss characteristics. There are many types of resonant techniques available such as reentrant cavities, split cylinder resonators, cavity resonators, etc. We will just look at a general overview of resonant measurements, the general ideas about using a cavity resonator. There are two types of resonant measurements that are generally used.

For permittivity measurements one uses perturbation methods. Perturbation methods are good for magnetic materials and medium to high loss material measurements as well. Low measurement method is a measurement on low loss materials using large samples. In general, the perturbation method is used more often. With resonance characteristics depending on the material under testing in a cavity its quality factor and resonance frequency can be monitored to determine the dielectric parameters. The

dielectric properties can be found by first measuring the resonant frequency. Then one can determine the quality factor of an empty cavity. The next step is to repeat the measurements after filling the cavity with the material under testing. If we use the frequency, volume, and q-factor one can calculate the permittivity or permeability of the material. One does not need to calibrate the network analyzer for this measurement. The network analyzer needs to have high frequency resolution in order to do this measurement. For example, Rohde and Schwarz network analyzer has an option to allow for this particular measurement. This option allows measurement with high frequency resolution up to one Hz. The advantages of resonant technique are the ability to measure very small material to test, and the use of approximate expression for fields in the sample and the cavity. The disadvantages of resonant technique are, the need for high frequency resolution vector network analyzer, and it is limited to narrow bands of frequencies [27] [32].

1.7 Measurement Procedure

The measurement setup includes a network analyzer, a software program that can be installed in the vector network analyzer, or in a remote computer and the sample holder for the material under test. The network analyzers can be used for the dielectric measurement. A network analyzer has a range of calibration techniques to suit different measurement techniques and allows for more accurate measurements. Other features such as time domain and embedding/de-embedding functions will give better accuracy of the measurement result. A function for direct extraction of the s-parameters is available on vector network analyzers. This is very important to have this function because it helps to increase the post processing of the s-parameters using some external software programs.

The external programs are then able to convert the s-parameters to the permittivity and permeability parameters [33]. There are many approaches for obtaining the permittivity and permeability from s-parameters. Table 1-2 gives an overview of the conversion techniques that are used to determine the dielectric properties.

Table 1-2: The difference between the conversion techniques.

Conversion techniques	S-parameters	Dielectric properties
NRW	S11,S21,S12,S22 or S11, S21	ϵ_r, μ_r
NIST iterative	S11,S21,S12, S22 or S11,S21	$\epsilon_r, \mu_r = 1$
New non-iterative	S11,S21,S12,S22 or S11,S21	$\epsilon_r, \mu_r = 1$
SCL	S11	ϵ_r

Each of the conversion techniques has different advantages and disadvantages. The selection of the technique depends on several different variables that one needs to consider for any projects. These factors include, measured s-parameters, sample length, the desired dielectric properties, speed of conversion, and accuracies in the converted results [21].

1.8 Nicholson-Ross-Weir (NRW) Technique

This is a technique that provides a way to directly calculate both permittivity and permeability from the s-parameters. It is probably the technique that is used the most to perform such conversion. If one wants to measurement the reflection coefficient and transmission coefficient then this requires all four s-parameters or a pair of s-parameters of the material under text to be measured. However, the technique diverges for low loss materials at frequencies corresponding to integer multiples of one-half wavelength in the

sample. This problem is due to a phase ambiguity, which will be look at later. So then, the technique is restricted to optimum sample thickness of $\lambda_g/4$, and the technique should be used for short samples. From our concrete pipe plots, one can see that the NRW technique is divergent at integral multiples of one-half wavelength in the sample.

This is because that at a point corresponding to the one-half wavelength the s-parameter (S_{11}) gets very small. For a small s-parameter (S_{11}) value the uncertainty in the measurement of the phase of S_{11} on the VNA is very large. Therefore the uncertainty causes the divergence at these frequencies. These divergences can be avoided by reducing the sample length. However, it is difficult to determine the appropriate sample length when its ϵ and μ are unknown. The advantages of this technique are that it is fast and applicable to waveguides and coaxial line. The disadvantages of this technique are that it divergences at frequencies corresponding to multiples of one-half wavelength, short samples should be used, and it is not suitable for low loss materials [34][20].

1.9 NIST Iterative Technique

NIST Iterative technique performs the calculation using a Newton Raphson's root finding technique. This technique is suitable for the calculation of permittivity only. It takes advantage of all four (S_{11} , S_{21} , S_{12} , S_{22}) or a pair of s-parameters of MUT to calculate the reflection and transmission coefficient. It works well if a good initial guess is available. This technique bypasses the inaccuracy peaks that existed in the NRW technique. The technique makes the correction when the sample thickness is an integer multiple of one half wavelength. It is suitable for long samples and characterizing low loss materials. By using this technique, a stable permittivity over the frequency spectrum can be obtained from the s-parameters. This technique allows measurements to be taken

on samples of arbitrary length. The technique minimizes the instability present in NRW technique by setting $\mu_r = 1$. One needs to remember that only non-magnetic materials can be measured using this technique. The advantages of NIST Iterative technique is smooth permittivity results, accurate, samples can be any length, and robust for low loss and high loss materials. The disadvantages of NIST Iterative technique are that it is applicable for permittivity measurement only, and one needs an initial guess of permittivity value [35].

1.10 New Non-Iterative Technique

The new non-iterative technique is quite similar to the NRW method. This technique is suitable for permittivity calculation for the case permeability $\mu_r = 1$. It takes advantage of all four s-parameters or just two s-parameters of MUT to calculate the reflection and transmission coefficients. The technique has the advantage of being stable over a whole range of frequencies for an arbitrary sample length. The technique is based on a simplified version of NRW method but no divergence is seen at frequencies corresponding to multiples of one half wavelengths in the sample. This technique does not need an initial estimation of permittivity. It can also perform the calculation very fast. The accuracies are comparable to the iterative technique. The technique uses a little different formulation from the NRW method. This technique can be easily extended to measuring other samples. It also has the permittivity and permeability appear in the expression of the effective electromagnetic parameters. The effective electromagnetic parameters represent a propagation mode. The advantages of new non-iterative technique are smooth permittivity results, accurate, length of the sample not important, fast, and finally no initial guess is required. The disadvantages of new non-iterative technique are that the method is applicable only for measuring the permittivity [12].

1.11 Short Circuit Line (SCL) Technique

Short circuit line technique is a one port measurement on a waveguide or a coaxial line. This technique does the calculation using the same Newton Raphson's numerical approach as the NIST iterative technique. The SCL technique is suitable for permittivity calculation only. It takes advantage of the S_{11} parameter of MUT to calculate the reflection coefficient. The method requires a good initial guess in order to obtain an accurate result. The technique also requires the input of sample length and position for accurate measurements. The advantages of the short circuit line technique are smooth permittivity results, accurate, arbitrary length of samples can be used, and finally prefer use for long samples for low loss materials. The disadvantage of the short circuit line technique is the need for an initial guess, iterative, and one needs accurate sample length [9].

In conclusion, in order to measure the dielectric properties of concrete pipe and clay pipe we need to know the appropriate measurement and conversion technique. It is necessary to use the right techniques for the material to be measured because specific techniques are applicable to specific materials. If the wrong techniques are used, the measurement will not be satisfactory. Besides the measurement and conversion techniques, speed and accuracy are important criterias too. Speed involves how fast the measurement techniques are able to extract the s-parameters and the speed of the conversion techniques. Accuracy depends on the calibration technique and the conversion technique used. Because this research used concrete pipe and clay pipe, which are solids, the measurement technique that has been used is the transmission/reflection method.

NRW was the conversion technique that this research used, but because of uncertainty in this technique we used a correction factor [12][36][37].

CHAPTER 2

THEORY OF THE DIELECTRIC PROPERTIES

2.1 Definition and Physics of Dielectric Properties

Materials can be characterized by electric permittivity ϵ , electric conductivity σ , magnetic permeability μ , and magnetic conductivity σ^* . The frequency-dependence of all these properties is termed dielectric dispersion. We can assume concrete to be as a homogeneous, isotropic, and lossless dielectric medium, although this is not totally the case. Dielectric properties of a material can be used to determine other material properties such as moisture content, and bulk density [38]. This section provides the background information regarding the theory of dielectric properties of materials in general.

Dielectric properties can be interpreted both microscopically and macroscopically.

Microscopically, dielectric properties represent the polarization ability of molecules in the material corresponding to an externally applied electric field. Macroscopically, dielectric properties are the relationship between the applied electric field strength E^* and the electric displacement D^* , both externally measured. Dielectric properties are the collective terms of electric permittivity ϵ , electric conductivity σ , magnetic permeability μ , and magnetic conductivity σ^* .

Materials are described and classified by these properties into various types, such as metals and dielectrics [30]. Our research is with concrete pipes, so the study will consider only isotropic materials. All of the properties of isotropic materials are described by first-order tensors. These quantities can be real or complex, depending on the nature of the material. When electric fields are applied to concrete pipes, the quantities are generally complex. Complex electrical permittivity ϵ (F/m) describes the ability of a material to interact with an applied electric field. It is defined as the ratio between the electric displacement D^* (C/m²) and the electric field E^* (V/m). Generally,

$$\vec{D}^* = \epsilon \vec{E}^* \quad (2.1)$$

where $\epsilon = \epsilon(\omega)$ for dielectric materials. It represents the ability of a material to permit an electric field to pass through the material [39]. For dielectric materials their frequency-dependent response is subject to applied electric fields, which is the result of the molecular polarizability. Their delayed and attenuated response is also observed and described as the dielectric dispersion phenomenon attributing to several polarization phenomena in the microscopic level. To account for these absorption and losses an imaginary part is needed in the dielectric description of the material property [40].

Therefore, the complex electrical permittivity (or complex permittivity) is defined as

$$\epsilon = \epsilon' + i(-\epsilon'') = \epsilon' - i\epsilon'' \quad (2.2)$$

where ϵ' is the real part of ϵ representing the ability of a material to store energy that is carried by the electromagnetic field transmitting through it, and ϵ'' is the imaginary part representing energy absorption and loss. The negative sign defines ϵ'' as applied since energy dissipation/loss occurs to the concrete pipes in our research. A positive sign of ϵ'' would suggest that energy is being created. The measured values of ϵ' and ϵ'' mainly

depend on measured frequency and temperature, while in some cases, as well as pressure [41]. For example, the Debye equations provide a frequency-dependent representation of ϵ' and ϵ'' , satisfying the Kramers-Kronig relations, as

$$\epsilon'(\omega) = \epsilon_i + \epsilon_s - \epsilon_i / (1 + (\omega\tau)^2) \quad (2.3)$$

$$\epsilon''(\omega) = \omega\tau(\epsilon_s - \epsilon_i) / (1 + (\omega\tau)^2) \quad (2.4)$$

where $\omega = 2\pi f$ is the angular frequency, f is the temporal frequency, ϵ_i is the permittivity measured by electric (ac) current field at frequency $\omega = \infty$, ϵ_s is the permittivity measured by the electric (dc) current field at frequency $\omega = 0$, and τ is the characteristic relaxation time [38]. The relaxation time is usually represented by,

$$\tau_t = \tau / 2\pi. \quad (2.5)$$

Materials whose response can be described by the Debye equations are called Debye material.

We find Kramers-Kronig relations by using Fourier Transforms. We begin with the relation between the electric field and displacement at some particular frequency ω .

$$\vec{D}(x, \omega) = \epsilon(\omega) \vec{E}(x, \omega) \quad (2.6)$$

where we note the two Fourier transform relations:

$$\vec{D}(x, t) = \frac{1}{\sqrt{2\pi}} \int_{-\infty}^{\infty} \vec{D}(x, \omega) e^{-i\omega t} d\omega \quad (2.7)$$

$$\vec{D}(x, \omega) = \frac{1}{\sqrt{2\pi}} \int_{-\infty}^{\infty} \vec{D}(x, t') e^{i\omega t'} dt' \quad (2.8)$$

and also, we have:

$$\vec{E}(x, t) = \frac{1}{\sqrt{2\pi}} \int_{-\infty}^{\infty} \vec{E}(x, \omega) e^{-i\omega t} d\omega \quad (2.9)$$

$$\vec{E}(x, \omega) = \frac{1}{\sqrt{2\pi}} \int_{-\infty}^{\infty} \vec{E}(x, t') e^{i\omega t'} dt' \quad (2.10)$$

Therefore:

$$\vec{D}(\mathbf{x}, t) = \frac{1}{\sqrt{2\pi}} \int_{-\infty}^{\infty} \varepsilon(\omega) e^{-i\omega t} d\omega \frac{1}{\sqrt{2\pi}} \int_{-\infty}^{\infty} \vec{E}(\mathbf{x}, t') e^{i\omega t'} dt' \quad (2.11)$$

$$\vec{D}(\mathbf{x}, t) = \varepsilon_0 \left\{ \vec{E}(\mathbf{x}, t) - \int_{-\infty}^{\infty} G(\tau) \vec{E}(\mathbf{x}, t - \tau) d\tau \right\} \quad (2.12)$$

where I have introduced the susceptibility kernel:

$$G(\tau) = \frac{1}{\sqrt{2\pi}} \int_{-\infty}^{\infty} \left(\frac{\varepsilon(\omega)}{\varepsilon_0} - 1 \right) e^{-i\omega \tau} d\omega \quad (2.13)$$

$$G(\tau) = \frac{1}{\sqrt{2\pi}} \int_{-\infty}^{\infty} \aleph_0(\omega) e^{-i\omega \tau} d\omega \quad (2.14)$$

where $\varepsilon(\omega) = \varepsilon_0 (1 + \aleph_0(\omega))$. This equation is nonlocal in time unless $G(\tau)$ is a delta function, which in turn is true only if the dispersion is constant [42]. To understand this consider the susceptibility kernel for a simple one resonance model. In this case we have

$$\aleph_0 = \varepsilon/\varepsilon_0 - 1 = \omega_p^2 / (\omega_0^2 - \omega^2 - i\gamma_0 \omega) \quad (2.15)$$

then,

$$G(\tau) = \frac{\omega_p^2}{2\pi} \int_{-\infty}^{\infty} \frac{1}{(\omega_0^2 - \omega^2 - i\gamma_0 \omega)} e^{-i\omega \tau} d\omega \quad (2.16)$$

This is an integral we can do using contour integration methods. We use the quadratic formula to find the roots of the denominator, and then write the factored denominator in terms of the roots:

$$\omega_{1,2} = -i\gamma \pm \sqrt{-\gamma^2 + 4\omega_0^2} / 2 \quad (2.17)$$

$$\omega_{1,2} = (-i\gamma / (2 \pm \omega_0 \sqrt{1 - u})) \quad (2.18)$$

where $u = \gamma^2 / 4\omega_0^2$ and $\nu_0 \approx \omega_0$ as long as $\omega_0 \gg \gamma/2$. Then,

$$G(\tau) = (2\pi i) \frac{\omega_p^2}{2\pi} \oint_c \left[\frac{1}{(\omega - \omega_1)(\omega - \omega_2)} \right] e^{-i\omega \tau} d\omega \quad (2.19)$$

If we close the contour in the upper half plane, we have to restrict $\tau < 0$, because otherwise the integrand will not vanish on the contour at infinity where ω the positive imaginary part has. If we close the integrand in the lower half plane, $\tau > 0$ and we have:

$$G(\tau) = \omega_p^2 e^{-\gamma\tau/2} \sin(\nu_0)/\nu_0 \theta(\tau) \quad (2.20)$$

where this is a function to enforce the $\tau > 0$ constraint. Then we can use complex variables and Cauchy's theorem to continue to solve the problem [43][44]. We start by noting that $G(\tau)$ is real, and then we get:

$$\frac{\varepsilon(\omega)}{\varepsilon_0} - 1 = iG(0)/\omega - G'(0)/\omega^2 + \dots \quad (2.21)$$

from which we can conclude that $\varepsilon(-\omega) = \varepsilon^*(\omega^*)$. Note the even/odd imaginary/real in the series, and $\varepsilon(\omega)$ is therefore analytic in the upper half plane and so we have:

$$\frac{\varepsilon(z)}{\varepsilon_0} - 1 = \frac{1}{2\pi i} \oint_c \frac{\varepsilon(\omega')}{(\varepsilon_0 - 1)(\omega' - z)} d\omega' \quad (2.22)$$

If we let $z = \omega + i\delta$, then we have:

$$1/(\omega' - \omega - i\delta) = P[1/(\omega' - \omega)] + i\pi\delta(\omega' - \omega) \quad (2.23)$$

If we substitute this into the integral above along the real axis only, we have:

$$\frac{\varepsilon(\omega)}{\varepsilon_0} = 1 + \frac{1}{i\pi} P \int_{-\infty}^{\infty} \frac{\varepsilon(\omega')}{(\varepsilon_0 - 1)(\omega' - \omega)} d\omega' \quad (2.24)$$

Although this looks like a single integral, because of the i in the denominator it is really two integrals. The real part of the integrand becomes the imaginary part of the result and vice versa. So what we have this is:

$$Re\left(\frac{\varepsilon(\omega)}{\varepsilon_0}\right) = 1 + \frac{1}{i\pi} P \int_{-\infty}^{\infty} \text{Im} \frac{\varepsilon(\omega')}{\varepsilon_0(\omega' - \omega)} d\omega' \quad (2.25)$$

$$Im\left(\frac{\varepsilon(\omega)}{\varepsilon_0}\right) = -\frac{1}{\pi} P \int_{-\infty}^{\infty} \text{Re} \frac{\varepsilon(\omega')}{(\varepsilon_0 - 1)(\omega' - \omega)} d\omega' \quad (2.26)$$

These are the equations that we know as the Kramers-Kronig relations [45]. A dimensionless representation is also used for defining the complex permittivity. The complex relative permittivity is defined by

$$\epsilon_r = \epsilon / \epsilon_0 = (\epsilon' - i\epsilon'') / \epsilon_0 = \epsilon'_r - i\epsilon''_r \quad (2.27)$$

where ϵ_0 is the electrical permittivity of free space, ϵ'_r is the dimensionless dielectric constant, and ϵ''_r is the dimensionless loss factor. It is only the dimensionless nature leading to the name “dielectric constant” since ϵ'_r is not a constant when considered over a range of frequencies [46]. The ratio between ϵ'_r and ϵ''_r is the loss tangent or dissipation factor, so when have:

$$\tan \delta = \epsilon''_r / \epsilon'_r = \epsilon'' / \epsilon' \quad (2.28)$$

This dimensionless representation (ϵ / ϵ_0 , $\tan \delta$) is simpler then and has an advantage over the original (ϵ' , ϵ'') representation because it clearly shows that the material is different from free space. Complex magnetic permeability μ describes the ability of a material to interact with an applied magnetic field. It is the ratio between the magnetic field flux density B and the magnetic field H.

$$\vec{B} = \mu \vec{H} \quad (2.29)$$

μ is a scalar for isotropic materials. The complex magnetic permeability is used when magnetic losses are present in the material [47][48].

$$\mu = \mu' - i\mu'' \quad (2.30)$$

where μ' and μ'' are the real and imaginary parts of the complex permeability. The negative imaginary part of μ suggests the energy dissipation. A dimensionless relative complex permeability can be further defined as

$$\mu_r = \mu' - i\mu'' / \mu_0 = \mu'_r - i\mu''_r \quad (2.31)$$

where μ_0 is the permeability of free space. Definitions of various materials are listed in Table 2-1.

Table 2-1: Types of magnetic materials

Description	Criterion
Feromagnetic	$\mu_r > 10$
Paramagnetic	$1 < \mu_r < 10$
Diamagnetic	$\mu_r < 1$
Non-magnetic	$\mu_r = \mu''_r = 1, \mu'''_r = 0$

Apparent electrical permittivity ϵ_a is defined by accounting for the direct current conductivity loss in the representation of complex permittivity. Since the imaginary part transmitting through the material [49]. The total energy dissipation in the material can be expressed by the dissipated or absorbed power using the complex Poynting vector theorem and the Maxwell's equations. When dealing with electromagnetic fields a way is needed to relate the concept of energy to the fields [50]. This is done by means of the Poynting vector:

$$\vec{P} = \vec{E} \times \vec{H} \quad (2.32)$$

where E is the electric field intensity, H is the magnetic field intensity, and P is the Poynting vector. The absolute value of Poynting vector is found to be the power density in an electromagnetic field. By using the Maxwell's equations for the curl of the fields along Gauss's divergence theorem and an identity from vector analysis, we may prove what is known as the Poynting theorem. The Maxwell's equations needed are

$$\nabla \times \vec{E} = -\partial \vec{B} / \partial t \quad (2.33)$$

$$\nabla \times \vec{H} = \vec{J} + \partial \vec{D} / \partial t \quad (2.34)$$

along with the material relationships:

$$\vec{D} = \epsilon_0 \vec{E} + \vec{P} \quad (2.35)$$

$$\vec{B} = \mu_0 \vec{H} + \mu_0 \vec{M} \quad (2.36)$$

or for isotropic materials

$$\vec{D} = \epsilon \vec{E} \quad (2.37)$$

$$\vec{B} = \mu \vec{H} \quad (2.38)$$

In addition, the identity from vector analysis,

$$\nabla \cdot (\vec{E} \times \vec{H}) = -\vec{E} \cdot (\nabla \times \vec{H}) + \vec{H} \cdot (\nabla \times \vec{E}) \quad (2.39)$$

is needed. If P_A is to be the power density, then its surface integral over the surface of a volume must be the power out of the volume. So next do the negative of the surface integral to obtain P , the power into the volume:

$$\vec{P}_A = - \oint \vec{E} \times \vec{H} \cdot d\vec{S}. \quad (2.40)$$

Now we can use Gauss's divergence theorem on the integral in equation (2.40), along with equation (2.39), we have:

$$\begin{aligned} \vec{P}_A &= - \oint (\vec{E} \times \vec{H}) \cdot d\vec{S} \\ \vec{P}_A &= \iiint -\nabla \cdot (\vec{E} \times \vec{H}) dV \\ \vec{P}_A &= \iiint \vec{E} \cdot (\nabla \times \vec{H}) + \iiint \vec{H} \cdot (-\nabla \times \vec{E}) dV \end{aligned} \quad (2.41)$$

Next, substituting from Maxwell's equations, we can obtain:

$$\vec{P}_A = - \oint \vec{E} \times \vec{H} \cdot d\vec{S} = \iiint \vec{E} \cdot \vec{J} dV + \iiint \vec{E} \cdot \partial \vec{D} / \partial t dV + \iiint \vec{H} \cdot \partial \vec{B} / \partial t dV \quad (2.42)$$

Equation (2.44) is the Poynting theorem. The complex Poynting vector \vec{p} is

$$\vec{P} = \frac{1}{2} \oint_s (\vec{E} \times \vec{H}^*) dS \quad (2.43)$$

where S is a closed surface and dS is a vector element of area directed outward from the volume V , H^* is the conjugate of the magnetic field H . The divergence theorem provides

$$\oint_S (\vec{E} \times \vec{H}^*) dS = \int_V \nabla \cdot (\vec{E} \times \vec{H}^*) dV. \quad (2.44)$$

From vector calculus we have

$$\nabla \cdot (\vec{E} \times \vec{H}) = (\nabla \times \vec{E}) \cdot \vec{H} - (\nabla \times \vec{H}) \cdot \vec{E} \quad (2.45)$$

with Maxwell's equations $\nabla \times \vec{E} = i\omega \vec{B}$ and $\nabla \times \vec{H} = i\omega \vec{D} + \vec{J}$, Ohm's law $\vec{J} = \sigma \cdot \vec{E}$, and $\vec{B} = \mu \vec{H}$, the complex Poynting vector becomes

$$\frac{1}{2} \oint_S (\vec{E} \times \vec{H}^*) d\vec{S} = \frac{1}{2} \int_V [(-i\omega\mu \cdot \vec{H}) \cdot \vec{H}^* + (i\omega\epsilon \cdot \vec{E} - \sigma \cdot \vec{E})] dV. \quad (2.46)$$

If we rearrange our equations, then

$$\text{Re} \left[\frac{1}{2} \oint_S (\vec{E} \times \vec{H}^*) (-d\vec{S}) \right] = \omega/2 \int_V (\mu'' \vec{H} \cdot \vec{H}^* + \epsilon'' \vec{E} \cdot \vec{E}^* + \sigma/\omega \vec{E} \cdot \vec{E}^*) dV \quad (2.47)$$

$$\text{Im} \left[\frac{1}{2} \oint_S (\vec{E} \times \vec{H}^*) (-d\vec{S}) \right] = \omega/2 \int_V (\mu' \vec{H} \cdot \vec{H}^* - \epsilon' \vec{E} \cdot \vec{E}^*) dV \quad (2.48)$$

where $-dS$ is the vector pointing toward the closed surface S and tangent to the surface boundary [51][52]. The real part of the complex Poynting vector is the dissipated energy P_{dis} absorbed by the material, which consists of three parts; magnetic loss, electric loss, and conductivity loss.

Since $\mu'' = 0$ for non-magnetic materials, P_{dis} becomes

$$\vec{P}_{\text{dis}} = \omega/2 \int_V (\epsilon'' + \sigma/\omega) \vec{E} \cdot \vec{E}^* dV = \omega/2 \int_V \epsilon \vec{E} \cdot \vec{E}^* dV \quad (2.49)$$

and the effective dielectric loss factor is

$$\epsilon''_e = \epsilon'' + \sigma/\omega \quad (2.50)$$

So then we can write an effective conductivity which is defined as

$$\sigma_e = \omega \epsilon''_e = \omega \epsilon'' + \sigma \quad (2.51)$$

where $\sigma = \sigma_s$ is the electrical conductivity measured at the static frequency ($\omega = 0$). This conductivity is the real part of the complex conductivity [52]. So now that we know the effective dielectric loss factor, we can define the apparent complex permittivity as

$$\epsilon_a = \epsilon'' - i\epsilon''_e = \epsilon' - i(\epsilon'' + \sigma_s/\omega) \quad (2.52)$$

Definitions of materials based on our apparent complex permittivity are listed in Table 2-2.

Table 2-2: Types of dielectric materials

Description	Criterion
Perfect Dielectric	$\epsilon'' > 0, \epsilon''_e = 0$
Imperfect Dielectric	$\epsilon' > 0, \epsilon''_e > 0$

Complex electrical conductivity σ describes the ability of a material to conduct an applied electric current, represented by the ratio between the electric current density \vec{j} and the electric field \vec{E} .

$$\vec{j} = \sigma \cdot \vec{E} \quad (2.53)$$

where σ is the scalar electrical conductivity for isotropic materials. Following the previously shown energy treatment for the definition of the complex permittivity, the complex electrical conductivity can be defined as

$$\sigma_a = i\omega\epsilon_a = i\omega(\epsilon' - i\epsilon''_e) = \sigma_e'' + i\sigma'' \quad (2.54)$$

where,

$$\sigma_e'' = \omega\epsilon_e'' = \omega\epsilon'' + \sigma_s \quad (2.55)$$

$$\sigma'' = \omega\epsilon''. \quad (2.56)$$

The defined effective conductivity is the real part of the complex apparent conductivity which can be defined as,

$$\sigma_e'' = \omega \epsilon_e'' = \sigma_e \quad (2.57)$$

The D.C. conductivity, a frequency-independent term, is part of the apparent complex conductivity in the definition. The D.C. conduction effect is significant only in low-frequency or high-temperature situations, while it is insignificant in microwave frequency because,

$$\omega \epsilon'' > \sigma_s . \quad (2.58)$$

By constructing this relationship, the definition regarding conductivity in complex apparent permittivity is connected to the complex apparent conductivity. This suggests that the behavior of this complex apparent conductivity is, by definition, similar to the one the complex apparent permittivity exhibits [53][54]. For example, in the Debye model, the real and imaginary parts of the complex apparent conductivity are,

$$\sigma_a = \sigma_e' + i\sigma'' \quad (2.59)$$

$$\sigma_e'' = \sigma_s + (\omega\tau)^2 (\sigma_\infty - \sigma_s) / (1 + (\omega\tau)^2) \quad (2.60)$$

$$\sigma'' = \omega \epsilon_\infty + \omega\tau (\sigma_\infty - \sigma_s) / (1 + (\omega\tau)^2) \quad (2.61)$$

where σ_∞ is the permittivity measured by an alternating field at frequency $\omega = \infty$, and σ_s is the permittivity measured by the direct current field at frequency $\omega = 0$. Comparing σ_e' with $\omega \epsilon_e''$ gives us

$$\epsilon_s - \epsilon_\infty = \tau (\sigma_\infty - \sigma_s). \quad (2.62)$$

The relaxation time can be determined to be

$$\tau = (\epsilon_s - \epsilon_\infty) / (\sigma_\infty - \sigma_s) . \quad (2.63)$$

The Debye-type behavior of complex electrical conductivity leads us to the loss tangent, which is,

$$\tan \delta = \epsilon_e'' / \epsilon'' = \sigma_e' / \sigma'' = \sigma_e' / \omega \epsilon'' = \omega \epsilon_e'' / \sigma'' \quad (2.64)$$

Those with a high conductivity are considered to be conductors and those without conductivity are insulators (see Table 2-3). Nonconductive materials are also called lossless. Materials, with slight conductivity are called low-loss [38][55][56][57].

Table 2-3: Summaries of various materials by conductivity.

Description	Criterion	Notes
Lossy	$0 < \tan \delta$	Electrical conductivity is present in the material.
Low-loss	$\tan \delta < 1$	General Definition
Lossless	$\tan \delta = 0$	Electrical conductivity is not present in the material.

2.2 Section II

2.2.1 Coaxial Transmission Line Theory

If we start with the wave equation in cylindrical coordinates, we have

$$1/\rho \partial/\partial\rho(\rho \partial V/\partial\rho) + 1/\rho^2 \partial^2 V/\partial\phi^2 + \partial^2 V/\partial z^2 = \nu^2 V \quad (2.65)$$

if we then separate variables,

$$V = R(\rho)\Phi(\phi)Z(z) \quad (2.66)$$

We know that R , Φ , and Z are functions, and ρ , ϕ , and z are coordinates, if we insert equation (2.67) into equation (2.66) and then divide by R , Φ , and Z , we obtain

$$1/\rho R \partial/\partial\rho(\rho \partial R/\partial\rho) + 1/\rho^2 \Phi \partial^2 \Phi/\partial\phi^2 + 1/z \partial^2 Z/\partial z^2 = \nu^2 \quad (2.67)$$

The third term is a function of z only. The sum of the three terms is a constant, and so the third term may be set equal to a constant a_z^2 ,

$$dZ^2/dz^2 = a_z^2 Z \quad (2.68)$$

This equation has a general solution of the form

$$X = C_1 e^{a_x x} + C_2 e^{-a_x x} \quad (2.69)$$

If we insert a_z^2 for the third term of equation (2.68) and multiply by ρ^2 , we obtain

$$\rho/R \partial [\rho(\partial R/\partial \rho)]/\partial \rho + 1/\Phi \partial^2 \Phi / \partial \varphi^2 + (a_z^2 - \nu^2)\rho^2 = 0 \quad (2.70)$$

The second term is a function of φ only. So we can equate this to a constant which can be represented by ν , then we obtain this equation for Φ ,

$$d^2 \Phi / d\varphi^2 = -\nu^2 \Phi \quad (2.71)$$

This equation also has a general solution like equation (2.69). Replacing the Φ term by ν^2 in equation (2.71) and multiply through by R , we have the equation for the radial function

$$\rho d/d \rho (\rho dR/d \rho) + [(a_z^2 - \nu^2)\rho^2 - \nu^2]R = 0 \quad (2.72)$$

This is a form of Bessel's equation. If we let $k^2 = (a_z^2 - \nu^2)$ and $x = k\rho$, this equation may be put in the standard form; x is a new variable and is not the x coordinate [58].

Equation (2.73), can then be written

$$x^2 d^2 R/dx^2 + x dR/dx + (x^2 - \nu^2)R = 0 \quad (2.73)$$

Since the Bessel equation is a second-order differential equation, it has two independent solutions. The solutions are obtained by assuming an infinite series solution of the form

$$R = \sum_{i=0}^{\infty} c_i x^{b+i} \quad (2.74)$$

The coefficients c_i and the constant b in the series are evaluated by substituting equation (2.75) into equation (2.74) [59]. The two solutions of equation (2.74) are Bessel function of the first kind and order ν :

$$J_\nu(x) = \sum_{m=0}^{\infty} (-1)^m (x/2)^{\nu+2m} / (m! \Gamma(m+\nu+1)) \quad (2.75)$$

$$j_{-\nu}(x) = \sum_{m=0}^{\infty} (-1)^m (x/2)^{-\nu+2m} / (m! \Gamma(m-\nu+1)) \quad (2.76)$$

When ν takes integer values, it can be replaced by $\nu = n$ and the Gamma function then becomes the factorial,

$$\Gamma(m + n + 1) = (m + n)! \quad (2.77)$$

The two solutions in equation (2.76) and equation (2.77) are then related by $J_\nu(x) = (-1)^n J_{-\nu}(x)$, so then they are not independent solutions. Another solution, known as the second-kind Bessel function of order n , represented by $N_n(x)$ may be obtained [58]. The first and second-kind Bessel functions of integral order are

$$J_n(x) = \sum_{m=0}^{\infty} (-1)^m (x/2)^{n+2m} / (m!(m+n)!) \quad (2.78)$$

$$N_n(x) = \sum_{m=0}^{\infty} J_n(x) \cos n\pi - J_{-n}(x) / \sin n\pi \quad (2.79)$$

The solution in cylindrical coordinates for integral values $\nu = n$ is

$$V = [C_1 J_n(k\rho) + C_2 N_n(k\rho)](C_3 \cos n\varphi + C_4 \sin n\varphi)(C_5 e^{a_z z} + C_6 e^{-a_z z}) \quad (2.80)$$

The solution for nonintegral values of ν , can be written

$$V = [C_1 J_\nu(k\rho) + C_2 J_{-\nu}(k\rho)](C_3 \cos \nu\varphi + C_4 \sin \nu\varphi)(C_5 e^{a_z z} + C_6 e^{-a_z z}) \quad (2.81)$$

Special cases occur if $a_z, \nu, \text{ or } \nu$ are zero. If $a_z = 0$, the Z function reduces to $Z = (C_5 z + C_6)$. If a_z and ν are both zero, then equation (2.73) becomes

$$\rho d[\rho dR / d\rho] / d\rho - \nu^2 R = 0 \quad (2.82)$$

which has a solution $R = (C_1 \rho^\nu + C_2 \rho^{-\nu})$. Finally, if $a_z, \nu, \text{ and } \nu$ are all zero, then the R solution becomes $R = C_1 \ln \rho + C_2$. The choice of the equation for a problem depends upon the boundary conditions [39][52][58][60].

In the coaxial line the principal mode is the TEM mode. It has no cutoff frequency and is the mode of operation of transmission lines at low frequencies or on direct current.

The coaxial transmission line can support TEM, TE, and TM modes (See Figure 2-1). However, it is normally operated at frequencies where only the TEM mode propagates [48].

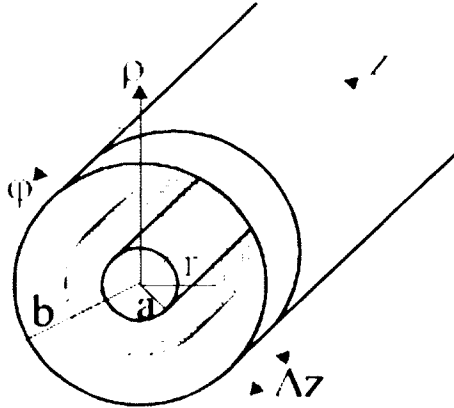


Figure 2-1: Coaxial line.

2.2.2 Coaxial Line TEM Modes

The transverse fields of the TEM mode can be written as

$$\vec{E}(\rho, \varphi, z) = \vec{e}(\rho, \varphi) e^{-j\beta z} \quad (2.83)$$

$$\vec{H}(\rho, \varphi, z) = \vec{h}(\rho, \varphi) e^{-j\beta z} \quad (2.84)$$

where $\vec{e}(\rho, \varphi)$ and $\vec{h}(\rho, \varphi)$ are equivalent to the electrostatic and magnetostatic fields for the coaxial geometry. The electrostatic field is that of a coaxial capacitor with voltage of V_0 between the cylindrical conductors.

$$\vec{e}(\rho, \varphi) = \vec{E}_0(\rho) = V_0 / \rho \ln(b/a) \vec{a}_\rho \quad (2.85)$$

The magnetostatic field is that of a coaxial transmission line carrying DC currents in opposite directions. For the magnetostatic field to be the static limit of a +z directed wave on the transmission line, the current in the inner conductor must be outward [61].

$$\vec{\mathcal{H}}(\rho, \varphi) = 1 / Z_{\text{TEM}} \vec{a}_z \times \vec{e}(\rho, \varphi) \quad (2.86)$$

$$Z_{\text{TEM}} = \eta = \sqrt{\frac{\mu}{\epsilon}} \quad (2.87)$$

$$\vec{\mathcal{H}}(\rho, \varphi) = \vec{H}_0(\rho) = V_0 / \eta \rho \ln(b/a) \vec{a}_\varphi \quad (2.88)$$

The TEM fields within the coaxial transmission line are

$$\vec{E}(\rho, \varphi, z) = \vec{e}(\rho, \varphi) e^{-j\beta z} = V_0 e^{-j\beta z} / \rho \ln(b/a) \vec{a}_\rho \quad (2.89)$$

$$\vec{H}(\rho, \varphi, z) = \vec{\mathcal{H}}(\rho, \varphi) e^{-j\beta z} = V_0 e^{-j\beta z} / \eta \rho \ln(b/a) \vec{a}_\varphi \quad (2.90)$$

The TEM mode represents the dominant mode in a coaxial line with a cutoff frequency of zero. However, higher order TE and TM modes can propagate in the coaxial line at sufficiently high frequencies [8][38][62].

2.2.3 Coaxial Line TE Modes

The longitudinal magnetic field of the TE modes within the coaxial transmission line must satisfy

where

$$\vec{H} = H_z \cdot \vec{a}_z$$

$$\nabla^2 H_z + k^2 H_z = 0 \quad (2.91)$$

$$H_z(\rho, \varphi, z) = h_z(\rho, \varphi) e^{-j\beta z} \quad (2.92)$$

so then, we can use the same general separation of variables solution that exists for circular waveguide [38].

$$H_z(\rho, \varphi) = R(\rho) P(\varphi) \quad (2.93)$$

$$R(\rho) = C J_n(k_c \rho) + D Y_n(k_c \rho) \quad (2.94)$$

$$P(\varphi) = A \sin n\varphi + B \cos n\varphi \quad (2.95)$$

Note that the ρ -dependent term includes both Bessel functions of the first and second kind. We cannot eliminate the Bessel function of the second kind from the solution since

$\rho = 0$ is not in the domain of interest[$a < \rho < b$] for the coaxial transmission line [49].

The general solution for the longitudinal magnetic field function is

$$\mathbb{H}_z(\rho, \varphi) = [CJ_n(k_c \rho) + DY_n(k_c \rho)][A \sin n\varphi + B \cos n\varphi] \quad (2.96)$$

while the longitudinal magnetic field is

$$H_z(\rho, \varphi, z) = [CJ_n(k_c \rho) + DY_n(k_c \rho)][A \sin n\varphi + B \cos n\varphi]e^{-j\beta z} \quad (2.97)$$

Since there is no longitudinal electric field for the TE modes, one can see that the only

TE boundary conditions for the coaxial transmission line are given as

$$\vec{E}_\varphi(a, \varphi, z) = 0 \quad \vec{E}_\varphi(b, \varphi, z) = 0 \quad (2.98)$$

where

$$E_\varphi = j\omega\mu/k_c^2 \partial H_z / \partial \rho \quad (2.99)$$

$$E_\varphi = j\omega\mu/k_c [CJ_n'(k_c \rho) + DY_n'(k_c \rho)](A \sin n\varphi + B \cos n\varphi)e^{-j\beta z} \quad (2.100)$$

The TE boundary conditions then yield the following,

$$CJ_n'(k_c a) + DY_n'(k_c a) = 0 \quad (2.101)$$

$$CJ_n'(k_c b) + DY_n'(k_c b) = 0 \quad (2.102)$$

This linear system of equations has a nontrivial solution only when the determinant is

zero:

$$J_n'(k_c a)Y_n'(k_c b) - Y_n'(k_c a)J_n'(k_c b) = 0 \quad (2.103)$$

The roots of this characteristic equation ($k_c = q'_{mn}$) define cutoff wavenumbers of the TE_{mn} modes for the coaxial line where m is the index on the roots and n is the order of the Bessel functions in the characteristic equation [58]. So we can then write

$$C/D = -Y_n'(k_c a)/J_n'(k_c a) = -Y_n'(k_c b)/J_n'(k_c b) \quad (2.104)$$

which then gives

$$R(\rho) = CJ_n(k_c \rho) + DY_n(k_c \rho) = C[J_n(k_c \rho) + D/C Y_n(k_c \rho)] \quad (2.105)$$

$$R(\rho) = C [J_n(k_c \rho) - J_n'(k_c a) / Y_n'(k_c a) Y_n(k_c \rho)] \quad (2.106)$$

$$R(\rho) = C' [Y_n'(k_c a) J_n(k_c \rho) - J_n'(k_c a) Y_n(k_c \rho)] \quad (2.107)$$

The resulting longitudinal magnetic field is then written as

$$H_z(\rho, \phi, z) = [Y_n'(k_c a) J_n(k_c \rho) - J_n'(k_c a) Y_n(k_c \rho)] [A \sin n \phi + B \cos n \phi] e^{-j\beta z} \quad (2.108)$$

Where the constant C' has been incorporated into the constants A and B. The resulting transverse fields of the TE_{nm} modes are

$$E_\rho(\rho, \phi, z) = -j\omega\mu / k_c^2 \rho \partial H_z / \partial \phi \quad (2.109)$$

$$E_\rho(\rho, \phi, z) = -j\omega\mu n / k_c^2 \rho [Y_n'(k_c a) J_n(k_c \rho) - J_n'(k_c a) Y_n(k_c \rho)] [A \cos n \phi - B \sin n \phi] e^{-j\beta z} \quad (2.110)$$

$$E_\phi(\rho, \phi, z) = j\omega\mu / k_c^2 \partial H_z / \partial \rho \quad (2.111)$$

$$= j\omega\mu / k_c [Y_n'(k_c a) J_n'(k_c \rho) - J_n'(k_c a) Y_n'(k_c \rho)] [A \sin n \phi + B \cos n \phi] e^{-j\beta z} \quad (2.112)$$

$$H_\rho(\rho, \phi, z) = -j\beta / k_c^2 \partial H_z / \partial \rho \quad (2.113)$$

$$= -j\beta / k_c [Y_n'(k_c a) J_n'(k_c \rho) - J_n'(k_c a) Y_n'(k_c \rho)] [A \sin n \phi + B \cos n \phi] e^{-j\beta z} \quad (2.114)$$

$$H_\phi(\rho, \phi, z) = -j\beta / k_c^2 \rho \partial H_z / \partial \phi \quad (2.115)$$

$$= -j\beta n / k_c^2 \rho [Y_n'(k_c a) J_n(k_c \rho) - J_n'(k_c a) Y_n(k_c \rho)] [A \cos n \phi - B \sin n \phi] e^{-j\beta z} \quad (2.116)$$

The cutoff frequency of the TE_{nm} mode may be defined in terms of the roots to the characteristic equation [32][52][63][64].

$$K_{c_{nm}} = 2\pi f_{c_{nm}} \sqrt{\mu\epsilon} = q'_{nm} \quad (2.117)$$

Solving for $f_{c_{nm}}$ we have,

$$f_{c_{nm}} = q'_{nm} / 2\pi \sqrt{\mu\epsilon} \quad (2.118)$$

The wavenumber for the TE_{nm} mode

$$\beta_{nm} = \sqrt{k^2 - k_{c_{nm}}^2} = \sqrt{k^2 - q_{nm}^2} = k \sqrt{1 - (f_{c_{nm}} / f)^2} \quad (2.119)$$

The wave impedance of the TE_{nm} mode is

$$Z_{TE_{nm}} = \vec{E}_\rho / \vec{H}_\phi = K \eta / \beta = \eta / \sqrt{1 - (f_{c_{nm}} / f)^2} \quad (2.120)$$

2.2.4 Coaxial Line TM Modes

where

$$\vec{E} = E_z \cdot \vec{a}_z$$

$$\nabla^2 E_z + k^2 E_z = 0 \quad (2.121)$$

$$E_z(\rho, \phi, z) = e_z(\rho, \phi) e^{-j\beta z} \quad (2.122)$$

The longitudinal electric field function of the coaxial TM modes satisfies the same differential equation as the magnetic field of the TE modes [65]. So then, we may write the solutions for $e_z(\rho, \phi)$ and $E_z(\rho, \phi, z)$ as

$$e_z(\rho, \phi) = R(\rho)P(\phi) \quad (2.123)$$

$$e_z(\rho, \phi) = [CJ_n(k_c \rho) + DY_n(k_c \rho)][A \sin n\phi + B \cos n\phi] \quad (2.124)$$

$$E_z(\rho, \phi, z) = [CJ_n(k_c \rho) + DY_n(k_c \rho)][A \sin n\phi + B \cos n\phi] e^{-j\beta z} \quad (2.125)$$

The TM boundary conditions for the coaxial line are

$$\vec{E}_\phi(a, \phi, z) = 0 \quad (2.126)$$

$$\vec{E}_\phi(b, \phi, z) = 0 \quad (2.127)$$

$$\vec{E}_z(a, \phi, z) = 0 \quad (2.128)$$

$$\vec{E}_z(b, \phi, z) = 0 \quad (2.129)$$

Again, we find that enforcement of the boundary condition on E_z automatically satisfies transverse field boundary condition. Application of the boundary condition on E_z gives us,

$$CJ_n(k_c a) + DY_n(k_c a) = 0 \quad (2.130)$$

$$CJ_n(k_c b) + DY_n(k_c b) = 0 \quad (2.131)$$

This linear system of equations has a nontrivial solution only when the determinant is zero:

$$J_n(k_c a)Y_n(k_c b) - Y_n(k_c a)J_n(k_c b) = 0 \quad (2.132)$$

The roots of this characteristic equation ($k_c = q_{nm}$) define cutoff wavenumbers of the TM_{nm} modes for the coaxial line [65]. So then, we can write

$$C/D = -Y_n(k_c a)/J_n(k_c a) = -Y_n(k_c b)/J_n(k_c b) \quad (2.133)$$

which gives us,

$$R(\rho) = CJ_n(k_c \rho) + DY_n(k_c \rho) \quad (2.134)$$

$$R(\rho) = C [J_n(k_c \rho) + D/C Y_n(k_c \rho)] \quad (2.135)$$

$$R(\rho) = C [J_n(k_c \rho) - J_n(k_c a)/Y_n(k_c a) Y_n(k_c \rho)] \quad (2.136)$$

$$R(\rho) = C' [Y_n(k_c a) J_n(k_c \rho) - J_n(k_c a) Y_n(k_c \rho)] \quad (2.137)$$

The resulting longitudinal electric field can be written

$$E_z(\rho, \phi, z) = [Y_n(k_c a) J_n(k_c \rho) - J_n(k_c a) Y_n(k_c \rho)] [A \sin n\phi + B \cos n\phi] e^{-j\beta z} \quad (2.138)$$

and the transverse fields can be written

$$E_\rho(\rho, \phi, z) = -j\beta/k_c^2 \partial E_z / \partial \rho \quad (2.139)$$

$$E_\rho(\rho, \phi, z) = -j\beta/k_c [Y_n(k_c a) J'_n(k_c \rho) - J_n(k_c a) Y'_n(k_c \rho)] [A \sin n\phi + B \cos n\phi] e^{-j\beta z} \quad (2.140)$$

$$E_\phi(\rho, \phi, z) = -j\beta/k_c^2 \rho \partial E_z / \partial \phi \quad (2.141)$$

$$E_\phi(\rho, \phi, z) = -j\beta n/k_c^2 \rho [Y_n(k_c a) J_n(k_c \rho) - J_n(k_c a) Y_n(k_c \rho)] [A \cos n\phi - B \sin n\phi] e^{-j\beta z} \quad (2.142)$$

$$H_\rho(\rho, \phi, z) = j\omega\epsilon/k_c^2 \rho \partial E_z / \partial \phi \quad (2.143)$$

$$H_\rho(\rho, \varphi, z) = j\omega\epsilon n / k_c^2 [Y_n(k_c a)J_n(k_c \rho) - J_n(k_c a)Y_n(k_c \rho)] [A \cos n\varphi - B \sin n\varphi] e^{-j\beta z} \quad (2.144)$$

$$H_\varphi(\rho, \varphi, z) = -j\omega\epsilon / k_c^2 \partial E_z / \partial \rho \quad (2.145)$$

$$H_\rho(\rho, \varphi, z) = -j\omega\epsilon / k_c [Y_n(k_c a)J'_n(k_c \rho) - J_n(k_c a)Y'_n(k_c \rho)] [A \sin n\varphi + B \cos n\varphi] e^{-j\beta z} \quad (2.146)$$

The cutoff frequency of the TM_{nm} mode is given by

$$k_{c_{nm}} = 2\pi f_{c_{nm}} \sqrt{\mu\epsilon} = q_{nm} \quad (2.147)$$

$$f_{c_{nm}} = q_{nm} / 2\pi \sqrt{\mu\epsilon} \quad (2.148)$$

The wavenumber for the TM_{nm} mode is

$$B_{nm} = \sqrt{k^2 - k_{c_{nm}}^2} = \sqrt{k^2 - p_{nm}^2} = k \sqrt{1 - (f_{c_{nm}} / f)^2} \quad (2.149)$$

The wave impedance of the TM_{nm} mode is

$$Z_{TM_{nm}} = \vec{E}_\rho / \vec{H}_\varphi = \eta\beta / k = \eta \sqrt{1 - (f_{c_{nm}} / f)^2} \quad (2.150)$$

In the coaxial line, we have two intensities, E_ρ and H_φ . If we obtain the curl equations and wave equations we have,

$$\nabla \times \vec{E} = -j\omega\mu\vec{H} \quad (2.151)$$

$$\nabla \times \vec{H} = (\sigma + j\omega\epsilon)\vec{E} \quad (2.152)$$

We can then express them in cylindrical coordinates, the equations then are written,

$$\partial E_\rho / \partial z = -j\omega\mu H_\varphi \quad (2.153)$$

$$\partial H_\varphi / \partial z = -j\omega\mu E_\rho \quad (2.154)$$

With a propagation term of the form $e^{j\omega t - \Gamma z}$, Equations (2.152) and (2.153) reduce to

$$\Gamma E_\rho = j\omega\mu H_\varphi \quad (2.155)$$

$$\Gamma H_\varphi = -j\omega\mu E_\rho \quad (2.156)$$

We can from this relationship obtain the characteristic wave impedance,

$$E_p / H_\phi = j\omega\mu / \Gamma = \Gamma / j\omega\varepsilon \quad (2.157)$$

Then we can solve equation (2.158) for Γ , we have

$$\Gamma = j\omega\sqrt{\mu\varepsilon} \quad (2.158)$$

If this is inserted into equation (2.158), we obtain

$$E_p / H_\phi = \sqrt{\mu/\varepsilon} = \eta \quad (2.159)$$

The propagation constant and characteristic wave impedance are therefore equal to the corresponding values in unbound dielectric [51]. Ampere's Law may be used to relate the magnetic intensity to the current [66]. For a current in the center conductor given by $I = I_0 e^{j\omega t - \Gamma z}$, Ampere's Law $\oint \vec{H} \cdot \vec{dl} = I$ yields $2\pi\rho H = I_0 e^{j\omega t - \Gamma z}$. Solving for H_ϕ and inserting this into equation (2.160) to obtain E_p , we have

$$H_\phi = I_0 / 2\pi\rho e^{j\omega t - \Gamma z} \cdot \vec{a}_\phi \quad (2.160)$$

$$E_p = \sqrt{\mu/\varepsilon} I_0 / 2\pi\rho e^{j\omega t - \Gamma z} \cdot \vec{a}_\rho \quad (2.161)$$

The potential rise from the outer conductor to the center conductor is found by inserting

E_p from equation (2.161) into $V = - \int_b^a E_p dp$, yielding

$$V = I_0 / 2\pi \oint \sqrt{\mu/\varepsilon} \ln b/a e^{j\omega t - \Gamma z} \cdot \vec{a}_\rho \quad (2.162)$$

The characteristic impedance of a coaxial line is equal to the ratio of voltage to current for the outgoing wave. Dividing the voltage in equation (2.163) by the current $I = I_0 e^{j\omega t - \Gamma z}$, we then have

$$Z_0 = V / I = 1 / 2\pi \sqrt{\mu/\varepsilon} \ln b/a \quad (2.163)$$

which agrees with the characteristic impedance. The curl equations (2.154) and (2.155) may be expressed in terms of voltage and current, whereas they take on the familiar form of the differential equations of a lossless transmission line. From equations (2.162) and (2.163) we obtain $E_p = V / [p \ln b/a]$. Also since $I = I_0 e^{j\omega t - \Gamma z}$, we have from equation (2.161), $H_\phi = I n / 2 \pi p$. Inserting these values of \vec{E}_p and \vec{H}_ϕ into equations (2.154) and (2.155) gives

$$\partial V / \partial z = -j\omega(\mu / 2 \pi \ln b/a)I = -j\omega LI \quad (2.164)$$

$$\partial I / \partial z = -j\omega(2 \pi \epsilon / \ln b/a)V = -j\omega CV \quad (2.165)$$

These are the transmission-line equations for a lossless line. The bracketed term in equation (2.164) is the inductance per unit length of line, while the bracketed term in equation (2.165) is the capacitance per unit length. Poynting's vector $\vec{P} = \vec{E} \times \vec{H}$, may be used to evaluate the instantaneous value of power density in an electromagnetic wave [32]. The intensity vectors are mutually perpendicular and the scalar value of Poynting's vector may therefore be written as $P = EH$. Since we will be dealing mostly with fields having sinusoidal time variation, it will be convenient to have an expression for the time-average power density. The time-average power flow at any point on a transmission line is $P_{av} = \frac{1}{2} VI \cos \theta$, where V and I are peak values and θ is the time phase angle between V and I . By analogy, the time-average power density in a uniform plane wave is $P_{av} = \frac{1}{2} E H \cos \theta$, where E and H are the peak values of the electric and magnetic intensities, and θ is the time phase angle between E and H . This may be shown to be equal to

$$P_{av} = \frac{1}{2} \text{Re} (\vec{E} \vec{H}^*) \quad (2.166)$$

where \vec{E} and \vec{H} are complex values, and \vec{H}^* is the complex conjugate of \vec{H} . By integrating Poynting's vector over the cross section of the dielectric, it may be shown that power is transmitted through the dielectric. We have shown that the time-average power through unit area of dielectric is $P_T = \frac{1}{2} E_p H_\phi$. The direction of power flow is mutually perpendicular to both E_p and H_ϕ and hence is in the z direction [36]. Dropping the term $e^{j\omega t - \Gamma z}$ in equations (2.161) and (2.162), we have for the amplitudes, $H_\phi = I_0 / 2\pi p$ and $E_p = \sqrt{\mu/\epsilon} (I_0 / 2\pi p)$. The time-average power density is therefore $p_T = (I_0^2 / 8\pi p^2) \sqrt{\mu/\epsilon}$. The total Power transmitted through the dielectric is found by integrating the power density over the cross section of the dielectric, or

$$P_T = \int_a^b p_T 2\pi p dp = I_0^2 / 4\pi \sqrt{\mu/\epsilon} \ln b/a \quad (2.167)$$

Since the voltage amplitude from equation (2.162) is $V_0 = (I_0 / 2\pi) \sqrt{\mu/\epsilon} \ln b/a$,

Equation (2.168) can be written as

$$P_T = \frac{1}{2} V_0 I_0 \quad (2.168)$$

where V_0 and I_0 are voltage and current amplitudes. Equation (2.168) is the time-average power flow in a lossless line having only an outgoing wave [60]. So then, the Poynting theorem shows that power flows through the dielectric of the coaxial line. If we need to calculate the dielectric properties of the coaxial line, we use the procedure proposed by Nicholson-Ross-Weir method. The following equations will be a good place to start:

$$S_{11} = \Gamma(1 - T^2) / (1 - T^2\Gamma^2) \quad (2.169)$$

and

$$S_{21} = T(1 - \Gamma^2) / (1 - \Gamma^2 T^2) \quad (2.170)$$

These parameters we will obtain directly from the vector network analyzers. The reflection coefficient can be written as:

$$\Gamma = x \pm \sqrt{x^2 - 1} \quad \text{where } |\Gamma| < 1 \quad (2.171)$$

This is required for finding the correct root and in terms of the s-parameter

$$X = S_{11}^2 - S_{21}^2 + 1 / 2S_{11} \quad (2.172)$$

The transmission coefficient can be written as:

$$T = S_{11} + S_{21} - \Gamma / (1 - (S_{11} + S_{21})\Gamma) \quad (2.173)$$

The permeability is then given as:

$$\mu_r = 1 + \Gamma / \Lambda (1 - \Gamma) \sqrt{1/\lambda_0^2 - 1/\lambda_c^2} \quad (2.174)$$

where λ_0 is the free space wavelength and λ_c is the cutoff wavelength. So then we have,

$$1/\Lambda^2 = (\epsilon_r * \mu_r / \lambda_0^2 - 1/\lambda_c^2) = (1/2\pi L \ln(1/T))^2 \quad (2.175)$$

The permittivity can then be written as:

$$\epsilon_r = \lambda_0^2 / \mu_r [1/\lambda_c^2 - (1/2\pi L - \ln(1/T))^2] \quad (2.176)$$

The last two equations (2.176) and (2.177) have an infinite number of roots since the imaginary part of the term $\ln(1/T)$ is equal to $j(\theta + 2\pi n)$ where $n = 0, \pm 1, \pm 2, \dots$ this is the integer of (L/λ_g) . The permittivity can be calculated from the equations (2.175) and (2.176) which λ avoids determining the n values. However, this is only valid for permittivity measurement if we assume $\mu_r = 1$. This is what we assume in is research [27]. We then have from equation (2.175),

$$1/\Lambda = \mu_r(1 - \Gamma) / (1 + \Gamma) \sqrt{1/\lambda_0^2 - 1/\lambda_c^2} \quad (2.177)$$

By setting this equation (2.179) equal to equation (2.176), the permittivity can be found,

$$1/\Lambda^2 = \mu_r^2(1-\Gamma)^2/(1+\Gamma)^2(1/\lambda_0^2 - 1/\lambda_c^2) = \epsilon_r \mu_r / \lambda_0^2 - 1/\lambda_c^2 \quad (2.178)$$

If we now solve for ϵ_r , which yields [32]

$$\epsilon_r = \mu_r (1-\Gamma)^2/(1+\Gamma)^2(1 - \lambda_0^2/\lambda_c^2) + \lambda_0^2/\lambda_c^2 \quad 1/\mu_r \quad (2.179)$$

CHAPTER 3

SAMPLE PREPARATION

3.1 Sample Preparation

Samples to be used for measurements must be prepared correctly. Test results are only as good as the specimens being tested. Proper preparations of the concrete and clay specimens are essential parts of the testing process. Solid cylindrical samples of the pipe material used in the measurements were machined to the dimensions of the coax waveguide fixtures. The sample must be made to fit correctly into the sample holder. A special drill bit was designed to make the samples that would fit into the sample holder. After the sample was drilled it still needed to be sanded and finished in order for it to fit correctly. One must realize that any scratches, nicks, and cracks may change the measured dielectric properties. So one must try to limit these problems on any sample that is made; also, one should be careful to minimize any unnecessary wear and tear on the sample. The sample length should be measured with precision at laboratory temperatures. The sample should fit as tightly as possible. When working with a tightly fit sample one must be careful not to destroy the sample when putting it into the sample holder. The gaps near the center conductor in the coaxial line are more serious than gaps near the outer conductor. The sample should be kept very clean and stored in a secure place. Finally, keep the gap between the sample and the guide walls to a minimum [15].

3.2 Drill Press

An indispensable tool in the machine shop is a drill press. The modern drill press has been around since the late 1800s. A drill press is preferable to a hand drill when the location and orientation of the hole must be controlled accurately. A drill press is composed of a base that supports a column; the column in turn supports a table. Work can be supported on the table with a vise or hold down clamps, or the table can be swiveled out of the way to allow tall work to be supported directly on the base. The height of the table can be adjusted with a table lift crank than locked in place with a table lock. The column also supports a head containing a motor. The motor turns the spindle at a speed controlled by a variable speed control dial. The spindle holds a drill chuck to hold the cutting tools. The Quill is moved up and down with a lever on the side as shown in the Figure 3-1.

There are four general instructions for operating a drill press.

1. Select the drill diameter that you need for the holes that you will be drilling.
2. Set the depth of the hole by adjusting the plunge depth on the right side of the spindle.
3. Clamp the work piece down securely to the table. Align the drill bit with the mark indicating where to drill the hole or holes in the work piece. Select the motor speed to match both the diameter of the drill and the material you are using.
4. Turn on the press and slowly lower the drill bit into the work piece until the spindle reaches the depth setting. If the setting is very deep in the work piece, back the bit up out of the hole periodically to clear the shavings from the hole. In our research with

concrete, concrete pipe, clay and clay pipe, water was needed for drilling the samples. The initial samples were obtained from coring the original structures (see Figures 3.2-3.8). The initial samples were from Lowe's and the TXI concrete company in Monroe, Louisiana [67][68].



Figure 3-1: Drill press used to cut samples.



Figure 3-2: Cutting with drill press.



Figure 3-3: Drill bit used to cut samples.



Figure 3-4: Samples of clay and concrete.



Figure 3-5: Machine used to sand off sample.



Figure 3-6: Samples placed in freshwater and saltwater.

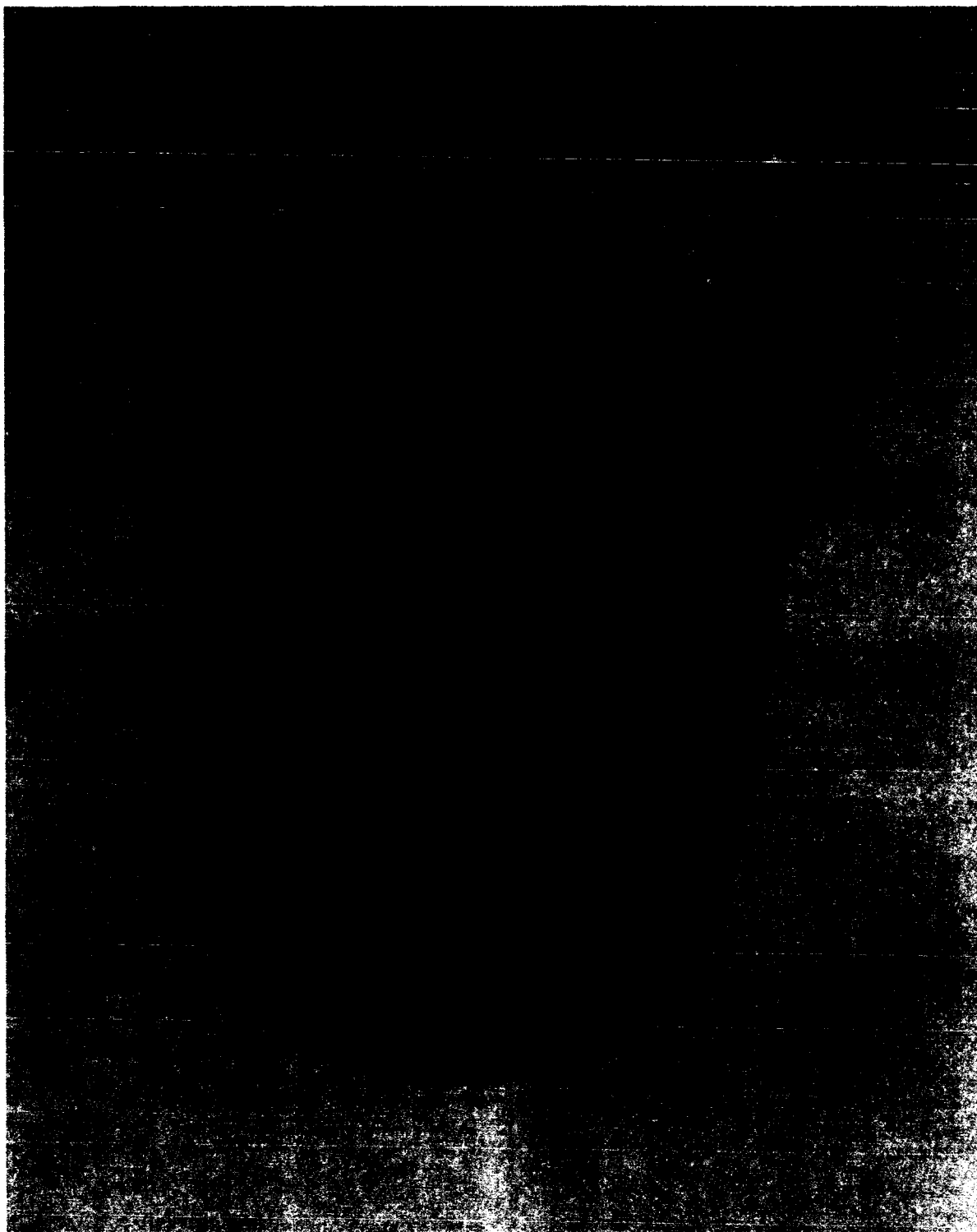


Figure 3-7: PVC sample.



Figure 3-8: Samples of the different materials used in research.

CHAPTER 4

PROPERTIES OF CONCRETE, CONCRETE PIPES, AND CLAY PIPES

Concrete is one of the most universally used construction material. It is among the few building materials produced directly on the job by the user. To know the proper mixture, it is important for the user to be able to identify desirable properties and components. Concrete is a mixture of aggregate and often controlled amounts of air held together by a hardened paste made from cement and water. Although there are other kinds of cement, the word cement, generally means Portland cement. A chemical reaction between the Portland cement and water, not the drying of the mixture, causes concrete to harden to a stonelike condition. This reaction is called hydration [69]. Because hydration, hardens the concrete, freshly placed concrete submerged underwater will harden. Concrete is a substance that can be cast or molded into any size or shape. Upon hydration of the cement by the water, concrete becomes stonelike in strength, durability, and hardness. Portland cement is a mixture of carefully proportioned and specially processed chemical combination of lime, silica, iron oxide, and alumina. Unless tests or experiences indicate that a particular water source is satisfactory, mixing water should be free from acids, alkalis, oils, etc. The basic ratio of water to cement determines the strength of concrete [70]. The less water in the mix, the stronger more durable and watertight the concrete should be. Too much water dilutes

the cement, resulting in weak concrete. Aggregate material (generally sand and stone or gravel) makes up between 60 to 80 percent of normal concrete. Aggregate is often washed when impurities are found that can retard cement hydration. All aggregate is screened to ensure proper size gradation because concrete differs from other cement-aggregate-mixtures in the size of its aggregate [71]. When cement is mixed with coarse aggregate of more than ¼-inch, plus fine aggregate and water, the product is concrete. The chemical and physical properties of the aggregate also affect concrete properties. Aggregate size, shape, and grade influence the amount of water required. Aggregate surface texture influences the bond between the aggregate and the cement paste. In properly mixed concrete, the paste completely engulfs each aggregate particle and fills all spaces between the particles.

The elastic properties of the aggregate influence the elastic properties of the concrete and the paste's resistance to shrinkage. Reactions between the cement paste and the aggregate can either improve or harm the bond between the two, which in turn affects the concrete's quality. All concrete contains some air. If air is chemically induced into the mixture, it is called entrained air. Air that is added to the mixture as a result of the mixing process is called entrapped air. Entrained air adds beneficial qualities to the concrete; however, entrapped air adds nothing to the mixture. Admixtures are substances added to concrete to alter its properties. They usually cause a chemical reaction within the concrete. Admixtures are normally classified into accelerators, retarders, air-entraining agents, water reducers, and pozzolans. Concrete has a great variety of applications because it not only meets structural demands but also lends itself readily to architectural treatment. In buildings, concrete is used for many applications like, foundations,

columns, footings, beams, and wall slabs; in short, concrete is an important building element. Other important concrete applications are in road pavements, airport runways, bridges, dams, irrigation canals, and water-distribution pipelines [14]. A great deal of concrete is used in manufacturing masonry units, such as concrete blocks and concrete bricks. Concrete and cement are among the most important construction materials. In general, concrete is fireproofed, watertight, and comparatively economical, and easy to make. It offers surface continuity and solidity and bond with other materials. Certain limitations of concrete cause cracking and other structural weaknesses that detract from the useful life of concrete structures.

Some of the principal limitations and disadvantages of concrete are: low tensile strength, thermal movements, drying shrinkage and moisture movements, creep, and permeability. The unit of measure for cement is the cubic foot (cf). Fine and coarse aggregate is measured by loose volume, whereas water is measured by the gallon. Concrete is usually referred to by cubic yards (cy). Concrete in a relatively fluid state can be readily molded by hand like a clump of modeling clay. A mix keeps all grains of sand and pieces of gravel or stones encased and held in place. The degree of plasticity influences the quality and character of the finished product. Significant changes in the mix proportions affect plasticity. Desirable properties of fresh concrete are: workability, nonsegregation, and uniformity. Hardened concrete is the end product of any concrete design. The essential properties it must have are strength, durability, and watertightness. Portland cements contain lime and minerals (like limestone, clay, and shale), silica, sand, iron ore, and aluminum [68][72]. These properties are shown in Table 4-1.

Table 4-1: Five types of standard specifications for Portland cement from the American Society For Testing And Materials

Type I. General purpose cement	Type I is used in pavement and sidewalk construction, bridges, sewers, water pipes, etc.	It is more available than the other types. Type I cement will reach its design strength in 28 days.
Type II. This is modified to resist a moderate sulfate attack. It usually generates less heat of hydration and at a slower rate than Type I.	Typical applications are drainage structures, and large structures in which its moderate heat of hydration produces only a slight temperature rise in the concrete.	Temperature rise can be a problem when concrete is placed in warm weather. Type II cement will reach its design strength in 45 days.
Type III. This is a high, early strength cement that produces strengths at an early age, usually seven days or less.	Type III permits fast form removal and, in cold weather construction, reduces the period of protection against low temperatures.	Although richer mixtures of Type I can obtain high early strength, Type III produces it more satisfactorily and more economically.
Type IV. This is a very special cement. It has low heat of hydration intended for applications requiring a minimal rate and amount of heat of hydration.	Type IV is used primarily in large concrete structures, such as gravity dams, where the temperature rise from the heat of hydration could damage the structure.	Type IV cement will reach its design strength in 90 days.
Type V. This concrete is sulfate-resistant.	It is used mainly where concrete is subject to severe sulfate action.	Type V cement will reach its design strength in 60n days.

Concrete proportions for a particular application are determined by the concrete's end use and by anticipated conditions at the time of placement. You must strike a balance between reasonable economy and the requirements for the job. Before proportioning a concrete mixture, one must have certain information about a job, such as the size and shape of structural members, the concrete strength required, and the exposure conditions. The w/c ratio is determined by the strength, durability, and watertightness requirements of the hardened concrete (see Table 4-2). Always remember that a change in the w/c ratio changes the characteristics of the hardened concrete. One can use the following table to

select a suitable w/c ratio for normal-weight concrete that will meet the anticipated exposure conditions [14].

Table 4-2: Maximum w/c ratio for various exposure conditions for concrete

Exposure Conditions	Normal-Weight Concrete, Absolute Water and Cement Ratio by Weight
Concrete protected from exposure to freezing and thawing or application of deicer chemicals	Select w/c on basis of strength, workability, and finishing needs.
Watertight Concrete	
In fresh water	0.50
In seawater	0.45
Frost resistant concrete	
Thin sections; any section with less than two -inch cover over reinforcement and any concrete exposed to deicing salts	0.45
All other structures	0.50
Exposure to sulfates	
Moderate	0.50
Severe	0.45
Placing concrete under water	Not less than 60 lb of cement per cubic yard
Floors on grade	Select w/c ratio for strength, plus minimum cement requirements.

Note that the w/c ratios in Table 4-3 are based on concrete strength under certain exposure conditions. If possible, perform tests using job materials to determine the relationship between the w/c ratio you select and strength of the finished concrete. One can use Table 4-3 as a guide. Enter Table 4-3 at the desired f'_c and read across to determine the maximum w/c ratio. You can estimate the values when both exposure conditions and strength must be considered. One uses the lower of the two indicated w/c ratios. If flexural strength rather than compressive strength is the basis for design, such as pavement, perform tests to determine the relationship between the w/c ratio and flexural strength.

An approximate relationship between flexural and compressive strength is:

$$f'_c = R^2 / K \quad (4.1)$$

where f'_c equals compressive strength in psi, R equals the flexural strength, in psi, and K which equals a constant that is generally between eight and ten [71].

Table 4-3: Maximum permissible w/c ratios for concrete when strength data is need for a specified job

Specified Compressive strength f'_c , in psi	Maximum absolute permissible w/c ratio, by weight	
	Non-air-Entrained Concrete	Air-Entrained Concrete
2500	0.67	0.54
3000	0.58	0.46
3500	0.51	0.40
4000	0.44	0.35
4500	0.38	Use trial batch method
5000	Use trial batch method	Use trial batch method

The proportions that one can arrive at in determining mixtures will vary somewhat on which method one uses. The variation is due to the empirical nature of the methods and does not necessarily imply that one method is better than another. One starts each method by assuming certain needs or requirements and then proceeds to determine the other variables. Since the methods begin differently and use different procedures, the final proportions vary slightly. This is to be expected and points out further the necessity of trial mixtures in determining the final mixture proportions. For variations in a mixture, note that for concrete used in slabs have minimum cement requirements depending upon the maximum size of the aggregates (see Table 4-4) [17][69].

Table 4-4: Minimum cement requirement for concrete that can be used in slabs of flatwork, aggregate size in inches and cement in lb/cy

Maximum Size of Aggregate, in inches	Cement, in lb/cy
1 ½	470
1	520
¾	540
½	590
3/8	610

One should use fine aggregate to fill spaces between coarse-aggregate particles and increase the workability of a mix. In general, aggregate that does not have a large grading gap or an excess of any size that does give a smooth grading curve, produces the best mix. One should use the largest practical size of coarse aggregate in the mix. The maximum size of coarse aggregate that produces concrete of maximum strength for a given cement content depends on the aggregate source as well as aggregate shape and grading. For pavement or floor slabs, the maximum size aggregate should not exceed one-third the slab thickness. One should use entrained air in all concrete exposed to freezing and thawing and, sometimes, under mild exposure conditions to improve workability. Always use entrained air in concrete paving, regardless of climatic conditions. Table 4-5 and Table 4-6 gives recommended total air contents of air-entrained concrete [73].

Table 4-5: Approximate mixing water and air content requirements for different slumps and maximum sizes of aggregate

Water, Pounds per Cubic Yard of Concrete, for indicated Maximum Sizes of Aggregate
Non-Air-Entrained Concrete

Slump, inches	3/8	1/2	3/4	1	1 1/2	2	3	6
1 to 2	350	335	315	300	275	260	240	210
3 to 4	385	365	340	325	300	285	265	230
6 to 7	410	385	360	340	315	300	285	-
Approx. amount of entrapped air	3	2.5	2	1.5	1	0.5	0.3	0.2

Table 4-6: Approximate mixing water and air content requirements for different slumps and maximum sizes of aggregates

Water, Pounds per Cubic Yard of Concrete, for Indicated Maximum Sizes of Aggregate
Air-Entrained Concrete

Slump, inches	3/8	1/2	3/4	1	1 1/2	2	3	6
1 to 2	305	295	280	270	250	240	225	200
3 to 4	340	325	305	295	275	265	250	220
6 to 7	365	345	325	310	290	280	270	-
Recommended average total air content, percent for level of exposure								
Mild exposure	4.5	4.0	3.5	3.0	5.0	2.0	1.5	1.0
Moderate exposure	6.0	5.5	5.0	4.5	4.5	4.0	3.5	3.0
Extreme exposure	7.5	7.0	6.0	6.0	5.5	5.0	4.5	4.0

The slump test measures the workability and consistency of concrete. Do not use it to compare mixes having completely different proportions or mixes containing different aggregate sizes. When testing different batches of the same mixture, change in slump indicate changes in materials, mix proportions, or water content. Table 4-7 shows the recommended slumps for various types of construction [14][70].

Table 4-7: Recommended slumps for various types of construction

Concrete Construction	Slump in	Maximum	Minimum
Reinforced foundation, walls, and footings	3		1
Plain footings, caissons, and substructure walls	3		1
Beams and reinforced walls	4		1
Building columns	4		1
Pavements and slabs	3		1
Mass concrete	2		1

With the w/c amounts determined, add sand, and gravel to yield a workable mix. Record the data and repeat the procedure until the concrete has desirable characteristics and a minimum cement content is obtained [74].

To summarize our discussion of concrete, we can see that concrete is everywhere. One just needs to take a moment and think about all the concrete structures that you have encountered today (see Figures 4.1-4.7). All of these concrete structures are created from a mixture of cement and water with added aggregate. It is important to distinguish between cement and concrete as they are not the same. Cement is made by combining a mixture of limestone and clay.



Figure 4-1: Concrete pipe.



Figure 4-2: Concrete building.

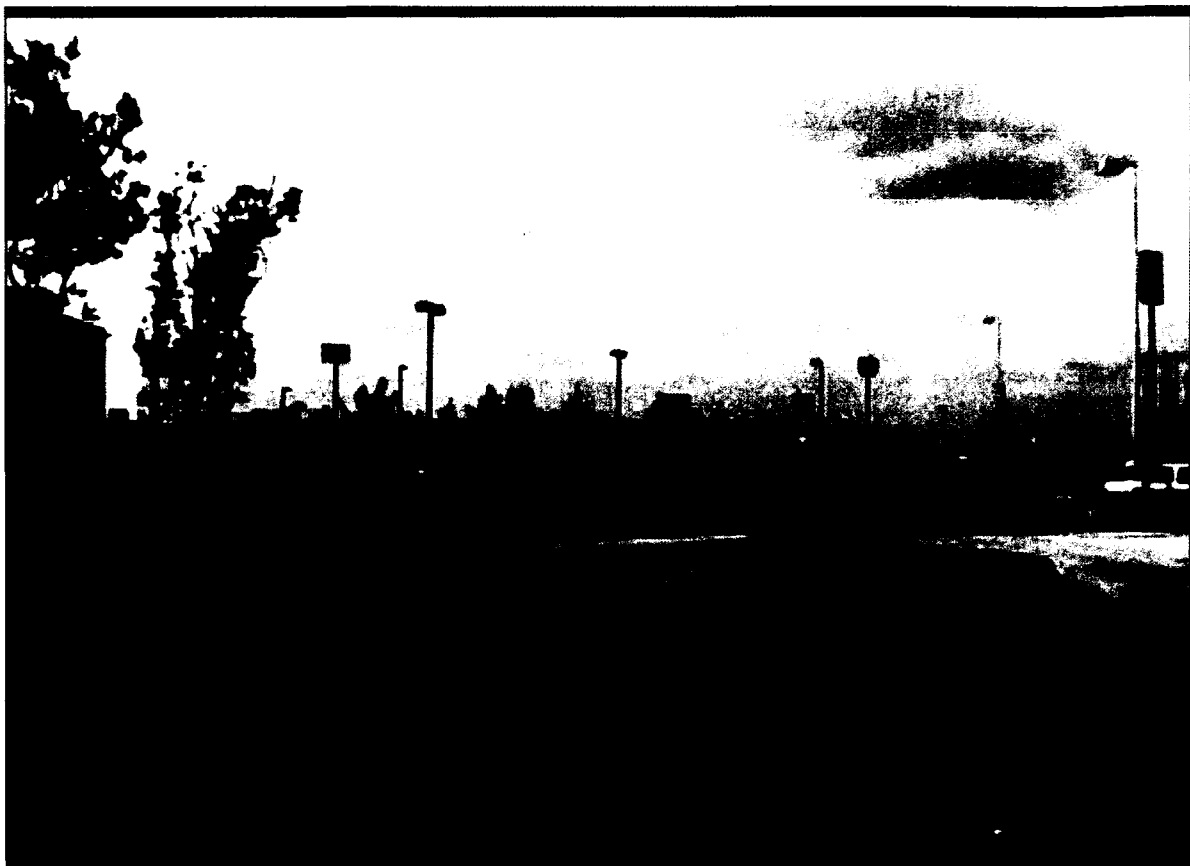


Figure 4-3 Concrete pavement.

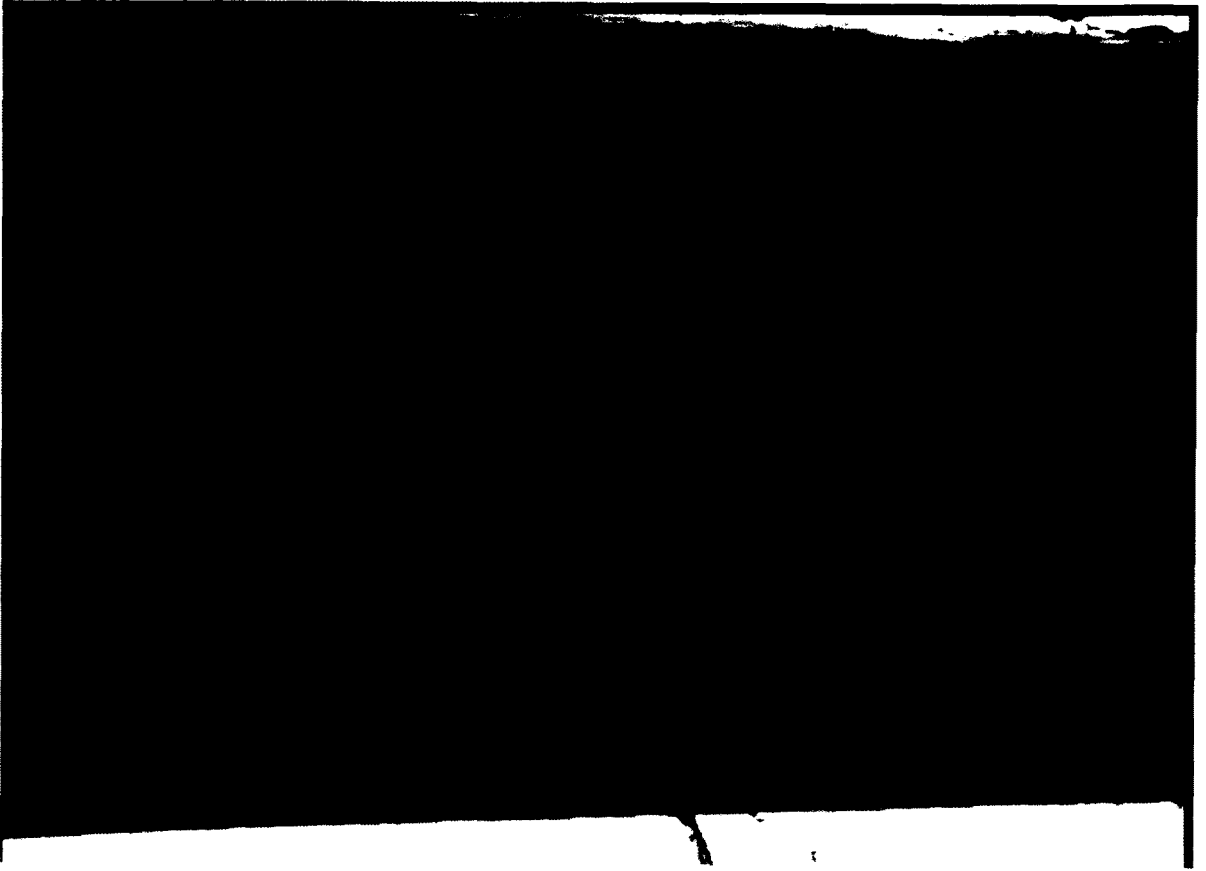


Figure 4-4: Concrete wall.



Figure 4-5: Concrete sidewalk.

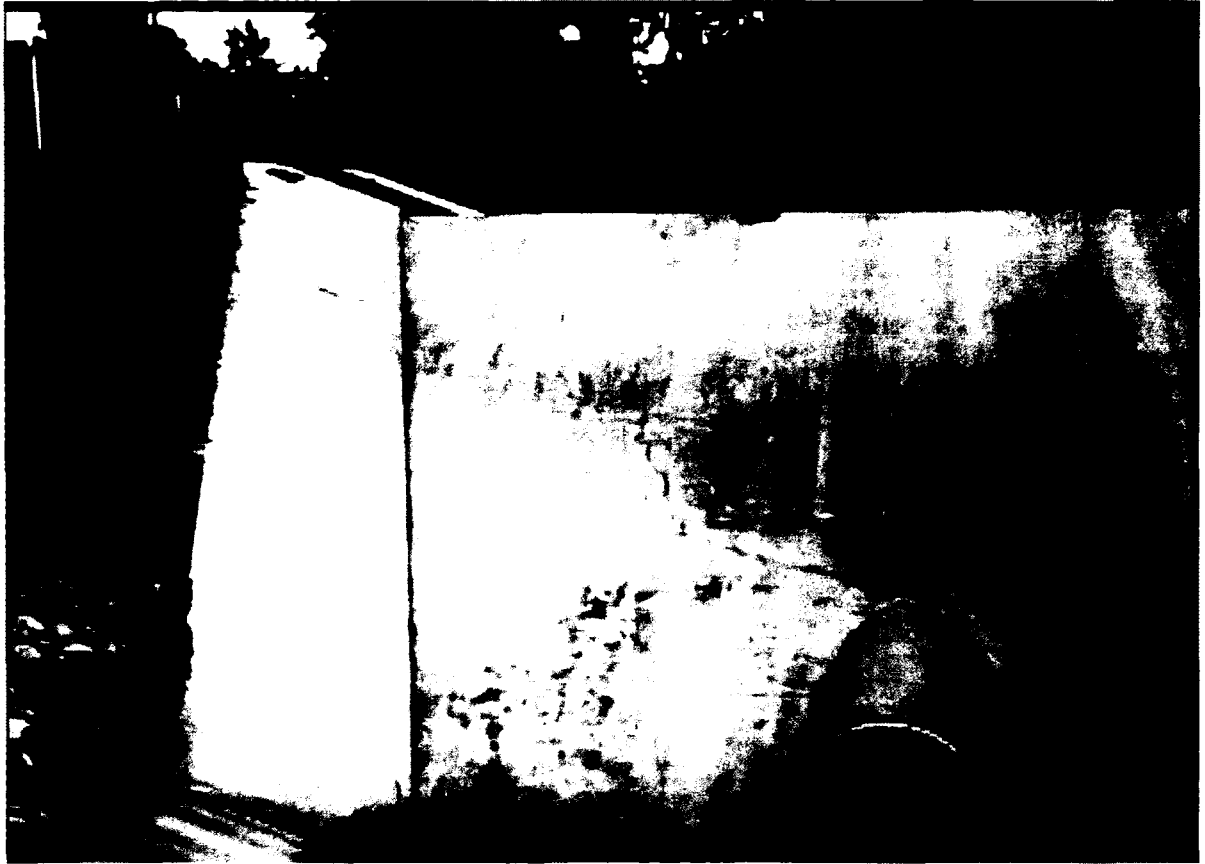


Figure 4-6: Concrete spillway.



Figure 4-7: Concrete bridge.

The product is an intimate mixture of compounds collectively called clinker. This clinker is finely ground into a powder form. The raw materials used to make cement are compounds containing some of the earth's most abundant elements, such as calcium, silicon, aluminum, oxygen, and iron. Water is a key reactant in cement hydration. The incorporation of water into a substance is known as hydration. Water and cement initially form a cement paste that begins to react and harden. This paste binds the aggregate particles through the chemical process of hydration. In the hydration of cement chemical changes occur slowly, eventually creating new crystalline products. The properties of this hardened cement paste, called binder, control the properties of the concrete. It is the inclusion of water into the product that causes concrete to set, stiffen, and become hard.

Once set, concrete continues to harden and become stronger for a long period of time, often up to several years. The strength of the concrete is related to the water to cement mass ratio and the curing conditions. A high water to cement mass ratio yields a low strength concrete. This is due to the increase in porosity, which is, created with the hydration process. Most concrete is made with water to cement mass ratio ranging from 0.35 to 0.6. Aggregate is the solid particles that are bound together by cement paste to create concrete. Aggregates can be fine, such as sand, or coarse, such as gravel. The relative amounts of each type and size of each type of aggregate determines the physical properties of the concrete. Sometimes other materials are incorporated into the batch of concrete to create specific characteristics. These additives are called admixtures. Admixtures are used to alter the fluidity of the cement paste, increase or decrease the setting time, increasing strength, or to extend the life of a structure. The making of concrete is a very complex process involving both chemical and physical changes [14].

4.1 Concrete Pipes

Concrete pipes are a precast product made in a factory setting. These products benefit from tight quality controls which are achieved at a production plant. Precast concrete pipes are produced in a highly controlled plant environment under rigid production standards and testing specifications. Concrete pipes come in a wide range of diameters, lengths, and with varying strengths. They have a proven track record and are custom designed for user's applications including draining, sewage, water supply, and irrigation.

There are five general types of concrete pipes which included: concrete culvert pipes, concrete stormwater pipes, concrete sewage pipes, concrete pressure pipes, and

concrete irrigation pipes. Precast concrete pipe are the strongest pipe available. It can be designed and plant tested to resist any load required. Unlike flexible pipe, it has minimal reliance on installation to support loads; it relies mostly on its inherent brute strength manufactured into the pipe. That adds up to a tremendous difference in the design, the installation and long-term success of a project. Compressive strengths for concrete pipe normally range from 4,000 psi to 8,000 psi; although, concrete pipe can be made beyond these standards. It is a function of other factors including, aggregates, and cement materials, the manufacturing process, curing process and mix design. Most concrete design strengths refer to a 28 day compressive strengths. It is not uncommon for 28 day tests to substantially exceed the specified design strengths.

Concrete pipe strength is standardized by ASTM C76 and AASHTO M170. Pipe is strength-tested in the plant using D-Load standards. Supporting strength of a pipe is determined under three-edge-bearing test conditions. Expressed in pounds per linear foot per foot of inside diameter, D-load tests the concrete pipe under severe loading conditions where there is no bedding, and no lateral support, under three-point loads [17][68]. The ASTM C76 (standard for four classes of reinforced concrete pipe) is:

- . Class I, II, III, IV, V
- . Class III: 1,350 lb/ft/ft
- . Class IV: 2,000 lb/ft/ft
- . Class V: 3,000 lb/ft/ft
- . Gasketed joints are tested to 13 psi

The ASTM C14 (non reinforced concrete pipe) standard is:

- . Class 1, 2, 3

. D/load expressed in lb/linear foot (to compare to reinforced divide by diameter)

Next we have the design loading used for determining concrete pipe strength for installations underneath traveled roadways. The AASHTO HS20 (standard for vehicle loads on pipes) is:

- . 16,000 lbs Axle Load
- . 10" x 20" Tire Footprint
- . 0 – 30% Impact load
- . Distributed 1.75H

Wire reinforcement in concrete pipe adds significantly to its inherent strength.

Wire reinforcement shaped as cages is a precision-fabricated mesh fabricated by automatic cage welding machines. The cage machines fabricate machine formed bells, are dimensionally stable, and have close engineered tolerances [69]. Reinforced concrete pipes have higher load capacities. Reinforced concrete pipe is a composite structure and specially designed to use the best features of both concrete and reinforcement. The concrete is designed for compressive force and the reinforcement for the tensile force. Unless the concrete cracks, the reinforcement is not being used to its design capacity. As more tensile forces are carried by the reinforcement, hairline cracks become visible, but these occur at loads well below the design loading of the reinforced member. Hairline cracks are not an indication of danger, distress, or loss of structural integrity.

Concrete pipe is generally designed to carry loads well within the engineered load bearing capacity of a pipeline, and hairline cracks do not occur. If hairline cracks do occur, they tend to seal themselves through a process called autogenous healing. Autogenous healing is the ability of concrete to repair itself in the presence of moisture.

Reinforced concrete pipe, unlike reinforced concrete beams and slabs, are buried where moisture conditions are present for autogenous healing to take place. Another important problem with concrete pipe is durability. With concrete pipe, durability deals with the life expectancy and enduring characteristics of its materials. The capability of pipe to perform as expected for the design life of a project is a fundamental engineering consideration, especially in today's economic environment, where requirements have been set in place to ensure a sustainable buried infrastructure. The design life of concrete pipes is generally between 70-100 years, and in many cases it will surpass those numbers. This means the expectation for precast concrete's functional life is at least twice as long as other materials. The reasons for this go far beyond concrete's innate strength.

Concrete also won't burn, rust, tear, buckle, deflect, and it is immune to the attack of most elements. It does not depend on whether the concrete pipe is buried or exposed. Quality concrete pipe densities typically range from 145-155 pounds per cubic foot. Usually the higher the density of the concrete pipe, then one can expect the greater the durability of the concrete pipe [16].

Technology is now in place for making concrete pipe more reliable than it has ever been before. Decades of research and development of many aspects of concrete pipe has enabled concrete pipe producers to change mixes, pipe design, and improve manufacturing processes to provide products that can withstand a complete range of underground environments. The dependability of concrete pipe is not just a matter of how a product performs on its own. It also has a lot to do with how well it is understood by the people who plan, design, construct, and install concrete pipe. In this important area, no

material is better understood and more commonly used in the field than concrete pipe [17]. This adds up to fewer mistakes and a greater level of confidence.

Concrete pipe is a rigid pipe that provides both structure and conduit when it arrives on site. Concrete pipe is a rigid pipe system that is over 85% dependent on the pipe strength and only 15% dependent on the strength derived from the soil envelope. The inherent strength of concrete pipe compensates for construction shortcomings and higher fill heights and trench depths. Flexible pipe is at least 95% dependent on soil support and the installation expertise of the contractor. Backfill must be properly engineered and applied to provide structure. Imported fill is usually required for flexible pipe systems. Concrete pipe is less susceptible to damage during construction, and maintains its shape, by not deflecting as does flexible pipe. As a rigid pipe, concrete pipe has high beam strength and can be pushed to proper grade. Only concrete pipe can bridge over uneven bedding without affecting the pipe hydraulics. Flexible pipe has a low beam strength stiffness and deflects with uneven bedding, thereby inducing strain along the pipe axis.

Deflection testing of flexible pipe is critical to measure the strain and any circumferential deflection. Allowable deflection of flexible pipe is 3% initial and 5% long term. Deflection testing should not end, or be taken when backfilling has been completed. Installation problems that may be associated with flexible pipe are deflection, deformation or buckling, wall strain, and buckling. Unlike thermoplastic conduits, concrete pipe will not burn. This is important for the planning of roads and highway cross drains in both urban and remote locations.

Concrete pipe is a good choice for construction site safety, public safety, and homeland security. Also, thermoplastic conduits are sensitive to extremes in temperatures that may cause joint separation, impact on wall stiffness, and strains on the corrugations of some thermoplastic products. Comparing the initial hard cost of materials is only the first step in seeing where the greatest value lies. There is an array of costs that arise after the initial purchase that can profoundly affect a project's bottom line. Concrete costs less than plastic or metal pipe to install, inspect and test. It also provides lower ongoing maintenance costs, and reduces risk of failure, early replacement or liability to the public. Concrete is one of the most widely used construction materials in existence. In virtually every major market, there is a local manufacturer that produces concrete pipe from local suppliers [16]. A least cost analysis is an effective method of evaluating two alternative materials with different service lives or economic equivalence.

The factors which affect the traditional analysis are project design life, material life, first cost, interest rate, inflation rate, replacement costs, and residual value. First cost is important to the engineer and owner, but does not reveal the entire cost of the pipeline. Least cost analysis should also consider costs to the replacement of potential catastrophic failures. Flexible pipe products may have lower initial costs, but they are not as cost effective as concrete pipe. Over the long term, flexible pipe has a shorter service life. In general, the true cost of flexible pipe can be twice that of concrete based on a 50-year or greater service life. Concrete pipe far out performs plastic or metal.

Concrete's rigidity and mass allow for easy and secure placement in a ditch, without disrupting line or grade. Also, precast concrete pipe joints are easily assembled, which helps minimize the time needed for installation. When installation time matters, or

when the soil poses challenges to installation, precast concrete pipe is quite simply the best choice. Concrete pipe has an unlimited range of pipe strengths from which to choose, and strength is demonstrated prior to installation. By choosing concrete pipe:

- 1) The designer has more control over pipe strength
- 2) There is less reliance on quality installation by the installer
- 3) There is lower embedment material cost and less compaction is required
- 4) It is easier to maintain grade and alignment and no excess deflection concerns
- 5) There is a lower life cycle cost of a project and lower maintenance costs
- 6) There is a reduced likelihood of failure and reduced overall liability to the public

A standard installation is used for precast concrete pipe beddings. Design of the pipe wall is based on the stresses and strains in the pipe [17]. This approach is more precise and can result in pipes that require less material. In addition, the standard installations approach permits greater choice of backfill materials, and needs less compaction of the backfill. Standard installations were adopted by the American Society of Civil Engineers in 1996. Standards installations provide several benefits when using concrete pipe [75][76].

- 1) Provides flexibility to meet design requirements and site conditions
- 2) Allows for narrower excavation limits and less expensive backfill material
- 3) Can reduce the level of compaction
- 4) Increases contractor productivity

There is a choice of types of standard installations that provide versatility to adapt to field conditions.

- 1) First Type: Highest quality installation using select granular soils with high compaction requirements for bedding.
- 2) Second Type: Allows silty granular soils less compaction required for bedding.
- 3) Third Type: Allows use of soils with less stringent compaction requirements for bedding.
- 4) Fourth Type: Allows use of onsite native material for bedding with no compaction required.

Some projects have design elements that are more complex than others. Precast concrete pipe provides solutions for these projects, whether they are open-cut, deep burials, tunnels, trenchless, shallow burials, or with vertical structures. Concrete pipe design is simple to do. Precast concrete pipe gives you strength and flexibility to ensure the success of your most demanding applications [76]. Pipes are made with a variety of sizes, shapes, joints, and seal options. There is also an array of linings and coatings that can handle the most aggressive environment. The main attributes of concrete pipe apply to sanitary, storm sewers and culverts.

Concrete pipes are used for storm drainage, roadway culverts, tunnels, and bridges. Concrete pipe accommodate great volumes of effluent in a tiny footprint. Concrete pipe offers a variety of joints from soil-tight to pressure. They are not affected by the type of backfill used for the installation. Joint performance must be demonstrated in the plant prior to pipe installation, and joint integrity can be field tested in a variety of ways. With concrete pipe, deflection will not compromise field joint test capability. The cross sectional rigidity of concrete pipe makes joint assembly a simple operation. Rigid

joint integrity will minimize the likelihood of embedment intrusion and subsidence of overfill. Types of concrete pipe joints are:

- 1) O-Ring Gaskets
- 2) Profile Gaskets
- 3) Mortar and Mastic Joints

O-Ring gaskets are used on all sanitary and some storm RCP where leak resistant joints are needed. These gaskets may be used in joints for low-head pressure applications. Profile gaskets are used on stormwater culverts and RCP storm and sanitary sewers. Mortar or mastic joints are used for storm sewers, culverts, and horizontal elliptical reinforced concrete pipe. Concrete pipe works very well in marshy environments. In these environments, the buoyancy of buried pipelines depends on the mass of the pipe material. Also, the buoyancy of buried pipe depends on the weight of the volume of water displaced by the pipe, the weight of the liquid load carried by the pipe, and the weight of the backfill material. Whenever the water table level is above the invert of the pipeline, the potential for floatation or buoyancy exists. Although the trench for a pipe installation in a marshy area is dewatered, the trench area downstream may become saturated. This can lead to a buoyancy effect on the pipe.

The mass of the concrete pipe generally counteracts this buoyancy force. The mass of the concrete pipe allows for: effective compaction of embedment and backfill, prevention of movement during backfilling, unlikely movement of structure following installation, reduces floatation, and reduces future damage [17]. The key to long term performance and efficiency lies in a materials ability to retain its original shape and alignment. Precast concrete pipes rigidity and mass allow it to greatly outperform flexible

pipe systems. For this reason, the hydraulic efficiency is greatly improved. The hydraulic capacity of all types of pipe depends on the smoothness of the interior pipe wall. The smoother the wall, the greater is the hydraulic capacity of the pipe. Smoothness of pipe is represented by Manning's roughness coefficient commonly called Manning's n . The lower the Manning's n value, the greater is the volume of water that will flow through the pipe.

Hydraulic analysis for drainage systems involves the estimation of the design flow rate based on watershed characteristics. The hydraulic design of a drainage system always includes an economic overview. A wide spectrum of flood flows with associated probabilities will occur at the site during its entire life. The benefits of constructing a large capacity system to accommodate all of these storm events with no detrimental flooding effects are normally outweighed by the initial construction costs. An economic analysis of the tradeoffs is performed with varying degrees of effort and overview. Risk analysis balances the drainage system cost with the damages associated with inadequate performance. There is no risk, when concrete pipe are used, because they have long service, and handle the requirements of a system's hydraulic design. Two basic values are often discussed when talking about the coefficient of roughness of a pipe. These two values are laboratory test values and design values. The difference between laboratory test values of Manning's " n " and accepted design values is significant. Manning's " n " values were obtained using clean water, smooth joints, no loads, and straight pipe lengths without bends, manholes, debris, or other obstructions. The laboratory results indicate only the differences between smooth wall and rough wall pipes. Rough wall pipe's " n " values are approximately 2.5 to three times those of smooth wall pipe. Smooth wall pipes

were found to have “n” values ranging between 0.009 and 0.010. Generally, engineers using concrete pipe and sewers have used 0.012 or 0.013 [17]. This design factor of 20 to 30 percent takes into account the differences between laboratory testing and actual installed conditions of various sizes as well as allowing for a factor of safety.

Research has concluded that designs using concrete pipe can be downsized by at least one size in most cases when compared to steel, aluminum, and lined corrugated HDPE pipe. It is critically important that the applied Manning’s “n” values are design values and not laboratory values. Using design values, concrete pipe has superior hydraulic characteristics, and engineers understand and possess proper verification of concrete pipe hydraulics. Batching and mixing operations in the industry’s premier plants have been upgraded over the past ten years. Characteristics of this operation of the pipe production process includes: computer controlled weighing and mixing systems, automated recording systems, and absorption testing. The American Concrete Pipe Association offers an ongoing quality assurance program so that pipes meet the standard required for each project. Historically, concrete is the most durable and sustainable material for major construction. It continues to function long after a projects life is reached. Precast concrete pipe’s staying power has another benefit; it’s not a passing fad.

When concrete pipe is specified, the projects you build today are more likely to be compatible with any future expansions or alterations. Precast concrete drainage products have a reputation for strength and durability. They will not burn, corrode prematurely, deflect or move off grade to reduce hydraulic performance, or collapse under loads designed into the pipe structure. Concrete is the world’s most commonly used building material, precast concrete infrastructure is quickly integrated into ecosystems. Today,

concrete is being recognized as a green material. Concrete pipe is suitable for many projects and fits sustainable development. Unlike plastic pipe, concrete is produced with natural materials. Manufacturing of concrete consumes less energy than plastic fabrication. It's also recyclable and has little if any environmental impact. The rigid nature of concrete pipe makes it ideal for removal and replacement.

The benefit of salvaging concrete pipe does not stop on the construction site. There are projects where concrete pipe has been excavated in industrial areas after decades of use, cleaned and reinstalled to continue performing as storm sewer pipe [16]. These pipes have been tested in laboratories, and it has been found to be stronger than when it was first tested. It is clear that concrete gets stronger over time. Concrete is a dielectric, nonmagnetic material. Dielectric materials are usually made up of atoms whose valence electron shells are nearly full, resulting in low conductivity. Using a coaxial transmission line, a particular material's dielectric properties can be tested as amounts of certain substances within it are varied. For concrete, there have been studies to ascertain the effects of different admixtures, the type of aggregate, water content, and curing time on dielectric properties. In general, the real part of the dielectric constant is larger when it is easier for the material to polarize, meaning that the ions are mobile and there is little crystallization [74].

The addition of chlorides increases the dielectric constant, as does the amount of water. The dielectric constant decreases over curing time, because the amount of water decreases during this time. Also, the dielectric constant of concrete is dependent on the constant of its aggregate: mixes containing limestone have a higher constant than those containing granite, this correlates with the fact that limestone itself has a higher constant

than granite does. There are certain concrete properties that influence the performance of concrete pipes. These properties include concrete compressive strength, density, absorption, water cement ratio, cement content and type, and aggregates. All of these factors would have an influence on the dielectric properties of concrete pipes. For example, the dielectric constant for concrete with coarse aggregates is higher than concrete with fine aggregates.

Compressive strengths for concrete pipes normally range from 4000 psi to 6000 psi [14]. Concrete strength is a function of many factors including, aggregates, cement material, manufacturing, curing process, and mix design. These factors must also play a role in the dielectric constant of concrete pipes, since concrete pipes strength is a function of these same factors. Concrete pipe design strengths refer to 28 days concrete strengths, but in actuality, the design strengths are obtained much earlier than 28 days. Quality concrete pipe densities typically range from 145-155 pounds per cubic foot. In general, the higher the density of concrete pipe, the greater the durability of the concrete, which leads us to believe that the dielectric constant could be affected by, changes in density.

Absorption is primarily used to check the density of the concrete. As with compressive strength, the absorption can be greatly influenced by the aggregates and the manufacturing process that is used for each concrete pipe. For example, ASTM C 76 specifies a maximum allowable absorption of 8.5% or 9%, for concrete pipe. Low water-cement (W/C) ratios are one of the trademarks of quality concrete pipe. Typical precast concrete pipe have W/C ratios that range from 0.33 to 0.45, with 0.53 being the maximum allowed by ASTM C 76. The cement content has always been a topic of

concern with concrete pipe. The key to proper cement content is proper design of the mix, with consideration of all material properties, manufacturing, and curing processes [17].

Materials used to manufacture concrete pipe consist of aggregates and manufactured products, such as Portland cement and reinforcing steel. Each of the components has a standard specifying its properties and methods of testing. Portland cement is a closely controlled chemical combination of calcium, silicon, aluminum, iron, and small amounts of other compounds. Gypsum, which regulates the setting time of the concrete, is added during the final process of grinding. In general, Portland cements may be composed of four principal compounds: tricalcium silicate, dicalcium silicate, tricalcium aluminate, and tetracalcium aluminoferrite. Portland cements are produced to meet CAN/CSA A-5 and classified into five types. This standard sets limits for chemical composition, fineness of grind, setting time, strength at certain ages, resistance to chemical attack, and rate of development of heat of hydration. Type-10 cement is general purpose cement suitable for all uses where the special properties of the other types are not required. Type-20 cement has a lower heat of hydration than Type-10, improved resistance to sulphate attack, and is intended for use in structures of considerable size [68]. Type-30 cement is used where high early strengths are desired, such as when forms need to be removed as soon as possible, or when the concrete must be placed in service as quickly as possible. Type-40 cement is used where the amount and rate of heat generated must be kept to a minimum. Type-50 cement is special cement intended for use in structures exposed to severe sulphate action.

The basic materials for concrete pipe then are, portland cement, fine aggregate, coarse aggregate, water, and, in some cases reinforcement. These are combined in a systematic manner, using quantities and proportions specially designed for each product [20]. Calculating the dielectric constant of a multi-phased heterogeneous composite like concrete is a challenging task. Chemical admixtures are also used in practice as a processing addition to aid in manufacturing and handling of concrete or as a functional addition to modify the properties of concrete. In our research, because of the difficulties in making our samples, we do not consider the problems of chemical admixtures or the microscopic structure in calculating the dielectric constant of clay, clay pipe, concrete, and concrete pipe [73][76].

4.2 Clay Pipes

The design of early sewers was a major problem because there were no standard sizes, strengths, quality tests or installation. In 1903, the ASTM started a committee to recommend standard specifications and tests for clay sewer pipes. Standard C 12 and many technical standards that followed covered all aspects of in-plant quality control testing, installation, jointing, bearing strength, chemical resistance and field acceptance testing. Many of these standards were industry firsts in sewer pipe field and represented major advances in wastewater transmission over the ensuing years. Piping materials are generally placed in one of two classifications: rigid or flexible.

Clay pipes are generally considered examples of a rigid pipe. Vitrified clay pipes are produced from the raw materials like clay, grog (chamotte) and water. Clay pipe is manufactured from clays and shales which are chemically inert. In the manufacturing process, various clays and shales are pulverized, screened, and placed in storage bins.

Blended materials are carried to the pugmill and mixed and moistened with water for a proper mix consistency for extrusion. The mix is then forced through a die into a vacuum chamber where trapped air is removed. This mixture is then machine-extruded in the form of a pipe. This fresh extruded pipe contains about 18 percent water and is called greenware. Greenware is placed in drying rooms to reduce the moisture content to about three percent.

The pipe is then taken to the kilns and preheated to approximately 110°C to drive off the remaining moisture. The pipe travels slowly through the kiln, reaching even higher temperatures where vitrification takes place. During vitrification the clay fuses into a very hard, chemically stable compound. Vitrified clay is very corrosion and abrasion resistant. Because of its inherent low strength, vitrified clay pipe is used for nonpressure applications. It is brittle and subject to impact damage; therefore, special care in handling is a requirement. Clay pipe is generally available in sizes ranging from four to 36 inches in diameter. However, it may be available in some locations in diameters up to 42 inches. The strength is determined by the three-edge bearing test, varies with diameter, and ranges from 2000 to 7000 lb/ft. This vitrified clay has exceptional properties in respect to chemical resistance, mechanical strength, impermeability, and hardness (See Table 4-8).

Table 4-8: Standards for clay pipe

ASTM C 700	Clay pipe, vitrified, and standard strength
ASTM C 425	Compression joints for vitrified clay pipe and fittings
ASTM C 301	Clay pipe, test methods
ASTM C 12	Installing vitrified clay pipe lines
ASTM C 828	Low-pressure air test of vitrified clay pipe lines

Highly developed manufacturing and preparation techniques have made it possible to upgrade an already proven product. Vitrified clay pipes are designed for sewers operating on gravity in municipal and industrial applications. Clay pipes are resistant to chemical attack in a pH-range from 0-14. They are also resistance to corrosion. The formation of H₂S in sewage is a consequence of the natural biological decomposition of sulphur containing organic and inorganic matter. H₂S mainly forms under anaerobic conditions by sulphate reducing bacteria in the slime of a matured sewer and to a lesser extent by bacteriological processes in the sewage. In gravity sewers the formation of H₂S commences after the oxygen originally present in the sewage has been consumed by manifold biological process. This is followed by the anaerobic decomposition with an ever increasing formation of H₂S which slowly escapes into the sewer atmosphere. Turbulence in the sewage stream increases the escape of the gaseous H₂S. The formation of H₂S is supported by long sewage flows, low flow velocities and high sewage temperatures.

Concrete pipes which contain limestone as the aggregate the effects of biological H₂S corrosion show later than on those having quart aggregate. Vitrified clay pipes are not affected by sulphuric acid, like concrete pipes. The mechanical resistance of vitrified clay pipes has developed greatly during the last decades. Vitrified clay pipes have the

same mechanical strength as reinforced concrete pipes from the series 135. The vitrified clay pipes have a life cycle of up to 100 years, even in the hardest conditions.

Furthermore, vitrified clay is the only material that resists regular rinsing and unclogging by means of high water pressure techniques. This means that vitrified clay pipe canals can be used over a longer period and that maintenance and replacement costs are lower than other types of pipes.

Clay pipes have high abrasion resistance. Vitrified clay materials are resistant to all types of chemicals over the entire wall thickness. The resistance of the vitrified clay materials and seals is tested using chemicals, including sulphuric acid at pH 0 and NaOH at pH 14. Clay pipes have a low heat expansion coefficient. In case of sudden temperature changes, it can be necessary to take protective measures. Most of the time because the clay pipes are underground, this is not a problem. The raw materials for manufacturing vitrified clay pipes are clay and recycled materials. Mining of the raw materials and subsequent restoration of a natural environment take place in an environmentally friendly way. Furthermore, the environmental impact of manufacturing of vitrified clay is relatively small compared with most other types of sewer materials. The long service life of vitrified clay pipe is an additional decisive factor in its use in sewers. Finally, no polluting products are created at the end of the life cycle of clay pipes. In situations where greater wall thickness is needed we can use a vitrified clay jacking pipe.

Vitrified clay jacking pipes have greater wall thickness than corresponding standard clay sewer pipes. That results in higher crown pressure ratings and higher resistance to ground and traffic loads. Strength in the length direction is the most

important factor for jacking pipes, because they must withstand the high jacking forces necessary to overcome the resistance of the cutting face and the external pipe surface. The longitudinal compressive strength of the surfaces that transfer the force between pipe sections must be at least 75 N/mm^2 . That is higher than values stated for other types of current jacking material. It allows very high jacking forces to be used. The glazed outer surface of the pipe strongly reduces friction between the pipe and surrounding soil. After being properly installed, clay pipes require very little maintenance. As vitrified clay scores very high with respect to all the requirements that must be imposed on sewer pipes, vitrified clay pipes attain very long and maintenance free lives. Clay is a naturally occurring material. It typically forms due to the weathering of feldspar:

Potash feldspar + water + carbon dioxide \Rightarrow kaolinite + quartz + potassium carbonate.

One of the major clay minerals is kaolinite. This is hydrous silicate of alumina, and some people use this formula for all clays. However, other clays minerals exist (nacrite, vermiculite, montmorillonite-smectite, illite, and chlorite). There are approximately 30 different types of clays, but most natural clays are mixtures of these different types, along with other weathered minerals. Clay may be classified as primary, colluvial, or secondary, depending on where it is located and how it got there. Primary clay is found at its origin, it tends to be white when it is fired. Colluvial clay is clay that has been naturally transported a short distance from its point of formation. Secondary clay is clay that has been naturally transported a great distance from its point of formation; this clay has many impurities, but is the most abundant.

Clay pipes are a mixture of different clay minerals, which makes it a multi-phased heterogeneous material. Dielectric constant is a measure of the polarizability of a

material. Polarization is the spatial separation of charges due to an applied electric field. The mechanisms that cause polarization depend on the frequency of the applied electric field and the composition of the material. Single phase, homogeneous materials experience only high frequency polarization mechanisms: electronic, ionic, and molecular [8].

Multi-phase heterogeneous materials experience these polarization mechanisms, as well as low frequency polarizations: interfacial spatial, bound water, and double layer. These property makes calculating the dielectric constant a difficult task. Daniels, 1996, reports that dry clay dielectric constant should be between two-six, and wet clay range between 15-40. These numbers can give us a guide, but with the different clay types we cannot be totally sure. Olhoeft, 1989, reports that kaolinite has a dielectric constant of 11.8 and quartz a dielectric constant of 4.5, but because clay pipe contain both quartz and kaolinite we need to consider the mixture when the dielectric constant is calculated. If a particular clay pipe contains more kaolinite than quartz we might be looking at a higher dielectric constant, than if the clay pipe contains more quartz than kaolinite. The raw materials of a vitrified clay pipe also include approximately 10 to 15 percent water. Water has a high dielectric constant, which must be considered. Free water has a higher dielectric constant than bound water.

Water has a high dielectric constant because water is a polar molecule which is free to rotate along the direction of an applied electric field, allowing alignment of the water molecules electric dipoles. Bound water has a lower dielectric constant than free water contained in the pore spaces, because its water molecules are absorbed to the surfaces of particles and the dipoles are immobilized. So if we want to calculate the

dielectric properties of clay pipes we need to account for the contributions to the dielectric constant from both bound and free water. So calculating the dielectric properties of clay pipes is complex, and there are many influencing factors.

CHAPTER 5

MEASUREMENT TECHNIQUES

Non-reinforced Concrete is a dielectric, nonmagnetic material. Dielectric materials are in general, made up of atoms whose valence electron shells that are nearly full, which results in low conductivity. In this kind of materials a dipole can be induced so that charge can be stored. Dielectric materials have complex permittivity, which describes the ability of the material to store energy, and this then describes the way in which the material interacts with electromagnetic waves [64]. The real part of the relative complex permittivity, which is the complex permittivity divided by the permittivity in free space, is known as the dielectric constant. This dielectric constant measures how much energy is stored in a material when applied from an external electric field. The imaginary part is known as the loss factor, and it measures how much energy is dissipated when applied from an external electric field [38]. Then by using these two values, the loss tangent, which is the ratio of energy lost to energy stored in a material, can be calculated [42]. The dielectric properties of materials have been tested at length in many studies using coaxial transmission lines. These transmission lines vary in design detail, but generally, they consist of two concentric, nonmagnetic conductors. The space between them is usually filled with an insulator, and electric fields are confined here, as is the sample, which is usually placed in the center of the tube.

To collect data, an impulse (VNA wave is sinusoidal) is sent into the sample. It propagates through the transmission line; and when it comes in contact with the sample, some amount of reflection will occur, depending on the materials dielectric properties. Then, the incident and reflected waves can be used to measure the permittivity of the sample. Signals are often received in the time domain, but they can be converted to the frequency domain using Fast Fourier Transform. Before use in experimentation, the coaxial transmission line is calibrated using materials whose dielectric constants are known, or can be calculated from expressions that have been developed [9]. Using this coaxial transmission line, a particular material's dielectric properties can be tested as amounts of certain substances within it are varied. For concrete, there have been studies to show the effects of different mixtures, the type of aggregate, water content, and curing time on dielectric properties.

In general, the real part of the dielectric constant is larger when it is easier for the material to polarize, meaning that the ions are mobile and there is little crystallization. In the findings of Pokkuluri and many other studies, the addition of chlorides increase the dielectric constant, as does the amount of free water. The dielectric constant decreases over the curing time, which we would expect because the amount of free water decreases during that time. Also, the dielectric constant of concrete is dependent on the constant of its aggregate. Concrete mixes that contain limestone have a higher constant than those containing granite, which should be correct because limestone itself has a higher constant than granite does [69].

In this paper the research shows the dielectric properties of concrete, concrete pipe, clay, and clay pipe that were measured using a two port coax and waveguide

measurement using a computer that was running Microsoft windows. We connected the two port device to the Vector Network Analyzer and the computer as seen in Figure 5-2.

One can also use a one port device as shown in Figure 5-1.

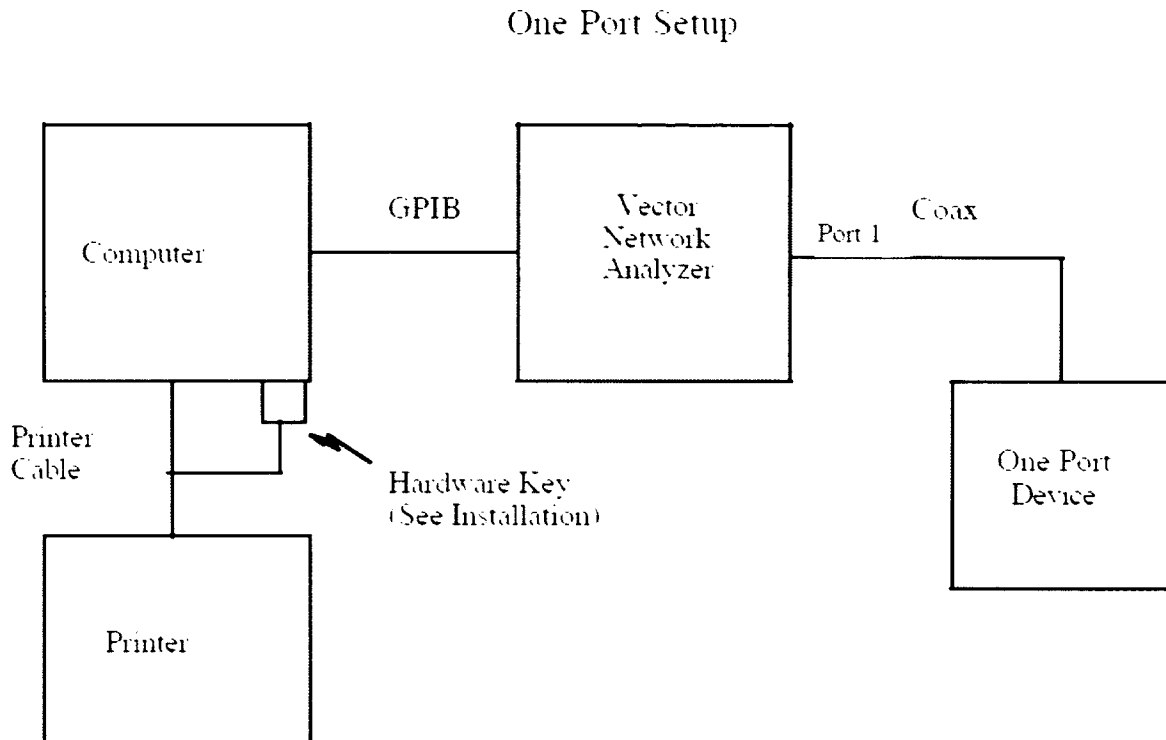


Figure 5-1: System connections one port.

Two Port Setup

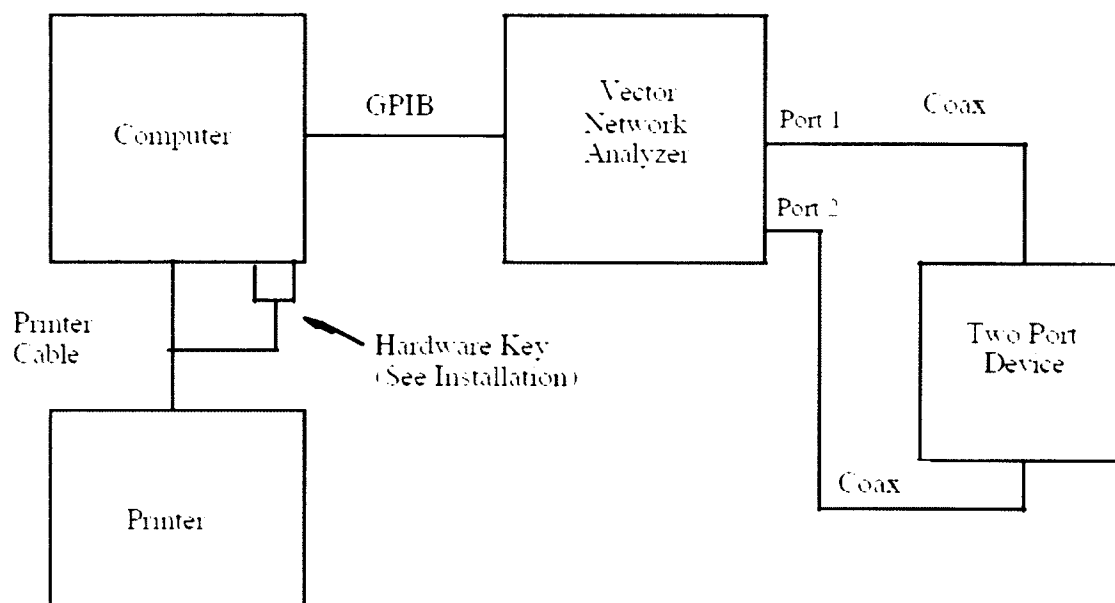


Figure 5-2: System connections two port.

The first step in making a measurement is to perform a calibration of the vector network analyzer. This was done from the MU-EPSLNTM program by selecting the appropriate calibration procedure. In general, TRL/LRL offers the best calibration followed by a SOLT (Short, Open, Load, Thru). One must realize that SOLT can only be done in coax. Simpler calibrations using just a short or thru may be more practical. One can decide what is needed in each situation. Two cables should be used to connect the fixture to the vector network analyzer. Adaptors can be used to connect the cables to the fixtures. Follow the instructions displayed on the computer screen. If the TRL/LRL calibration is used, the sample holder or a through standard is used as the through delay in the calibration and the two adaptor sections are clamped together for the zero length through. Once the calibration is complete it can be stored for later use. Solid samples

need to be machined to the dimensions of the coax fixtures. Then the samples may be slipped over the center conductor and placed anywhere along the conductor; however placement at the ends should be avoided. A tight fit on the center conductor is required for good measurements.

Slight over sizing of the sample gives good contact to the outer conductor [67]. Over sizing also helps provide good contact to the waveguide sample holders. Sometimes, however, this over sizing can lead to the braking apart of the sample itself. Depending on the sample that is used care must be taking not to destroy the sample. Samples must be measured precisely, before taking the measurement. After that, you are ready to start taking data on the sample. The vector network analyzer calibration is initiated by pressing the analyzer button on the main window dialog box and then selecting calibrate. Selecting the analyzer button in the main menu and then “next measurement” button initiates the measurement sequence. No measurement can be performed until a valid network analyzer calibration can be completed. In order to begin a measurement the user must choose raw measurement, measure reference data, or divide by reference.

The raw measurement makes a corrected S-parameter measurement according to the calibration method used without any other modification. A reference data measurement makes corrected S-parameter measurements to be used later as a reference. This allows for full S-parameter measurements to be made and immediately divided by a selected reference data set. When the measurement is complete, the user is prompted to enter a title of one or more lines to describe the measurements. Dielectric samples, where $\mu = 1$, are best proceeded with Epps from transmission reduction. The plot menu then

allows the user to select one of five data categories to plot: reference, measurement, time domain, permeability, or permittivity. Plot selection of measurement data allows one S-parameter or all four S-parameters, depending on the measurement, one can then choose between magnitude, real & imaginary or rectangular plot. The resistivity, capacitance, or inductance thin sheet approximations, which are computed from the measurement data, may also be plotted on a rectangular grid. The plot menu allows the user to select one of four categories to list: measurement data, permeability data, permittivity data, and conductivity data.

Within each category, the user may select any number of data sets present from measurement or reduction (see Figures 5-3 to 5-11). One port measurements can be done with two port coaxial and Free Space Setups. First, the standard two port TRL/LRL calibration should be done. Then a short circuit should be attached to one end of the empty sample holder or at a suitable location in a free space setup. The unused port can be left open and ignored [19]. The measurement of the short circuit must be stored as a reference. Although all four S-parameters are measured, only the S-parameter corresponding to the short circuit should be stored as a reference. Next the sample is placed in the sample holder. The sample must be placed against the short for a short circuit measurement. For an open circuit coax measurement the short is used to determine the sample position, but the short is removed before the measurement begins.

After the measurement is complete the appropriate S-parameter is divided by the corresponding reference. One needs to understand that the open circuit has no free space equivalent. This data can be stored on the disk and used in the calculations. The division step must not be performed for the reduction where $\mu = 1 - j0$. Keep in mind that the

reference must have been measured and stored for the reduction to work well. Also, the sample does not have to be placed at the short circuit or open circuit end, any termination can be used as long as it is identical to the termination stored in the reference. The sample offset is measured from the TRL/LRL calibration plane [9][34][66][22].

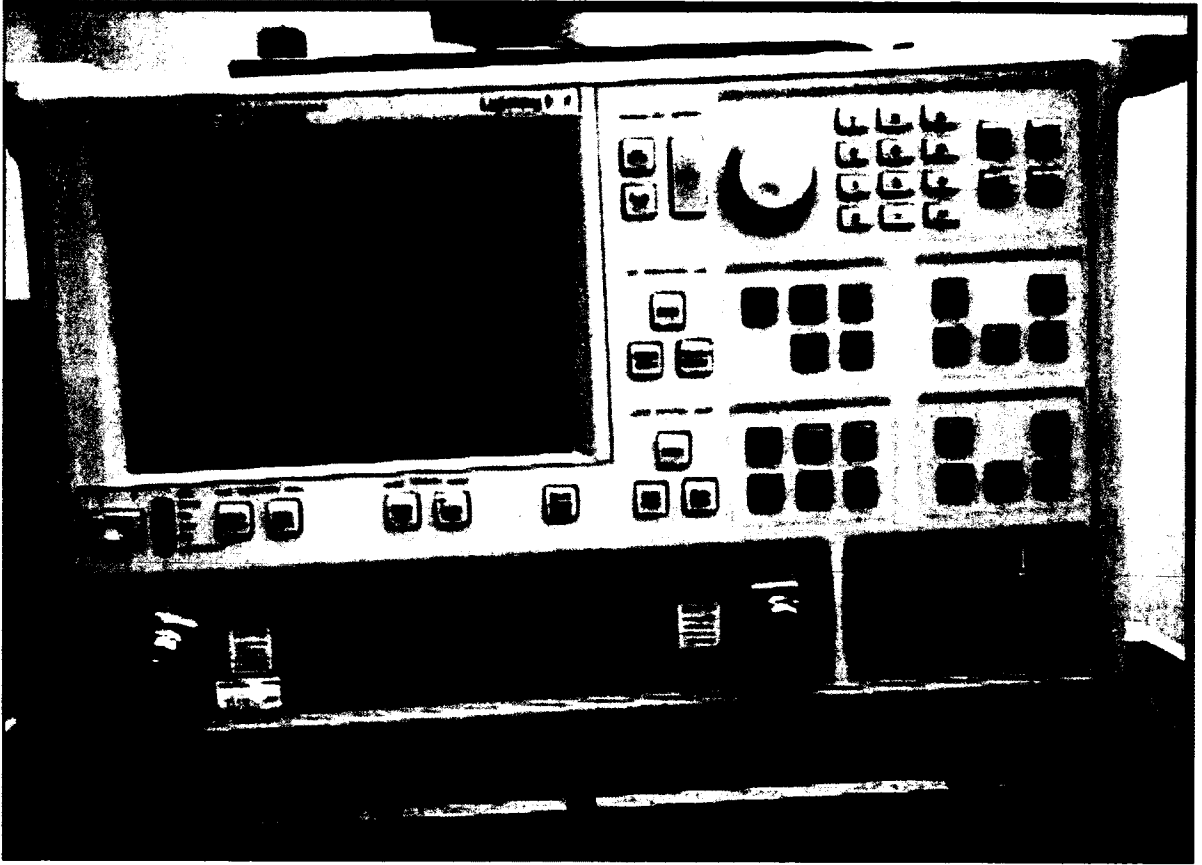


Figure 5-3: Vector network analyzer.

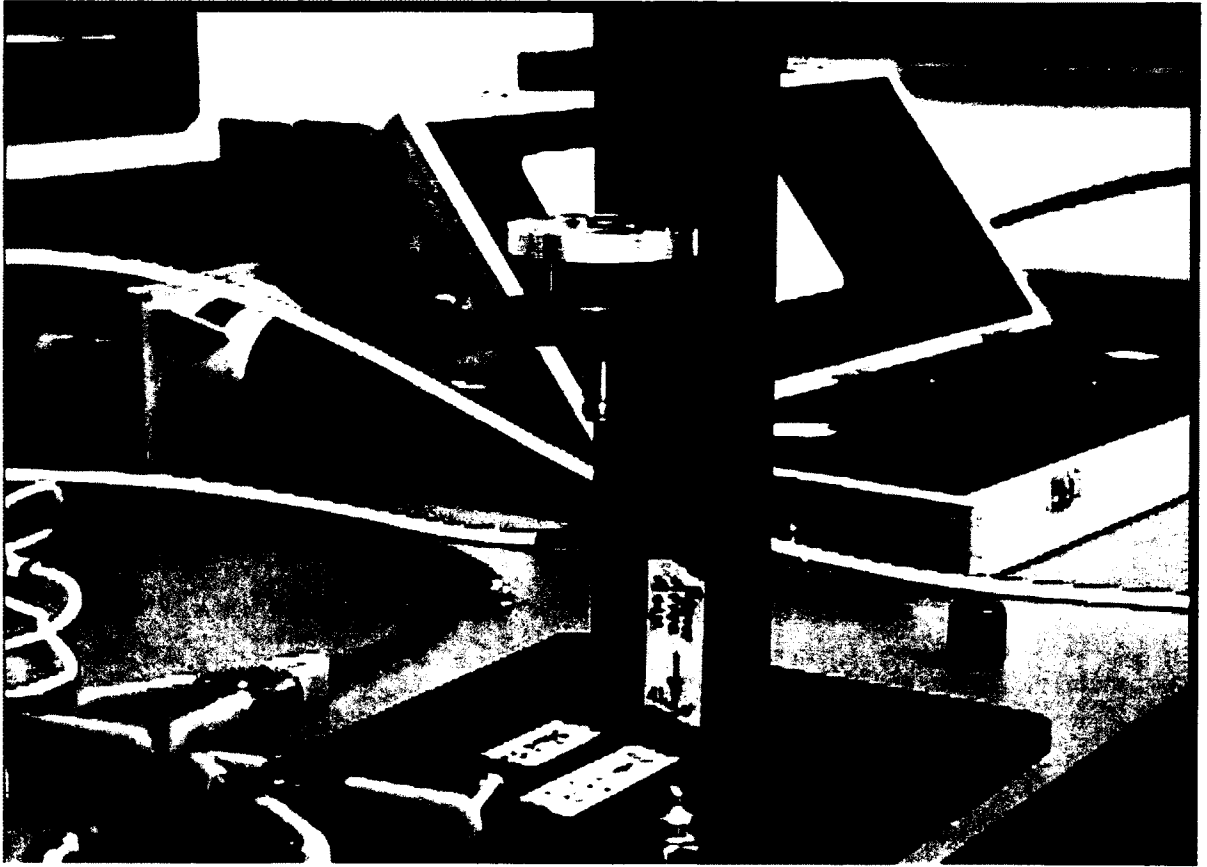


Figure 5-4: Sample holder.

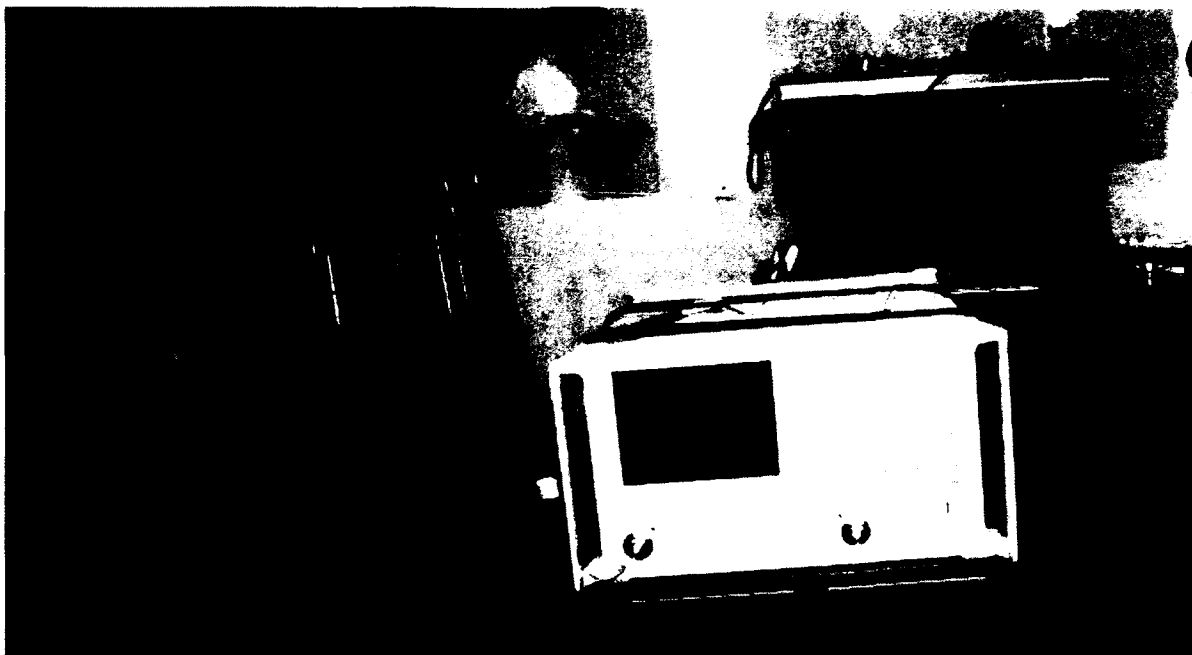


Figure 5-5: Look at VNA and oscilloscope.



Figure 5-6: Sample holders and some samples.

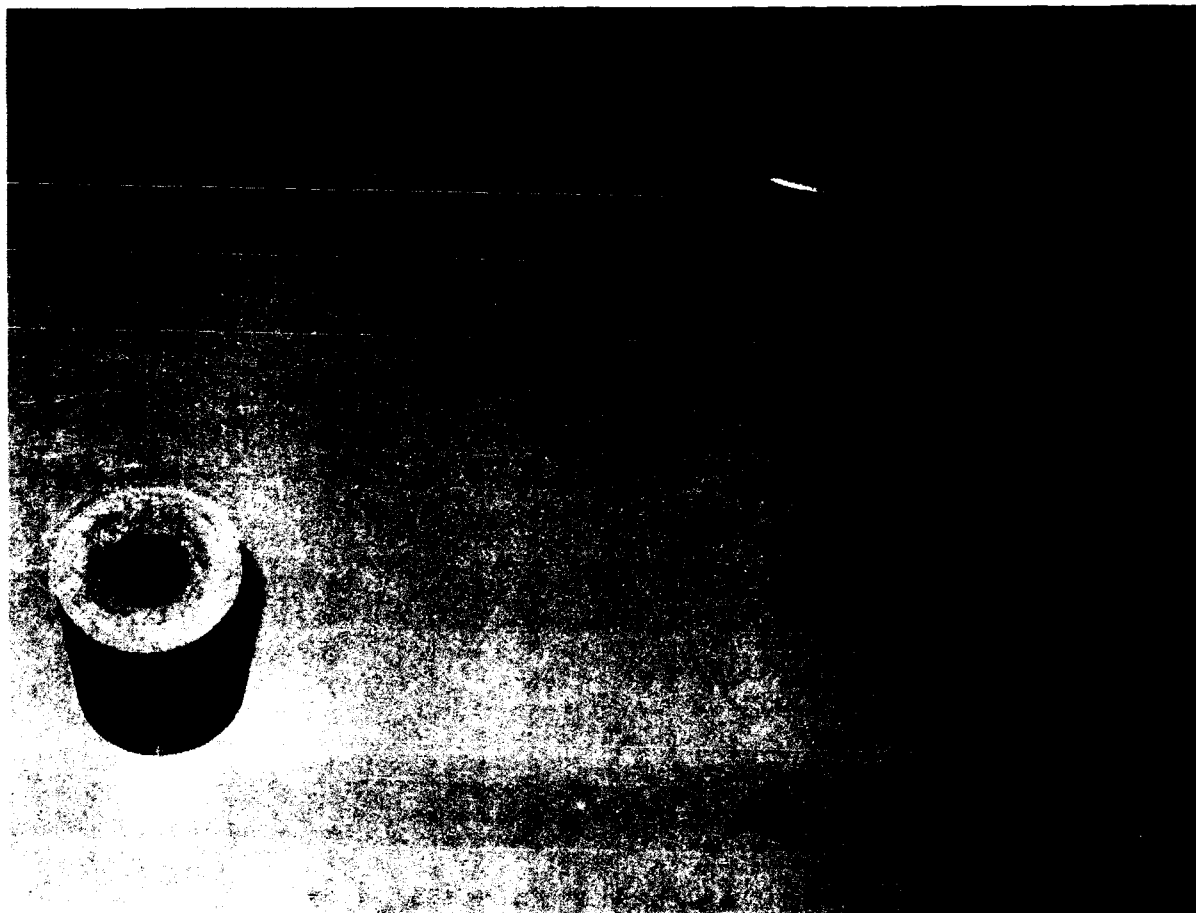


Figure 5-7: PVC sample with computer.

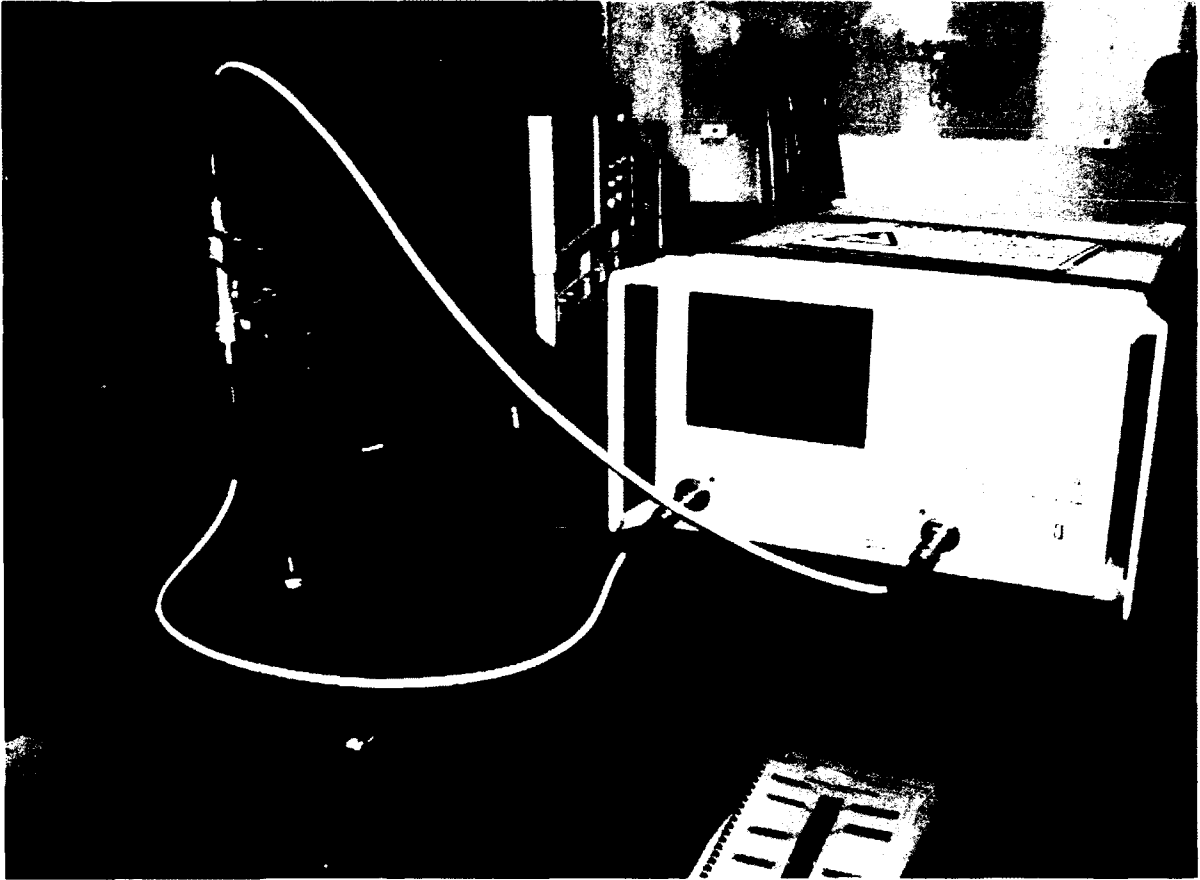


Figure 5-8: All three components: computer, vna, and holder ready to take data.

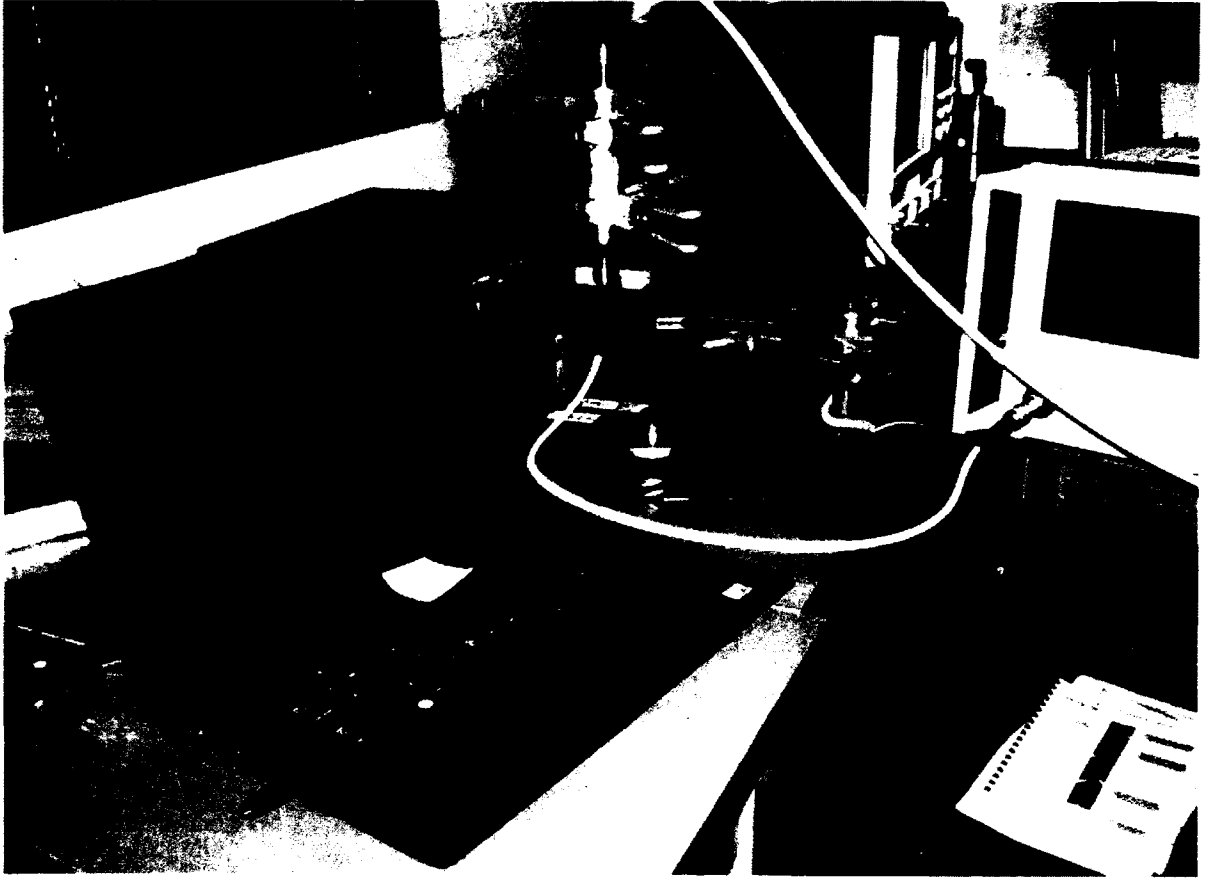


Figure 5-9: Equipment and computer needed for data collecting.

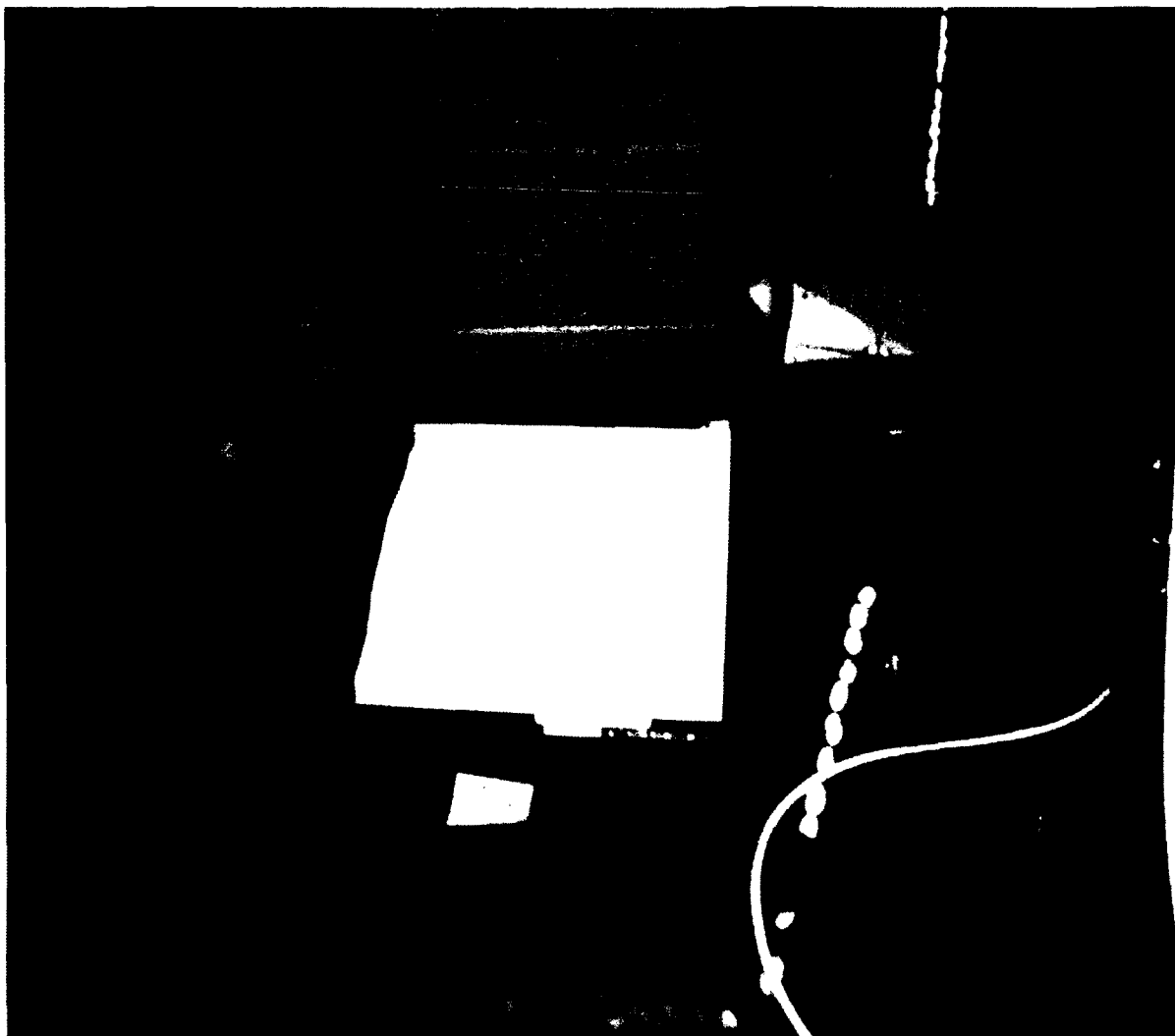


Figure 5-10: Computer graphing.

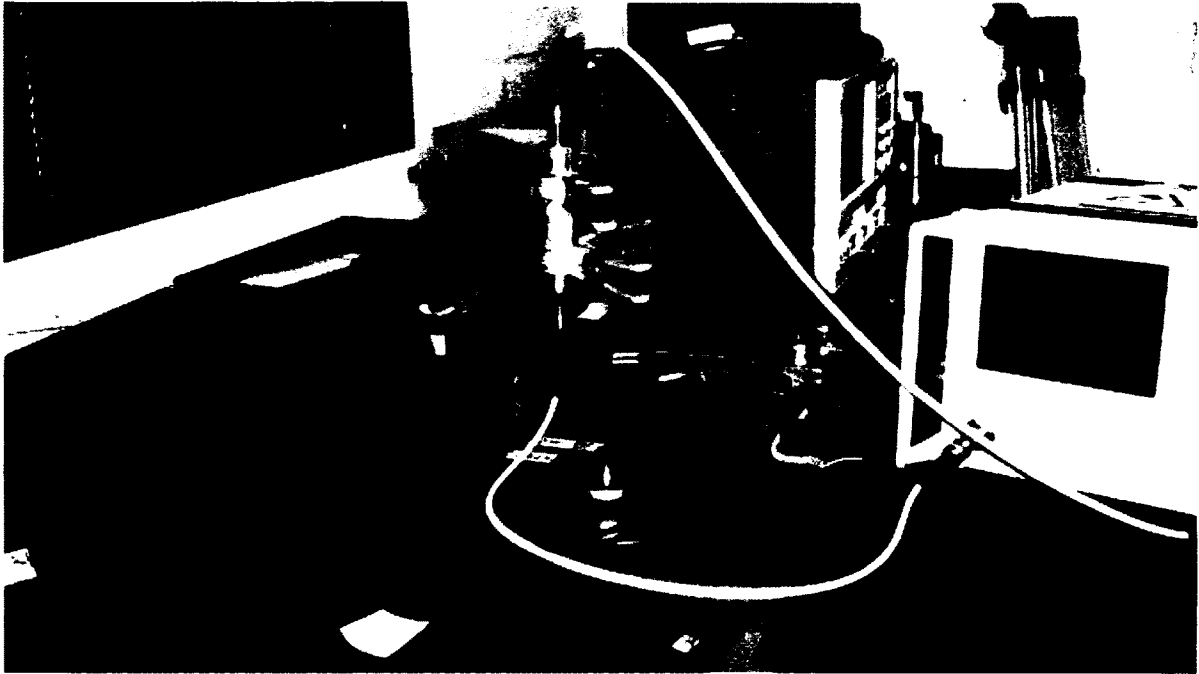


Figure 5-11: Starting data collection process.

5.1 Fundamentals of a Vector Network Analyzer

Vector network analyzers are powerful instruments that provide unparalleled accuracy. Vector network analyzers have many applications, and are particularly useful in measuring linear characteristics of radio frequency components and devices. Because a vector network analyzer is a closed stimulus response system, you can measure radio frequency characteristics with precision. You can also use a VNA in more specific applications, such as signal integrity → materials measurement. Also, a VNA can measure device magnitude, phase, and impedance. Network is a frequently used term that has many modern-day definitions. With respect to a VNA, a network is a group of interconnected electrical components. One function that a VNA performs is to quantify the impedance mismatch between two radio frequency components to maximize power efficiency and signal integrity.

Each time a radio frequency signal leaves one component and enters another, portions of the signal are reflected and transmitted. For example, let us consider light from a source that directs an incident signal at a lens. The lens is analogous to an electrical network [10]. As light hits the lens, depending on the lens' properties, some of the light is reflected back at the source, and some is transmitted through. Conservation of energy requires that the sum of the reflected and transmitted signal equals the source or incident signal. One can ignore any loss due to heat, which will be very small. We can define a reflection coefficient (Γ), a vector quantity with both magnitude and phase, as the ratio of light reflected to the total incident light. Similarly, the transmission coefficient (T) is the vector ratio of transmitted light to the incident light. These two values are shown in Figure 5-12.

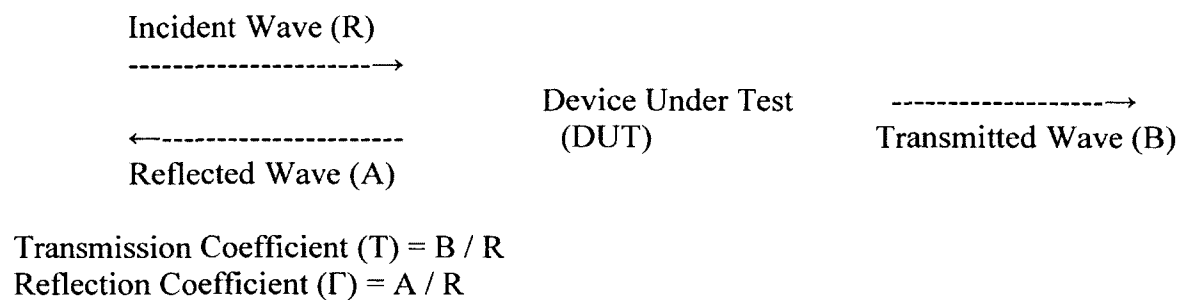


Figure 5-12: Transmission (T) and reflection (Γ) coefficients.

By using the ratio of reflected or transmitted light to the incident light, you gain insight into the performance of the device under test (DUT). If we think back on the light analogy, if the DUT were a mirror, you would want high reflectivity. If the DUT were a camera lens, you would want it to be highly transmissive [25]. Sunglasses may have both reflection and transmissive properties. Similar practical measurements can be made in

electrical networks. A VNA generates a sine wave signal, typically across a range of frequencies. The DUT responds with the incident signal being transmitted through the DUT and reflected back from it. The amount of transmitted and reflected signal usually changes with frequency. The response of the DUT to the incident signal is a result of the DUT properties, as well as any discontinuities in the characteristic impedance of the system. For instance, a bandpass filter is highly reflective out of band, but highly transmissive in band. If the DUT is slightly off the characteristic impedance resulting in an impedance mismatch, the DUT could generate additional unwanted responses. The goal is to develop a measurement methodology that accurately measures the DUT response while minimizing or eliminating uncertainties [13] [33][77].

5.2 Vector Network Analyzer Measurements

Reflection coefficient (Γ) and transmission coefficient (T) are the ratio of reflected signal divided by the incident signal or transmitted signal divided by the incident signal, respectively. Modern VNA expands on this idea with scattering parameters, or S-parameters. S-parameters are complex vector quantities that represent the ratio of two radio frequency signals. S-parameters have a magnitude and phase, or in Cartesian form, real and imaginary terms. S-parameters are expressed as S_{xy} where X represents the DUT output port being measured and Y denotes the DUT input port stimulated by the incident radio frequency signal. S_{11} is defined as the ratio of the energy reflected at port one to the incident signal placed on port one. S_{21} is defined as the ratio of the energy transmitted through the DUT present at port two to the incident signal placed on port one [77].

Both of these quantities, S_{11} and S_{21} , are referred to as forward S-parameters because the incident signal originates from the radio frequency source on port one. With the incident source on port two, S_{22} becomes the ratio of the energy reflected by port two, divided by the incident source energy at port two. Then S_{12} is the ratio of the energy transmitted through the DUT present at port one to the incident signal placed on port two. These are the reverse S-parameters. You can expand this concept with multiport or N-port S-parameters. The total number of S-parameters required to fully describe the radio frequency characteristics of a device is given by the number of device ports squared. S-parameters that describe transmission, such as S_{21} , are analogous to other familiar terms including gain, insertion loss, or attenuation. S-parameters that describe reflection, such as S_{11} , correspond to voltage standing wave ratio, return loss, or reflection coefficient. S-parameters also have other advantages. They are widely used in modern radio frequency measurements.

They are easily translated into H, Z, or other parameters. You can use S-parameters for multiple devices to produce a composite result. Also, of even greater importance, S-parameters are ratios. As a result, you do not need to precisely set the incident source power to some absolute value. Any offset in the input is reflected in the DUT response and canceled out when the ratio of the incident and transmitted or reflected signals is calculated [12][77].

5.3 Network Analyzer Architectures

Network analyzers are available as both vector and scalar instruments. Scalar instruments were popular in the past because of their simplicity and lower cost. Vector network analyzers offer better error correction and more complex measurement capability. With new advances in technology, vector network analyzers are a signal source, which produces the incident signal, which is either swept or stepped in frequency. Also, one can adjust the power level when it is needed for each application. This source feeds into the DUT input via the signal separation section, also known as a test set. At this stage, the reflected and transmitted signals are separated into components. For each frequency point the processor measures the individual signals, and computes the parameter value. User calibration provides error correction that is applied to the data. Finally, when you interactively use a vector network analyzer, you can view these corrected values on a display, which shows the parameters and offers other functionality, such as scaling. Test sets are designed as either transmission/reflection or full S-parameter. T/R architecture includes a stable source that supplies a sine wave signal at a given frequency and power.

A reference receiver, R, connected with a power divider, measures incident signal magnitude and phase [77]. The incident signal exists the network analyzer via port one and enters the DUT input. The receiver directional coupler measures any signal reflected back to port one. With their functions being similar, you can use either directional couplers, or resistive bridges to separate signals, based on performance, frequency range, and cost requirements. The signal transmitted through the DUT enters vector network analyzer port two, where the B receiver measures signal magnitude and phase. Receivers

have different architectures, depending on the desired characteristics. They can be thought of as narrowband receivers with a down converter, IF bandwidth filter, and vector detector. They produce real and imaginary signal components from which magnitude and phase can be derived. In addition, all receivers share the same phase reference with the source, allowing one to measure their phase with respect to the source incident signal. The fundamental network analyzer architectures are mostly implemented in the test set where signal separation occurs. Once the analyzer measures both magnitude and phase for the incident signal and transmitted or reflected signals, it computes the four S-parameter values [77][78].

R = reference receiver
A and B are receivers

$$\text{Forward Return Loss} = S_{11} = \frac{A}{R_f} \quad (5.1)$$

$$\text{Forward Insertion Loss} = S_{21} = \frac{B}{R_f} \quad (5.2)$$

$$\text{Reverse Return Loss} = S_{22} = \frac{B}{R_r} \quad (5.3)$$

$$\text{Reverse Insertion Loss} = S_{12} = \frac{A}{R_r} \quad (5.4)$$

In selecting the proper vector network analyzer architecture, one should consider the application, performance, required accuracy, and cost among other factors.

Understanding the sources of uncertainty in a vector network analyzer helps one develop a sound user calibration approach. The first uncertainty is the transmitted and reflected signal loss across frequency [28]. Next is the difference between the DUT input impedance and the network analyzer or system impedance. The same concept applies to the DUT output impedance. These are the source match and load match, respectively. The efficiency of the directional couplers used for signal separation also requires

consideration [77]. An ideal directional coupler produces an output signal in the coupled arm that is proportional to the measured signal traveling in one direction of the main arm.

A directional coupler should produce no output for a signal traveling in the opposite direction. However, this generally is not the case. Although very small, a signal traveling in the opposite direction through a real-world coupler produces an unwanted response at the coupler output. This unwanted signal is defined as the coupler leakage. The final problem for one to consider is isolation. A small amount of incident signal is radiated from port one and is detected at the port-two receiver. In vector network analyzers, this unwanted leakage is usually small. It does not impact the measurement unless the DUT has high loss. Accounting for isolation during calibration is optional, but recommended, in vector network analyzers. The sources of uncertainty in the forward direction of a two-port vector network analyzer include transmission and reflection tracing; load and source match; and isolation. If one combines the forward direction and the reverse direction there are a total of 12 error terms [79].

5.3.1 Calibration

RF instrument calibration involves periodically returning an instrument to a certified calibration laboratory to ensure it is operating within manufacturer specifications. The laboratory traces the instrument performance back to a standard body, like the National Institute of Standards and Technology. Vector network analyzers are no exception. They too require periodic calibration in order to achieve high accuracy. The calibration must also be performed frequently so that standards are being kept. This is accomplished with a set of calibration standards from a vector network analyzer

calibration kit. By comparing known values, stored in the vector network analyzer, against measured values of the calibration standards, a set of correction factors is created.

These are applied to the data during the post-calibration measurements to compensate for the sources of error discussed earlier. Many factors determine how often user calibration is performed [77]. Items you should consider include the required measurement accuracy, environmental conditions, and the repeatability of the DUT connection. Typically, vector network analyzer need user calibration every few measurements. You should use verification standards, identification of the sources of measurement uncertainty, and personal experience to determine how often to calibrate. Three families of calibration are commonly used in vector network analyzer calibration: Short, open, load, through (SOLT), Through, reflect, line, (TRL), Automatic calibration using an external automatic calibration module. Each calibration family has a variety of implementations. Which method you use depends on the DUT, test system, and measurement requirements. Regardless of which calibration method you choose, you should avoid random sources of error. Reducing the IF bandwidth and using averaging reduces noise, providing better results. Quality components, solid measurement practices, and a thorough understanding of the calibration procedure and instruments are all equally important when calibrating vector network analyzers [77].

5.3.2 Process Requirements

When making precise measurements with a vector network analyzer, you need to understand and correctly implement each step in the process for best results. Use quality components and sound measurement practices. The best vector network analyzer is ineffective if the quality of the RF connection to the DUT is not par with the required

system accuracy. It is useful to develop a process when using a vector network analyzer. A process reinforces good practices and helps you improve results. One can follow this general framework for using a vector network analyzer: prepare, practice, calibrate, and perform.

When properly used, a vector network analyzer is one of the most accurate RF instruments. It is capable of accuracies of ± 0.1 db and ± 0.1 degree. They make precise, repeatable RF measurements. Modern vector network analyzer offer configurations, and measurement capabilities as extensive as the range of applications they cover. Selecting the proper instrument, calibration, and features, along with using sound RF measurement practices, can give one excellent results [77][80].

CHAPTER 6

RESULTS

This research represents the results of complex permittivity measurement for dielectric materials at microwave frequencies. It was based on measuring S_{ij} scattering parameters using a Vector Network Analyzer by (TRL) calibration. In this research concrete, concrete pipe, clay, clay pipe, and soils were tested. Cylindrical samples specimens were made using a drill press. The specimens were drilled from different types of materials; like clay, clay pipe, concrete, concrete pipe, and soil. Dimensions of the specimens varied from three cm to four cm in diameter to four to five cm in height. A number of different conditions of the specimens were used for the measurements (1) saturated specimens with moisture on the inside for one month or more, (2) air dried specimens exposed to just room temperature and humidity, and finally (3) specimens were placed into saltwater (NaCl solution one M) for one month or more. We also calculated the percentage of moisture content for our samples. The percentage of moisture content is the ratio between the amount of moisture in the specimen at the time of measurement and the absolute dry mass of the specimen. The samples were oven dried for two days(see Table 6-1).

Table 6-1: Percentage of moisture content, $m[\%]$.

$$m = (W_n - W_s) / W_s \times 100$$

W_n = Mass of specimen at time of measurement

W_s = oven dried mass

		Wet	Dry mass	Percent of moisture $m[\%]$
Water	Concrete Pipe	23.244 grams	19.058 grams	21.964
Water	Clay Pipe	28.099 grams	26.063 grams	7.811
Saltwater	Concrete Pipe	22.715 grams	19.353 grams	17.371
Saltwater	Clay Pipe	32.458 grams	30.061 grams	7.973

6.1 Data Correction for Graphs

Every measurement is subject to error. This universally accepted truth is the result of everyday experience. From the simplest type of measurement, to the most refined type of measurement, errors are bound to creep in. For the graphs the following correction was used to improve our accuracy and precision.

C_m = concrete measurement of permittivity

p_m = PVC sample measurement of permittivity

p_T = PVC sample theoretical value of permittivity

so then,

$$\frac{C_m}{p_m} \times p_T =$$

An example,

$$\text{If } C_m = 3.89, p_m = 2.78, \text{ and } p_T = 3.00 \text{ then,} \\ 3.89/2.78 \times 3 = 4.19$$

That would then be the new corrected data, the program continues until all data is corrected, then it will create a new graph.

The Nicholson-Ross-Weir technique provides a way to directly calculate both permittivity and permeability from the s-parameters. It is probably the technique that is used the most to perform such conversion. If one wants to measurement the reflection

coefficient and transmission coefficient then this requires all four s-parameters or a pair of s- parameters of the material under test to be measured. However, the technique diverges for low loss materials at frequencies corresponding to integer multiples of one-half wavelength in the sample. This problem is due to a phase ambiguity. So then, the technique is restricted to optimum sample thickness of $\lambda_g/4$, and the technique should be used for short samples. From our concrete pipe and clay pipe plots, one can see that the NRW technique is divergent at integral multiples of one-half wavelength in the sample.

This is because that at a point corresponding to the one-half wavelength the s-parameter (S_{11}) gets very small. For a small s-parameter (S_{11}) value the uncertainty in the measurement of the phase of S_{11} on the VNA is very large. Therefore the uncertainty causes the divergence at these frequencies. These divergences can be avoided by reducing the sample length. However, it is difficult to determine the appropriate sample length when its ϵ and μ are unknown. The advantages of this technique are that it is fast and applicable to waveguides and coaxial line. The disadvantages of this technique are that it divergences at frequencies corresponding to multiples of one-half wavelength, short samples should be used, and it is not suitable for low loss materials [34][20]. These errors clearly show up in the graphs of the permittivity of clay pipes and concrete pipes. So to correct for this, all the data that was collected over a two year period was study, and the corrected data is shown in the final figures (see Figures 6-1 through 6-12).

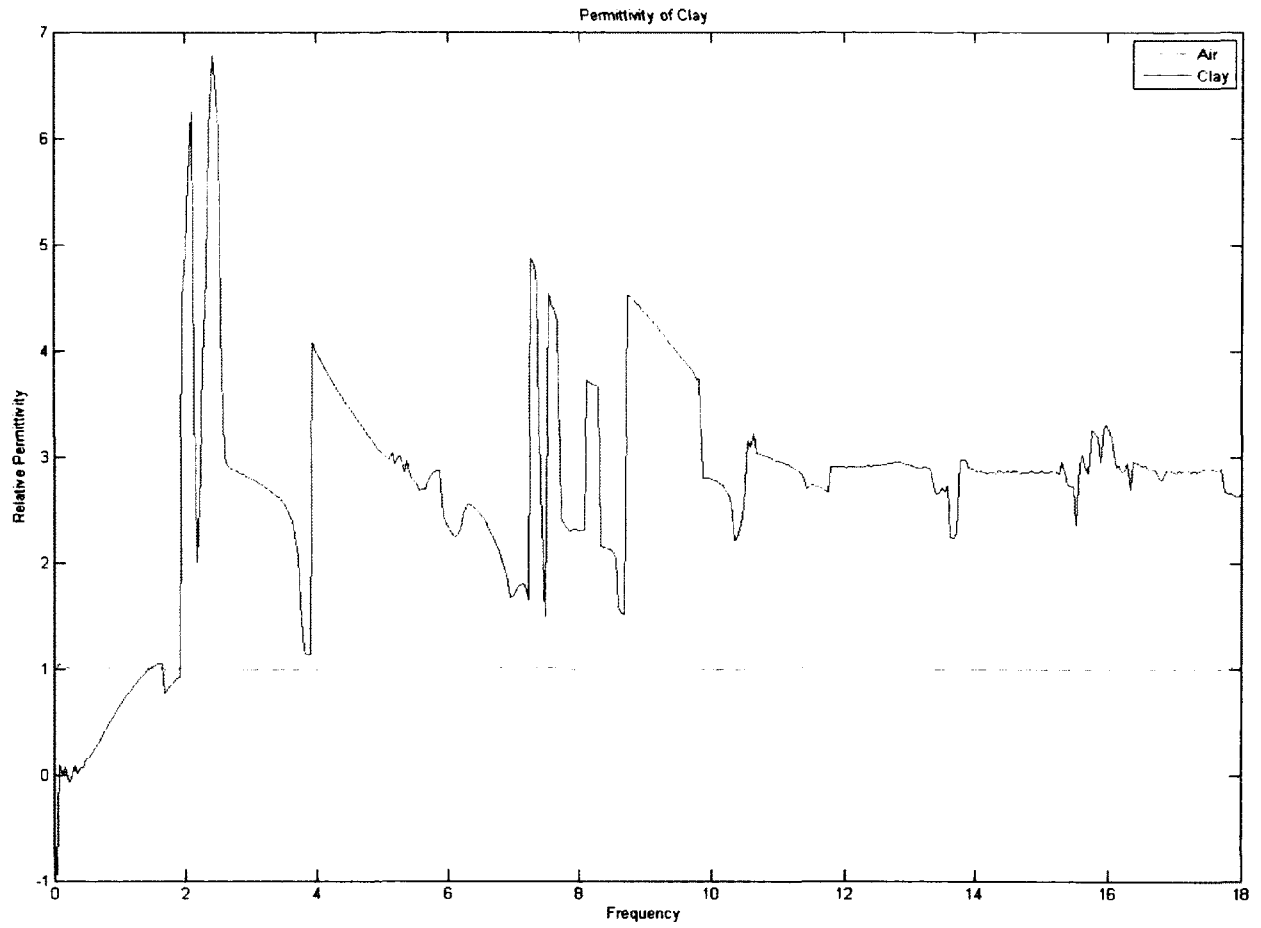


Figure 6-1: Permittivity of dry clay (frequency in Ghz).

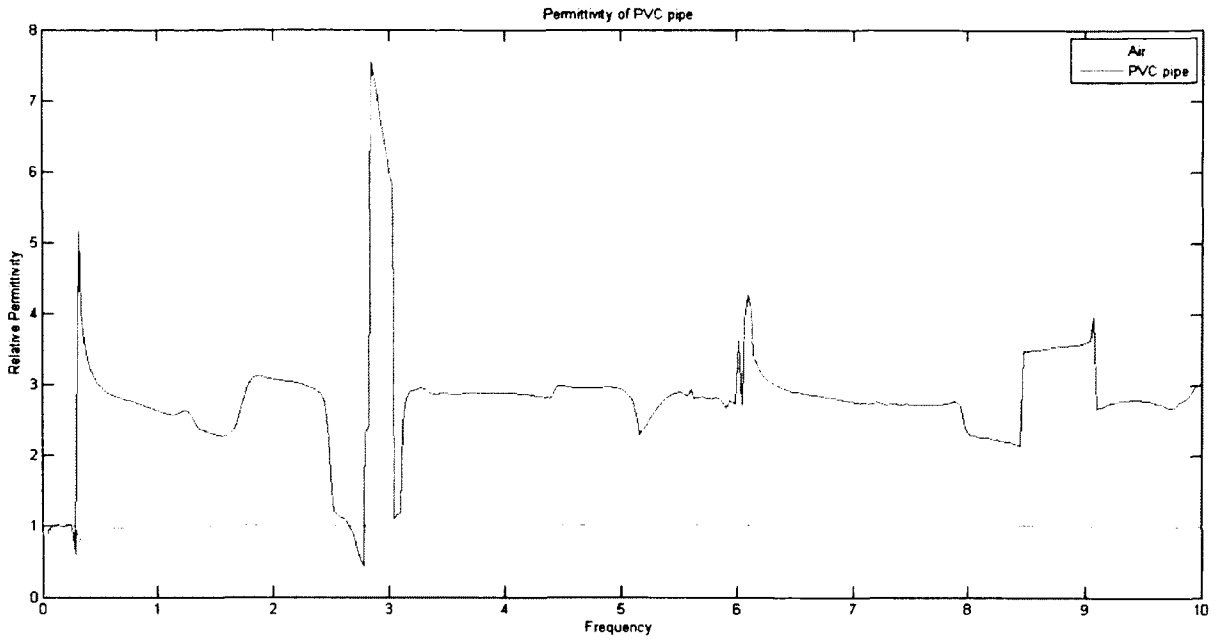


Figure 6-2: Permittivity of PVC pipe (frequency in Ghz).

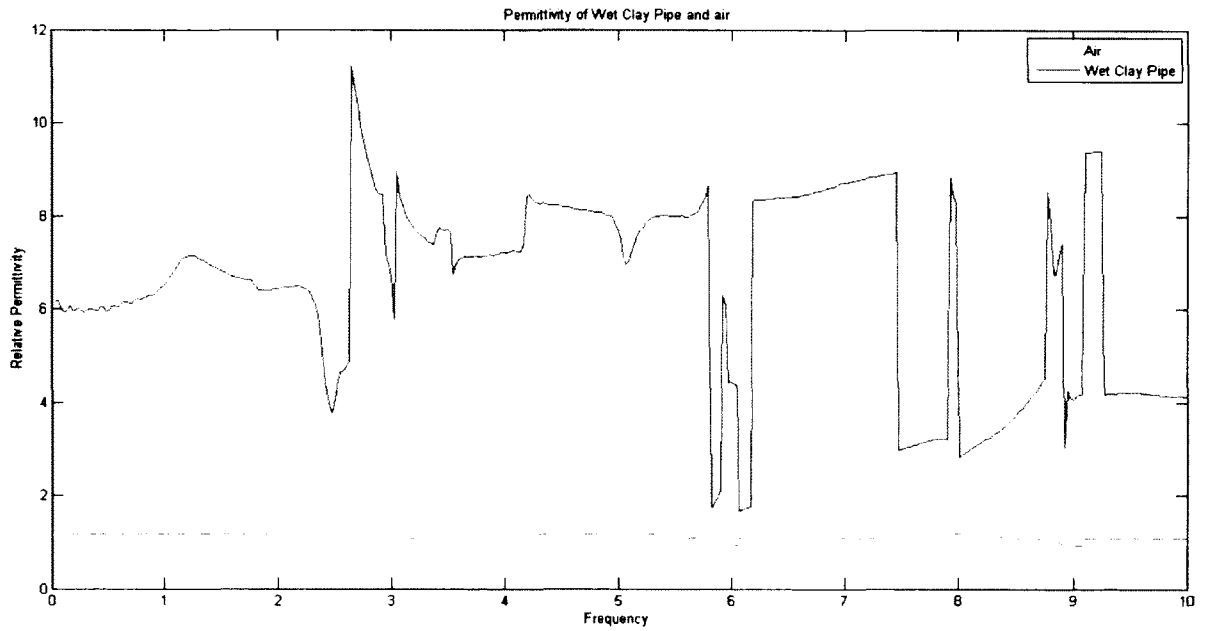


Figure 6-3: Permittivity of wet clay pipe and air (frequency in Ghz).

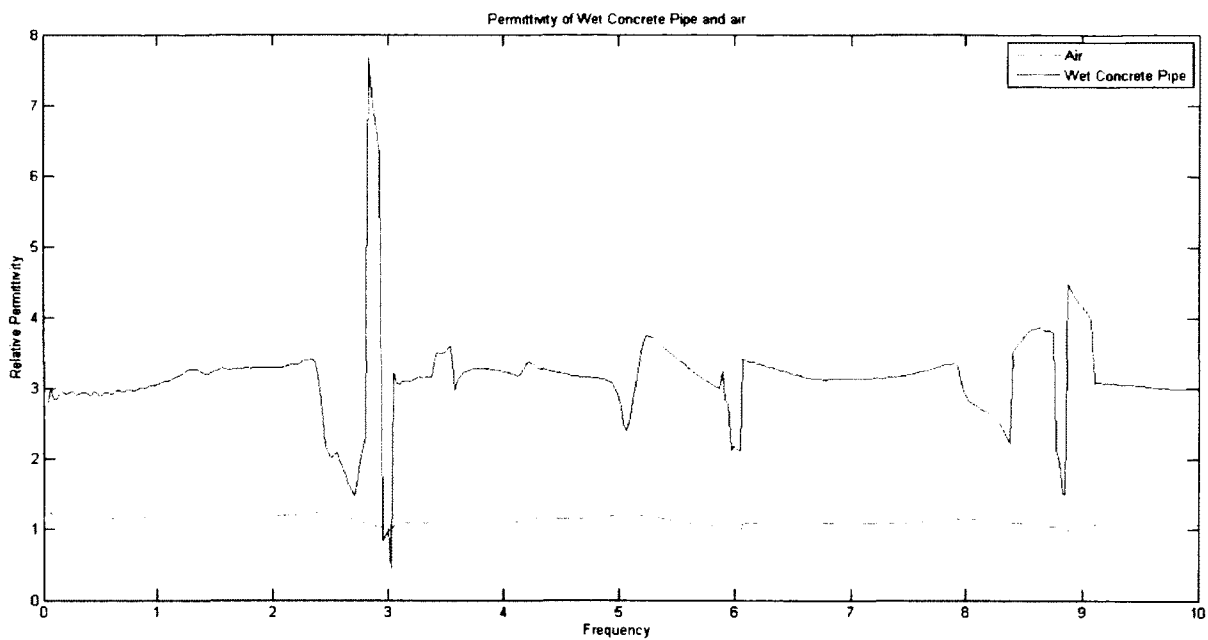


Figure 6-4: Permittivity of wet concrete pipe and air (frequency in Ghz).

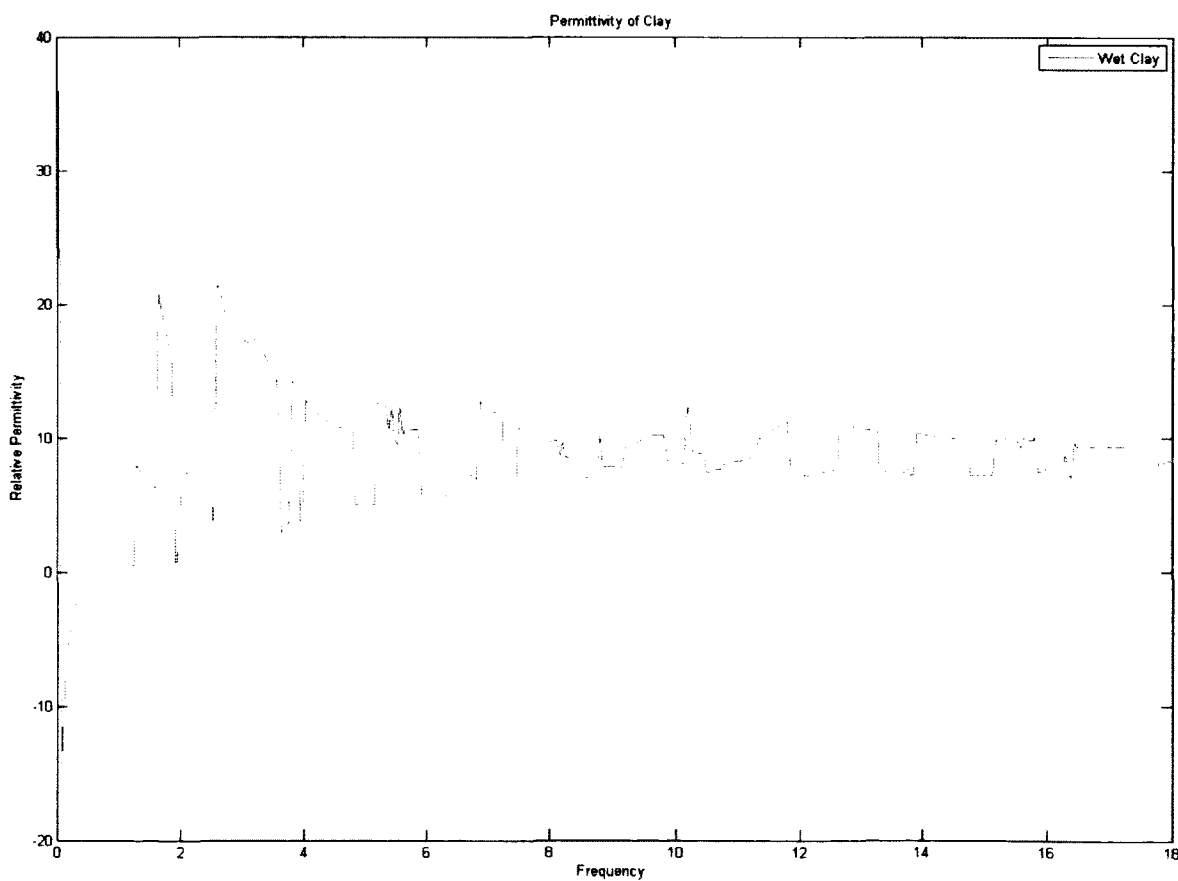


Figure 6-5: Permittivity of wet clay (frequency in Ghz).

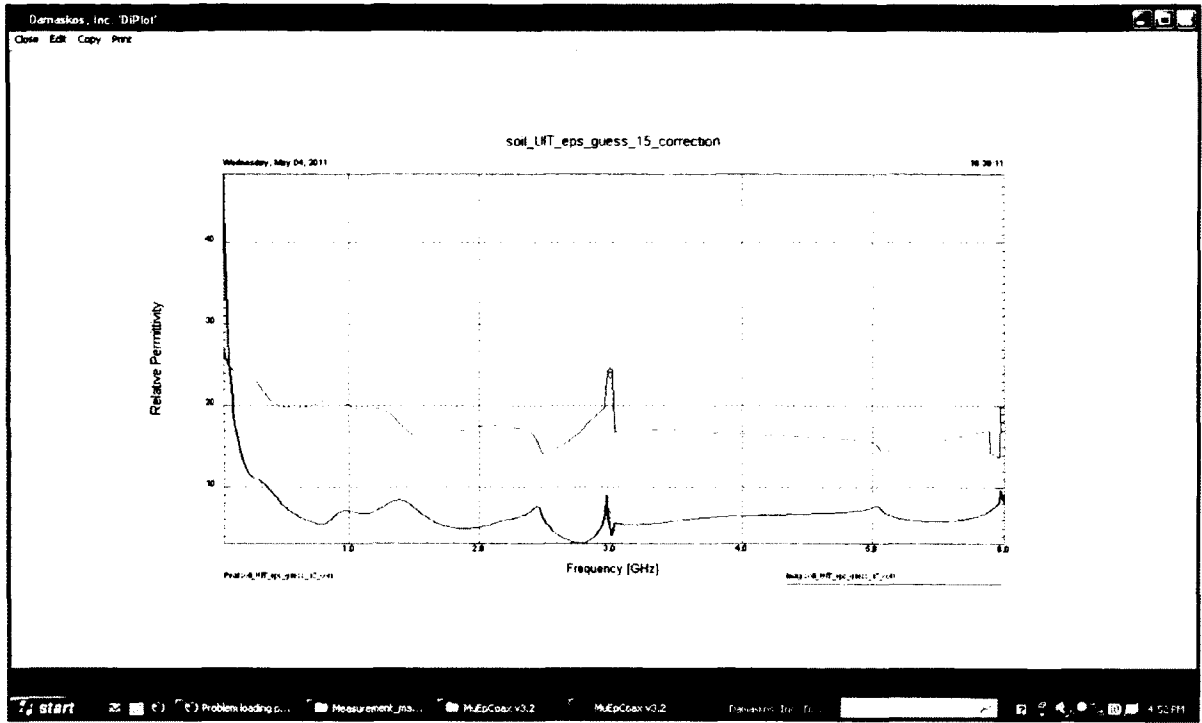


Figure 6-6: Permittivity of soil (directly from the program).

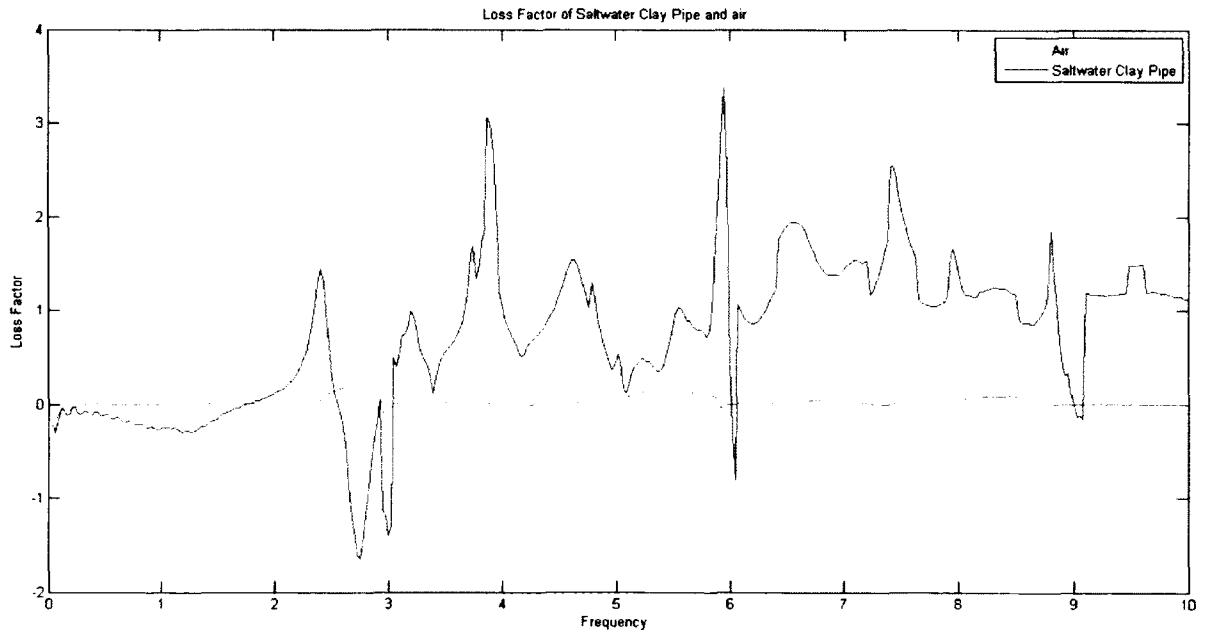


Figure 6-7: Loss factor of saltwater clay pipe and air (frequency in Ghz).

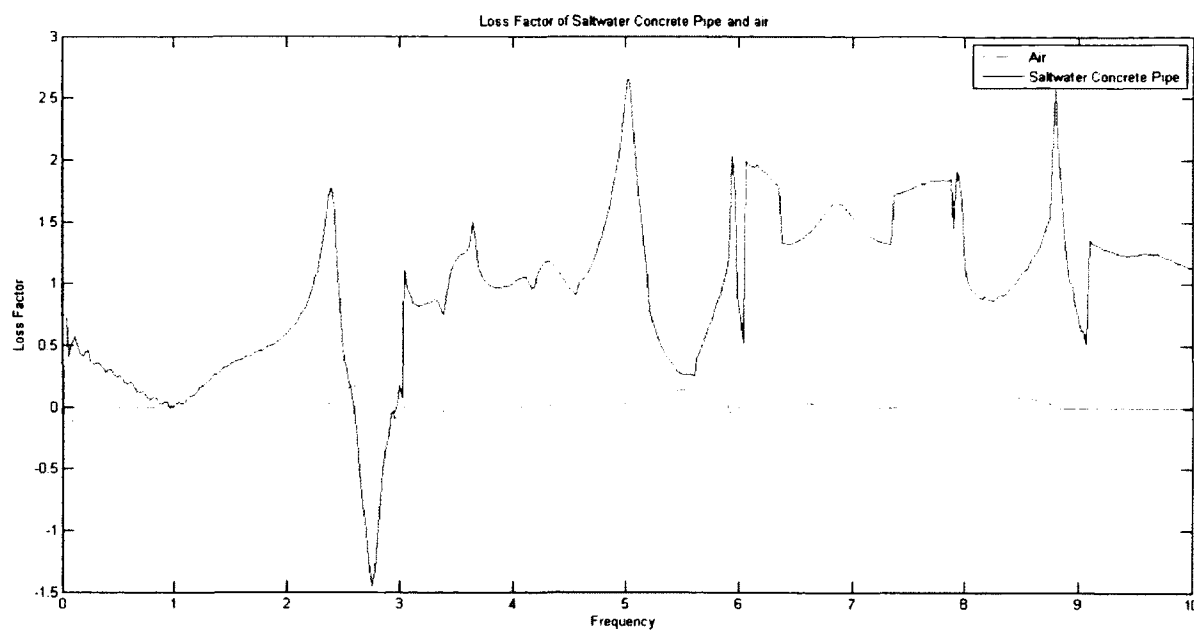


Figure 6-8: Loss factor of saltwater concrete pipe and air (frequency in Ghz).

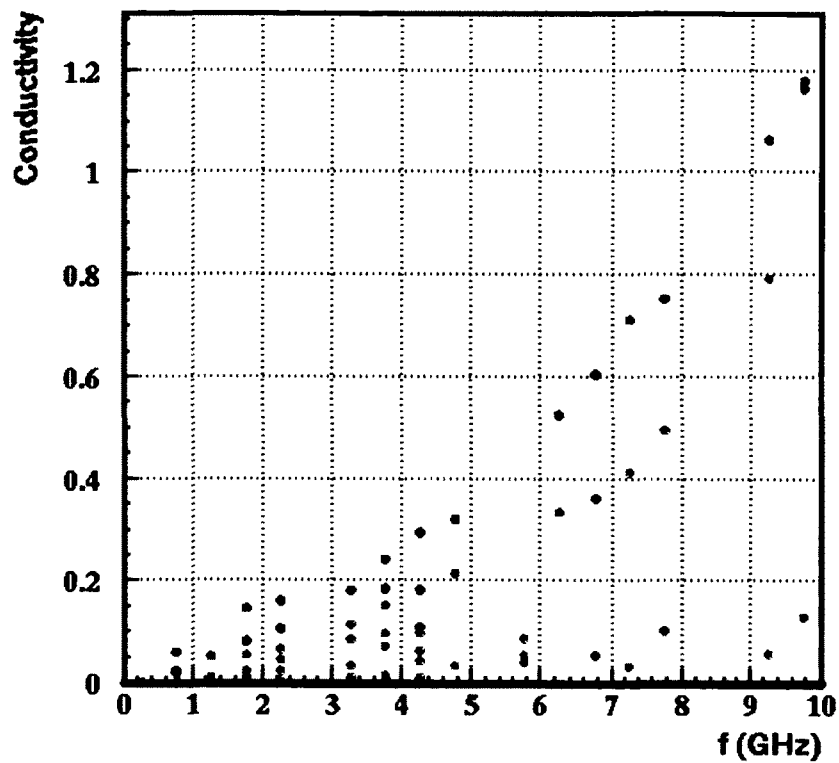


Figure 6-9: Conductivity of concrete. Red dots represent dry concrete, green dots represent wet concrete, and blue dots represent saltwater concrete (conductivity is in S/m).

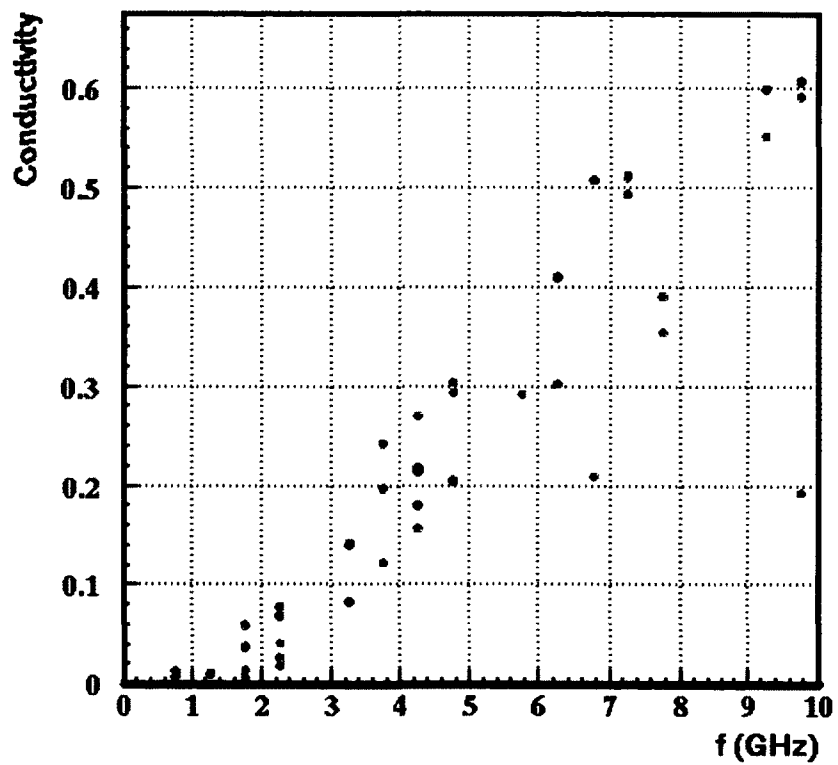


Figure 6-10: Conductivity of clay. Red dots represent dry clay, green dots represent wet clay, and blue dots represent saltwater clay (conductivity is in S/m).

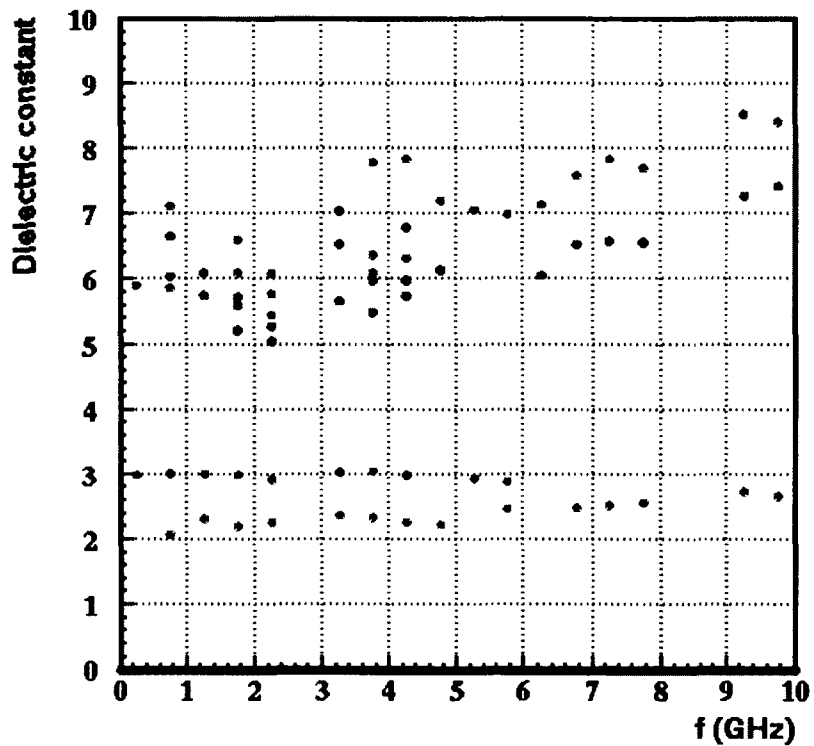


Figure 6-11: Dielectric constant for concrete. Red dots represent dry concrete, green dots represent wet concrete, and blue dots represent saltwater concrete.

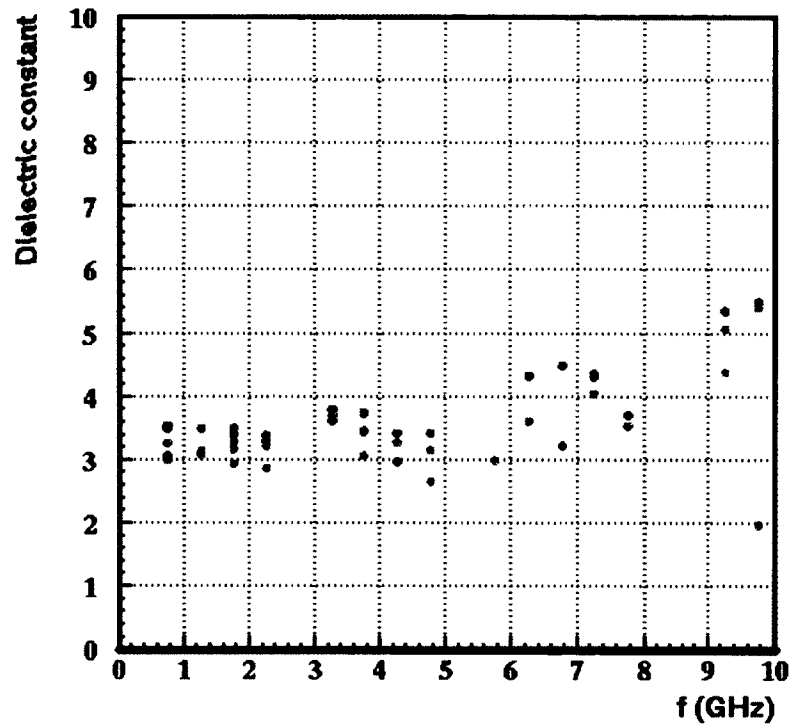


Figure 6-12: Dielectric constant of clay. Red dots represent dry clay, green dots represent wet clay, and blue dots represent saltwater clay.

CHAPTER 7

SUMMARY AND CONCLUSIONS

7.1 Summary

A dielectric material is a material which conducts electromagnetic waves, and is commonly referred to as an insulator. The transition from insulator to conductor is a gradual one without any clear cut-off point, and many existing materials exhibit both properties. If the conductivity of a material is high, it attenuates electromagnetic waves to a larger extent, thus resulting in a lower penetration depth. The two significant properties of a dielectric material are the real and imaginary parts of its complex dielectric permittivity. The real part is associated with the phase velocity and the imaginary part signifies the conductivity or attenuation of electromagnetic waves in the medium. The dielectric permittivity is often called the dielectric constant. This term is a misleading one, since this property of a dielectric material varies with several factors. A dielectric material increases the storage capacity of a capacitor by neutralizing charges at the electrode surfaces. This neutralization can be imagined to be the result of the orientation or creation of dipoles opposing the applied field. Such polarization is proportional to the polarizability of the dielectric material; that is, the ease with which it can be polarized. Polarizability is defined as the average induced polarization per unit field strength. The greater the polarizability of a material, the greater will be its dielectric constant.

The dielectric constant of a material is not a constant, but is a function of the polarizability which is in turn a function of frequency, temperature, local fields, applied field strength, availability and freedom of charge carriers within the dielectric, and local field distortions. The dielectric conductivity is also affected by the same factors. This is because the dielectric conductivity is a function not only of ohmic conductivity but also of the power consumed in polarizing the material. Moisture and chloride are the two constituents which have the most effect on the dielectric properties of concrete and clay. In general, the real part of the dielectric constant is larger when it is easier for the material to polarize, meaning that the ions are mobile and there is little crystallization. The addition of chlorides increases the dielectric constant, as does the amount of water. The dielectric constant decreases over curing time, because the amount of water decreases during this time. Also, the dielectric constant of concrete is dependent on the constant of its aggregate: mixes containing limestone have a higher constant than those containing granite, this correlates with the fact that limestone itself has a higher constant than granite does [15].

There are certain concrete properties that influence the performance of concrete pipes. These properties include concrete compressive strength, density, absorption, water cement ratio, cement content and type, and aggregates. All of these factors would have an influence on the dielectric properties of concrete pipes. For example, the dielectric constant for concrete with coarse aggregates is higher than concrete with fine aggregates. Compressive strengths for concrete pipes normally range from 4000 psi to 6000 psi. Concrete strength is a function of many factors including, aggregates, cement material, manufacturing, curing process, and mix design. These factors must also play a role in the

dielectric constant of concrete pipes, since concrete pipes strength is a function of these same factors. Concrete pipe design strengths refer to 28 days concrete strengths, but in actuality, the design strengths are obtained much earlier than 28 days. Quality concrete pipe densities typically range from 145-155 pounds per cubic foot. In general, the higher the density of concrete pipe, the greater the durability of the concrete, which leads us to believe that the dielectric constant could be affected by, changes in density.

Clay pipes are a mixture of different clay minerals, which makes it a multi-phased heterogeneous material. Dielectric constant is a measure of the polarizability of a material. Polarization is the spatial separation of charges due to an applied electric field. The mechanisms that cause polarization depend on the frequency of the applied electric field and the composition of the material. Single phase, homogeneous materials experience only high frequency polarization mechanisms: electronic, ionic, and molecular [8].

Multi-phase heterogeneous materials experience these polarization mechanisms, as well as low frequency polarizations: interfacial spatial, bound water, and double layer. These property makes calculating the dielectric constant a difficult task. Dry clay dielectric constant should be between two-six, and wet clay range between 15-40. These numbers can give us a guide, but with the different clay types we cannot be totally sure. Kaolinite has a dielectric constant of 11.8 and quartz a dielectric constant of 4.5, but because clay pipe contain both quartz and kaolinite we need to consider the mixture when the dielectric constant is calculated. If a particular clay pipe contains more kaolinite than quartz we might be looking at a higher dielectric constant, than if the clay pipe contains more quartz than kaolinite. The raw materials of a vitrified clay pipe also include

approximately 10 to 15 percent water. Water has a high dielectric constant, which must be considered. Free water has a higher dielectric constant than bound water.

Water has a high dielectric constant because water is a polar molecule which is free to rotate along the direction of an applied electric field, allowing alignment of the water molecules electric dipoles. Bound water has a lower dielectric constant than free water contained in the pore spaces, because its water molecules are absorbed to the surfaces of particles and the dipoles are immobilized. So if we want to calculate the dielectric properties of clay pipes we need to account for the contributions to the dielectric constant from both bound and free water. So calculating the dielectric properties of clay pipes is complex, and there are many influencing factors.

7.2 Conclusions

In conclusion, it appears that at under dry conditions, the dielectric constant of concrete pipes and clay pipes does not vary much over the measured frequency range. However, the change of the dielectric constant of concrete pipe and clay pipe becomes significant as the moisture level increases. Moisture content is one of the major constituents which influence the electromagnetic properties of concrete pipe and clay pipe. Loss factor of clay pipe and concrete pipe is the imaginary part of the complex permittivity. The loss factor is divided by the dielectric constant over the frequency range to obtain the loss tangent. The loss tangent of concrete pipe increases as frequency increases, the effect of water on the lossiness of concrete pipe is shown in the Figure 6-8. Also the loss tangent of concrete pipe specimens with higher moisture content show higher loss tangent values than those with less moisture content.

The significance of conductivity is that the penetration depth of the wave in concrete pipe is inversely proportional to the conductivity. The conductivity in concrete pipes varies depending on the type of cement used in the sample. Saltwater has almost the same effects on concrete as water. The dielectric constant of concrete in saltwater is almost the same as the dielectric constant of wet concrete. In general, the dielectric constant of saltwater is just a little less than the dielectric constant of wet concrete. Saltwater has a more significant influence on the loss part of the Dielectric constant than the real part (See Figure 6-1 to Figure 6-12).

7.3 Recommendations for Future Work

In future research the concentration of saltwater can be increased or decreased to see how it affects the dielectric constant. Also, the temperature could be changed to see how it affects the dielectric constant.

REFERENCES

- [1] R.L.Sterling, J. Anspach, E. Allouche, J. Simicevic, W. Rogers, and K. Hayes, "Encouraging in locating and characterizing underground utilities," Report to the SHRP2 Program, *Transportation Research Board*, NAS. 2009.
- [2] Battelle Memorial Institute, White paper on Rehabilitation of wastewater collection and water distribution systems. Contract No. EP-C-05-057, Task Order No. 58. 2008.
- [3] NIST. "Advanced sensing technologies for the infrastructure: Roads, highways, bridges, and water." 2008.
- [4] Z.Tan and I.D.Moore, "Effect of backfill erosion on moments in buried rigid pipes," *Transportation Research Board Annual Conference*, Washington, D.C., January, p. 29, 2007.
- [5] *Insituform*, "How a sinkhole forms," 2009.
- [6] S.B.Costello, D. N.Chapman, C.D. F. Rogers, and N. Metje, "Underground asset location and condition assessment technologies." *Tunneling and Underground Space Technology* 22 (5-6), 524-542. 2007.
- [7] A. Jaganathan, E. N. Allouche, and N. Simicevic, "Pipeline scanning: Novel technology for detection of voids and internal defects in non-conductive buried pipes," In: Proceedings of NO-DIG International conference, Brisbane, Australia. 2010.
- [8] A.R.Von Hippel, *Dielectric Materials and Applications*. The Technology Press of M.I.T. and John Wiley & Sons, Inc., 1954.
- [9] J.Baker-Jarvis, E. J. Vanzura, and W. A. Kissick, "Improved technique for determining complex permittivity with the transmission/reflection method," *IEEE Transactions on Microwave Theory and Techniques* 38(8): 1096-1103, 1990.
- [10] U.C.Hasar, "Permittivity measurement of thin dielectric materials from reflection-only measurements using one-port vector network analyzers," *Progress In Electromagnetics Research*, PIER 95, pgs. 365-380, 2009.

- [11] Z. Ma, and S. Okamura, "Permittivity determination using amplitudes of transmission and reflection coefficients at microwave frequency," *IEEE Microwave Theory and Technology*, Vol. 47, no. 5 pgs. 546-550, 1999.
- [12] J. Baker-Jarvis, C. Jones, B. Riddle, M. Janezic, R. Geyer, J. H. Grosvenor Jr., and C. Weil, "Dielectric and magnetic measurements: A survey of nondestructive, quasi-nondestructive, and process-control techniques," *Research in Nondestructive Evaluation* 7(2-3): 117-36, 1995.
- [13] R. Clarke, *A Guide to the Dielectric Characterization of Materials at RF and Microwave Frequencies*, National Physical Laboratory; NPL; 2003.
- [14] P. K. Mehta, *Concrete: Structure, Properties and Materials*, Prentice Hall, Englewood Cliffs, NJ, 1986.
- [15] O. Buyukozturk and H. C. Rhim, "Modeling of electromagnetic wave scattering by concrete specimens," *International Journal of Cement and Concrete Research*, V. 25 No. 5, pp. 1011-1022, 1999.
- [16] R. J. Goodfellow, "Concrete for underground structures: guidelines for design and construction," *Society for Mining, Metallurgy, and Exploration*, 2011.
- [17] A. P. Moser, "Buried pipe design," In: McGraw-Hill *Professional Engineering*, 2nd ed., McGraw-Hill, 2001.
- [18] G. H. Haggis, J. B. Hasted, and T. J. Buchanan, "The dielectric properties of water in solutions," *Journal of Chemical Physics*, 29: 1452-1465; 1952.
- [19] K. H. Wong, "Using precision coaxial air dielectric transmission lines as calibration and verification standards," *Microwave Journal* pp. 83-90; 1988 December.
- [20] Rohde and Schwarz, "Measurement of dielectric material properties," *Application Note*, Application Center Asia/Pacific, RAC0607-0019, CY Kuek 07, 2006.
- [21] U. Kaatze, "Techniques for measuring the microwave dielectric properties of materials," *Metrologia*, Vol. 47, No. 2, S91-S113, 2010.
- [22] W. Su, O. A. Hazim, I. L. Al-Qadi, and M. C. Riad, "Permittivity of Portland cement concrete at low rf frequencies," *Materials Evaluation*, Apr., pp. 496-502. 1994.
- [23] M. D. Belrhiti, S. Bri, A. Nakheli, M. Haddad, and A. Mamouni, "Complex permittivity measurement for dielectric materials at microwave frequencies using rectangular waveguide," *European Journal of Scientific Research*, Vol. 49, No.2 (2011), pgs. 234-248, 2011.

- [24] A. C. Lynch, "Relationship between permittivity and loss tangent," *Proc. IEEE* 118: 244-246; 1971.
- [25] A. E. Bailey, *Microwave Measurement*, London: Peter Peregrinus; 1985.
- [26] N. Marcuvitz, *Waveguide Handbook*, New York, Dover Publications, 1951.
- [27] Ai Huang, *Recent Advances in Dielectric Materials*, Nova Science Publishers, 2009.
- [28] M. A. Marsland and S. Evans, "Dielectric measurements with an open-ended coaxial probe," *IEE Procedure*, 134: 341-349;1987.
- [29] R. Olmi, M. Bini, A. Ignesti, and C. Riminesi, "Nondestructive permittivity measurement of solid materials," *Measurement Science Technology* 11: 1623-1629; 2000.
- [30] J. Muscil and F. Zacek, *Microwave Measurements of Complex Permittivity by Free Space Methods and Their Applications*. New York, Elsevier, 1986.
- [31] D. K. Ghodgaonkar, V. V. Varadan, and V.K. Varadan, "Free-space measurement of complex permittivity and complex permeability of magnetic materials at microwave frequencies," *IEEE Transactions on Instrumentation and Measurement*, Vol. 39 Issue 2, pgs. 387-394, 1990.
- [32] C. Cook, *The Theory of the Electromagnetic Field*, Prentice-Hall, 1975.
- [33] U. C. Hasar, "Unique permittivity determination of low loss dielectric materials from transmission measurements at microwave frequencies," *Progress in Electromagnetics Research*, Vol. 107, 31-46, 2010. Baker-Jarvis, J., Transmission/reflection and short-circuit line permittivity measurements, *National Institute of Standards and Technology Note* 1341; July. 1990.
- [34] W. B. Weir, "Automatic measurement of complex dielectric constant and permeability at microwave frequencies," *Proceedings of the IEEE* 62(1): 33-36, 1974.
- [35] D. Manohar, D. Jagadeswara, C. Reddy, P. Tiemsinu, and R. Cravey, "A new approach to estimate complex permittivity of dielectric materials at microwave frequencies using waveguide measurements," *IEEE*, Vol. 45, No. 3, pgs. 359-366., 1997.
- [36] M. Sadiku, *Elements of Electromagnetics*, 4th ed., Oxford University Press, Inc., New York, USA, 2007.

- [37] U.S.Inan and A.S. Inan, *Electromagnetic Waves*, Prentice Hall, Upper Saddle River, Nj, USA, 2000.
- [38] H. Frohlich, *Theory of Dielectrics*. Oxford University Press, 1958.
- [39] R. Elliott, *Electromagnetics*, McGraw-Hill, 1966.
- [40] F. M. Lea, *The Chemistry of Cement and Concrete*, Chemical Publishing Company, Inc., New York, NY, 1971.
- [41] R. Grag, "Analytical and computational methods in electromagnetics," *Artech House*, pg. 551, 2008.
- [42] P. Debye, *Polar Molecules*, Dover Publications, Inc., 1929.
- [43] M. Weiner, *Electromagnetic Analysis Using Transmission Line Variables*, 2nd ed., World Scientific, 2010.
- [44] K. Lonngren, *Electromagnetics with Matlab*, Cambridge International Science Publishing, 1997.
- [45] K.S. Cole and R.H. Cole, "Dispersion and absorption in dielectric I: Alternating current characteristics," *The Journal of Chemical Physics*, 9:341, 1941.
- [46] Y. Pochi, Y. Amnon, and C. Hong, "Electromagnetic propagation in periodic stratified media. I. general theory," *Journal Optical Society of America*, Vol. 67, Number 4, April 1977 pp. 423-438.
- [47] A. B. Constantine, *Advanced Engineering Electromagnetics*, John Wiley & Sons, 1989.
- [48] R. A. Harris, On harmonic functions, *American Journal of Mathematics*, XXXIV, pgs. 391-420, 1912.
- [49] A. Papoulis, *The Fourier Integral and Its Applications*, New York: McGraw-Hill; 1987.
- [50] C. H. Durney, *Introduction to Modern Electromagnetics*, McGraw-Hill, 1969.
- [51] H. R. Hertz, *Electric Waves*, Macmillian and Co., Ltd., London, 1900.
- [52] L. Lewin, *Advanced Theory of Waveguides*, London, England: Illiffe; 1951.
- [53] R. W. Ziolkowski and E. Heyman, Wave propagation in media having negative permittivity and permeability, *Physical Review*, E 64: 056625-1.15; 2001.

- [54] E. B. Graham, J. Pierrus, and R. E. Raab, "Multipole moments and Maxwell's equations," *Journal of Physics B: Optical Physics* 25: 4673-4684; 1992.
- [55] P. Mazur and B. R. A. Nijboer, "On the statistical mechanics of matter in an electromagnetic field," *I, Physica* 19: 971-986, 1953.
- [56] M. Mandel and P. Mazur, "On the molecular theory of the dielectric relaxation," *Physica* 24: 116-128;1958.
- [57] J. E. Gubernatis, "Scattering theory and effective medium approximations to heterogeneous materials," *Physica* 24: 84-96,1978.
- [58] G. N. Watson, *A Treatise on the Theory of Bessel Functions*, 2nd ed., Cambridge University Press, New York, 1966.
- [59] R. Hargreaves, "A diffraction problem and an asymptotic theorem in bessel's series," *Philosophical Magazine* (6) XXXVI, pgs. 191-199, 1918.
- [60] J. A. Kong, *Electromagnetic Wave Theory*, 2nd ed. , John Wiley & Sons, New York, 1990.
- [61] F. Bowman, *Introduction to Bessel Functions*, Dover Publications, Inc., New York, NY, 1958.
- [62] J. D. Kraus, and D. A. Fleisch, *Electromagnetics with Applications*, 5th ed., McGraw-Hill, New York, USA, 1999.
- [63] C. Kittel, *Introduction to Solid State Physics*, 6th Ed., New York, John Wiley, 1986.
- [64] P. Cornille, "Advanced electromagnetism and vacuum physics," *World Scientific*, 2003.
- [65] H. C. Chen, *Theory of Electromagnetic Waves: A Coordinate-Free Approach*, McGraw-Hill, New York, 1983.
- [66] C. Smyth, *Dielectric Behavior and Structure*. McGraw-Hill Book Company, Inc., 1955.
- [67] M.R.Taherian, D. J. Yeun, T. M. Habashy, and J. A. Kong, "A coaxial-circular waveguide for dielectric measurement," *IEEE Tranaction Geoscience Remote Sensing*, 29:321-330.,1991.
- [68] S. Popovics, *Concrete Materials: Properties, Specifications and Testing*, 2nd ed., Noyes Publications, New Jersey, 1992.

- [69] J. D. Dewar and R. Anderson, *Manual of Ready-mixed Concrete*, 2nd ed., Blackie Academic & Professional, 2003.
- [70] A. J. Boyd and S. Mindess, "Cement and concrete: Trends and challenges, materials science of concrete," *American Ceramic Society*, 2002.
- [71] S. Mindess and J. F. Young, *Concrete*, Prentice-Hall, Inc., New Jersey, NJ, 1981.
- [72] T. C. Powers, "Structure and physical properties of hardened portland cement paste," *Journal of American Ceramic Society*, Vol. 61, No. 1, pgs. 1-5., 1958.
- [73] P. Collins, R. Legault, and K. Frampton, *Concrete: The Vision of a New Architecture*, 2nd ed., McGill-Queen's University Press, 2004.
- [74] P. Bhatt, T. J. MacGinley, and B. S. Choo, *Reinforced Concrete: Design Theory and Examples*, 3rd ed., Taylor & Francis, 2006.
- [75] P. Neelakanta, *Electromagnetic Materials*, London: CRC Press; 1995.
- [76] M. G. Richardson, "Fundamentals of durable reinforced concrete," In: *Modern Concrete Technology*, Spon Press, 2002.
- [77] R. B. Marks, "A multiline calibration for network analyzers," *IEEE Trans. Microwave Theory and Techniques* 39: 1205-1215; 1991.
- [78] H. E. Bussey and J. E. Gray, "Measurement and standardization of dielectric samples," *IRE Transactions on Instrumentation* I-11(3):162-165; 1962.
- [79] S. Laurens, J. P. Balayssac, and J. Rhazi, Nondestructive evaluation of concrete moisture by GPR: experimental study and direct modeling, *Materials and Structures*, 2005, (38): 827-832.
- [80] E. Heyman, B. Mandelbaum, and J. Shiloh, *Ultra-wideband short-pulse Electromagnetics*, 4, Kluwer Academic Publishers, 2002.

APPENDIX A

TIME DOMAIN TESTS

Attenuation/Transmission Loss in Concrete Using Time Domain Measurements- Preliminary Results

Experiment 1 (Preliminary study)

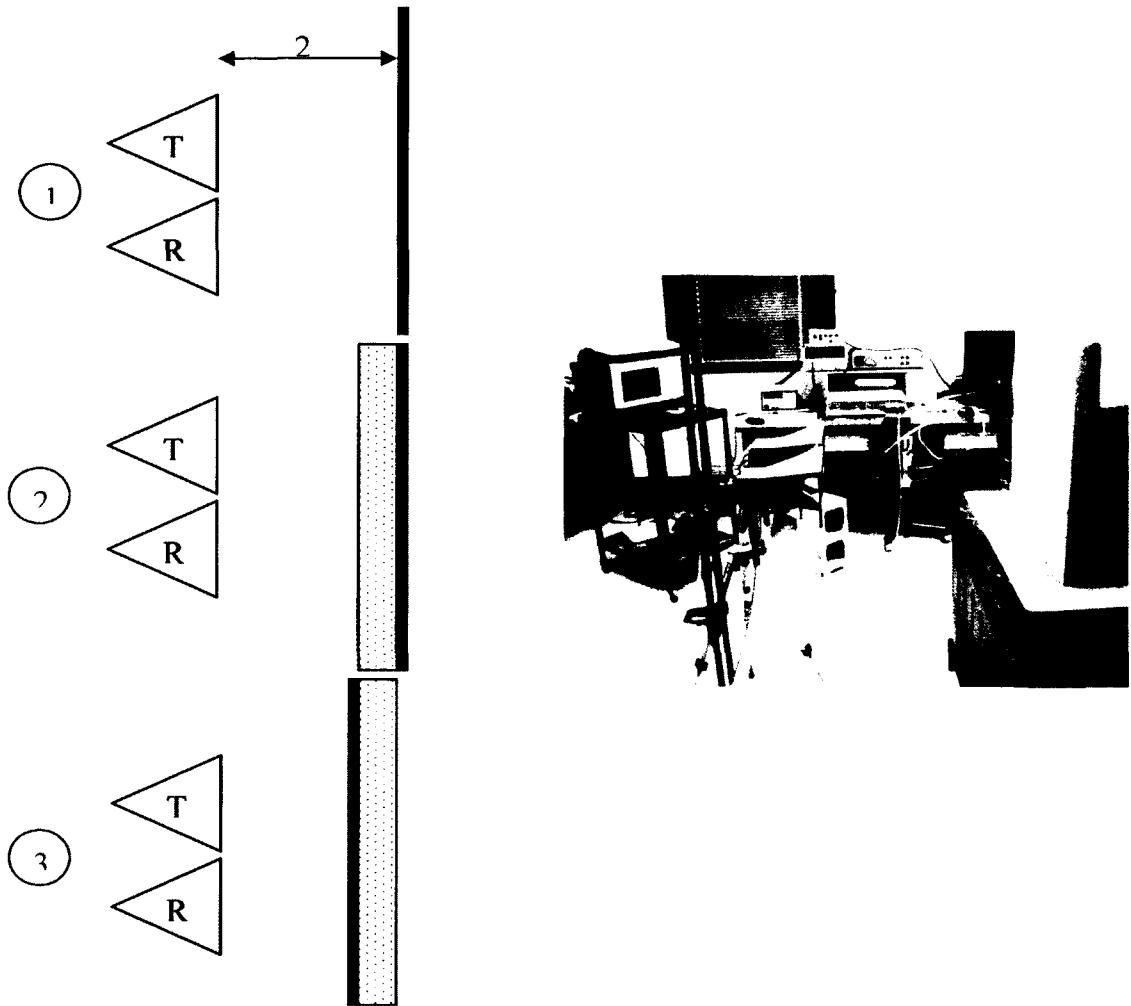


Figure A-1: Experiment one setup.

(left) - Three individual measurements used in the experiment; (right)- photograph of the experimental setup showing two double ridged horn antenna placed in front of a concrete block (2' square and 1.5 inch thick) backed with a metal plate. Also seen on the photograph are the oscilloscope and the pulse generator.

Highlights of the Test

1. Input Pulse to drive the transmit horn is a Gaussian pulse with width (FWHM) of ~ 200 ps.
2. Sample used - non-reinforced dry concrete block with moisture content around 7-8% . Moisture content was measured using a General tools handheld moisture meter (see Figure A-2) which is typically used to measure moisture in construction materials such as concrete, wood and dry wall. It has accuracy of $\pm 3\%$ which is not adequate. A better instrument with accuracy of $\pm 1\%$ will be purchased.



Figure A-2: Moisture measurement instrument manufactured by general tools.

Experiment 2 (Concrete and Concrete + Metal)

Figures A-3 and Figure A-4 show the attenuation of signal due to the presence of concrete is very low (about two - three dB drop between one and five GHz). It is expected that the energy within the pulse used in the final prototype would be concentrated within three and five GHz.

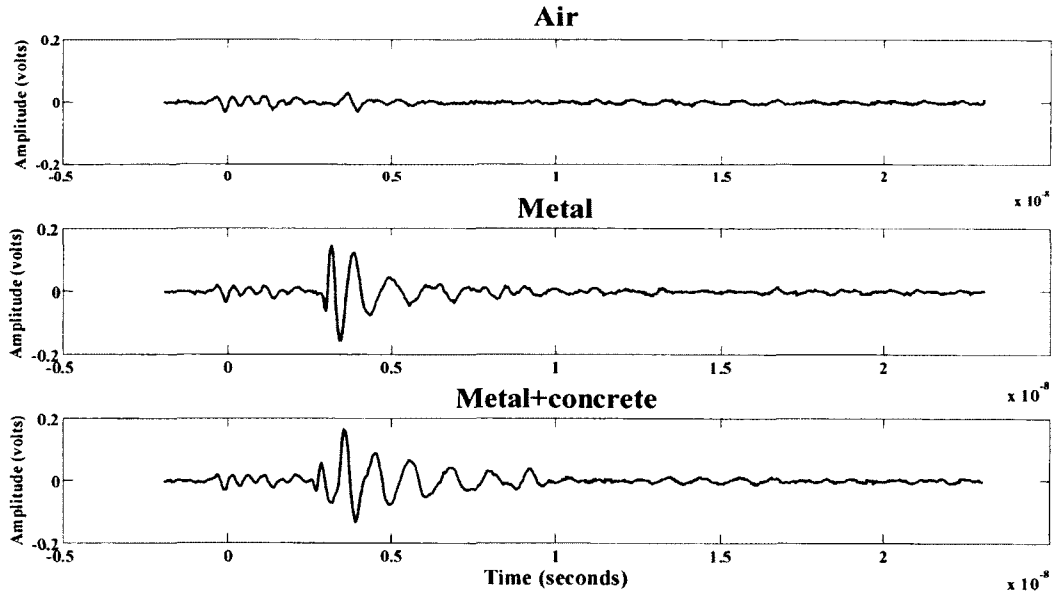


Figure A-3: Time domain plots obtained during Experiment 1.

(**Top:** no object was present in front of the antennas, **middle:** metal plate was present 2' away from the antennas & **bottom:** concrete block was placed in front of the metal plate) (Figure A-3) obtained using Fourier decomposition

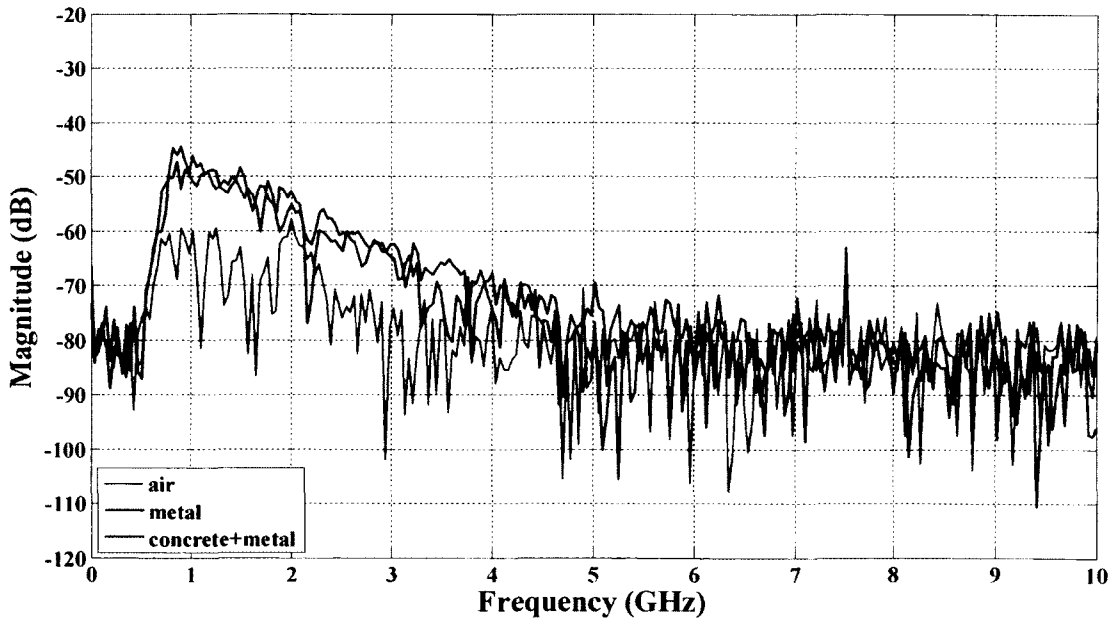


Figure A-4: Magnitude spectrum of the data collected during Experiment 1.

Figure A-5 represents the setup for Experiment 2 (horn antennas are separated by a distance of 172 cm). Photograph in the bottom right shows the placement of two horn antennas. Photograph in the bottom left shows the four inch square steel grid used as a sample during the experiment

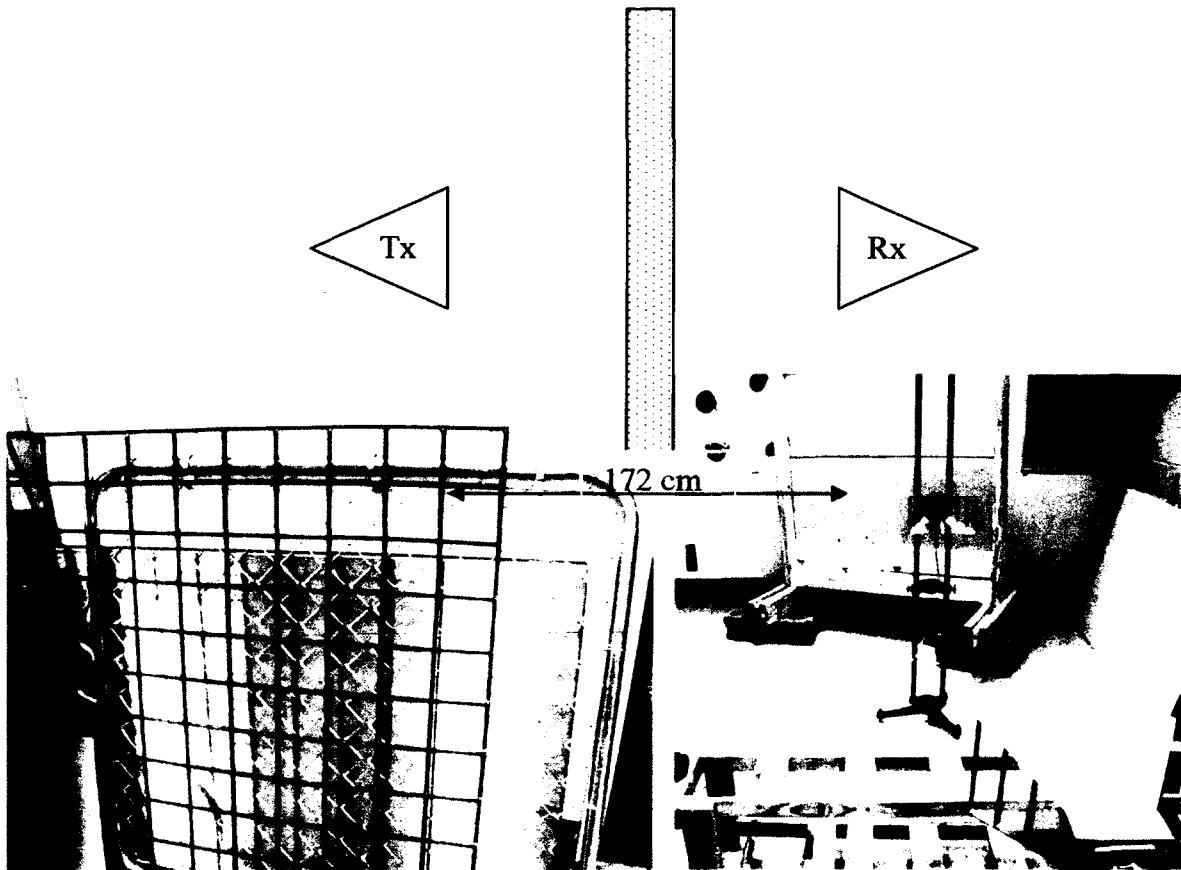


Figure A-5: Experiment 2.

In this test, a Gaussian pulse with a width (FWHM) of ~ 200 ps was used to excite the transmitting horn and the signal from the receiving horn was digitized using Tektronix oscilloscope. These sample types are shown in Table A-1.

Table A-1: List of sample types used during Experiment 2.

No.	Sample type placed in between horns
1	Open space
2	Metal plate (4' x 4')
3	2 inch square steel grid
4	4 inch square steel grid
5	8 inch square steel grid
6	concrete wall (4' x 4'x 2") + 2 inch square steel grid
7	concrete wall (4' x 4'x 2") + 4 inch square steel grid

Figure A-6 and Figure A-7 show the magnitude of the transmitted signal between two horn antennas dropped about eight dB (compared against the open space measurement) from one and five GHz for the case of concrete wall backed by a two inch steel grid. The drop in transmission for all other samples were below six dB. The transmission loss measurement obtained during Experiment 2 with pulsed signal is similar to the results obtained using CW signal (using VNA). Figure A-8 gives the transmission loss measurements performed using a configuration similar to Experiment 2 with the pulse generator and oscilloscope replaced by a vector network analyzer.

Time domain plots of the signal measured by the receiving horn antenna during Experiment 2. Three curves top, bottom and middle, correspond to the samples numbers one, six and seven from Table A-1.

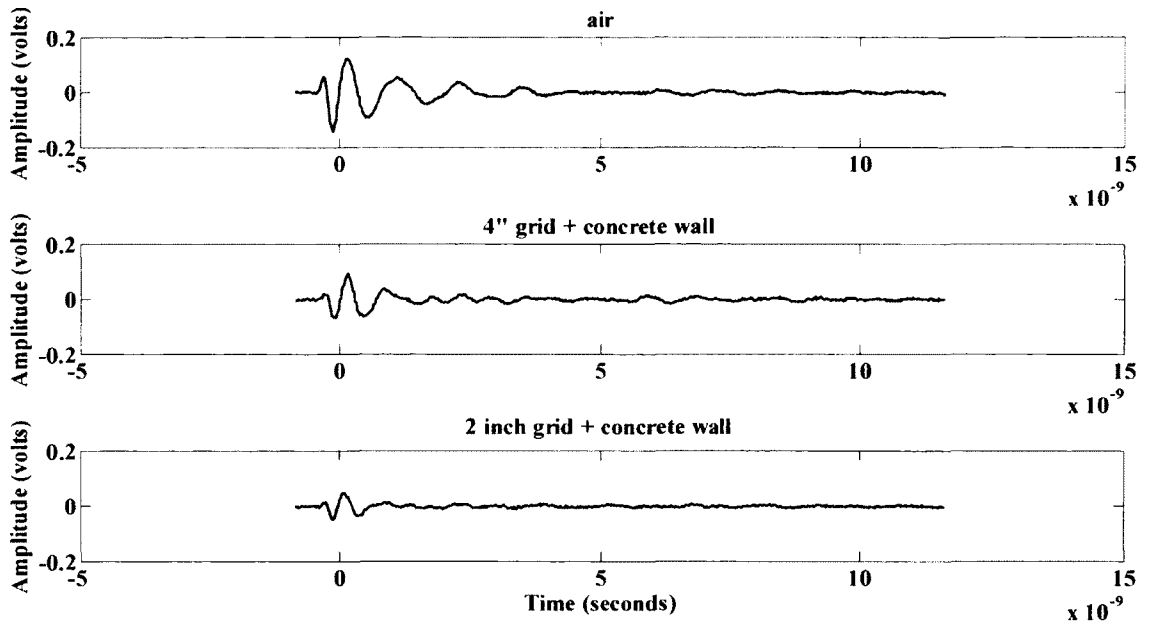


Figure A-6: Time domain plots.

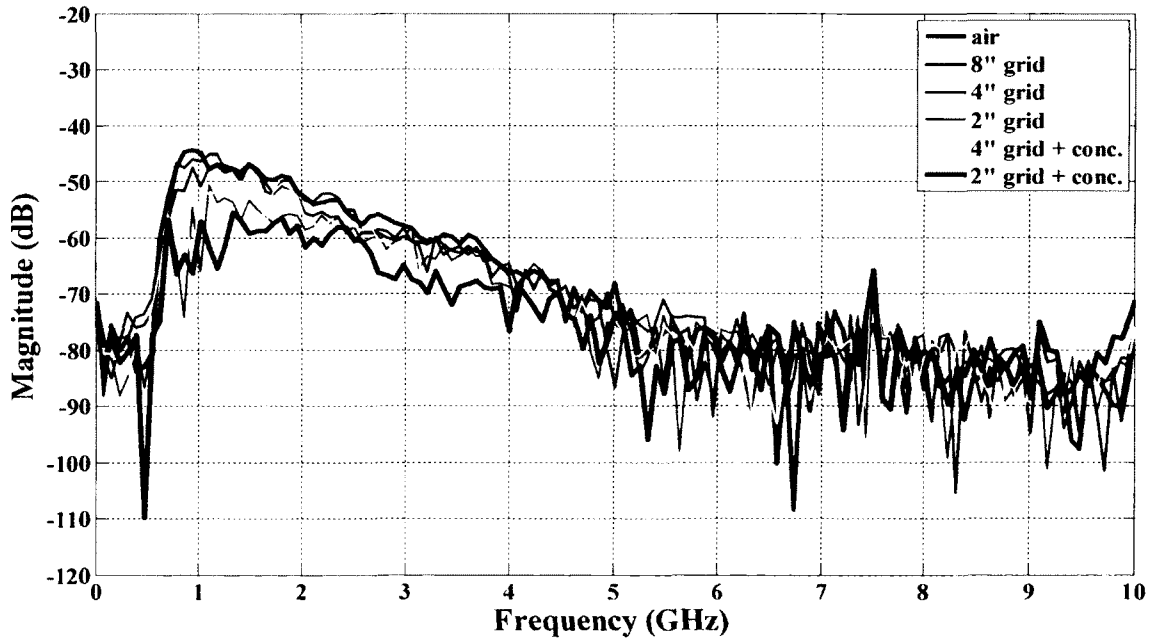


Figure A-7: Magnitude spectrum of the transmitted signal between two horns with different samples placed in between the antennas.

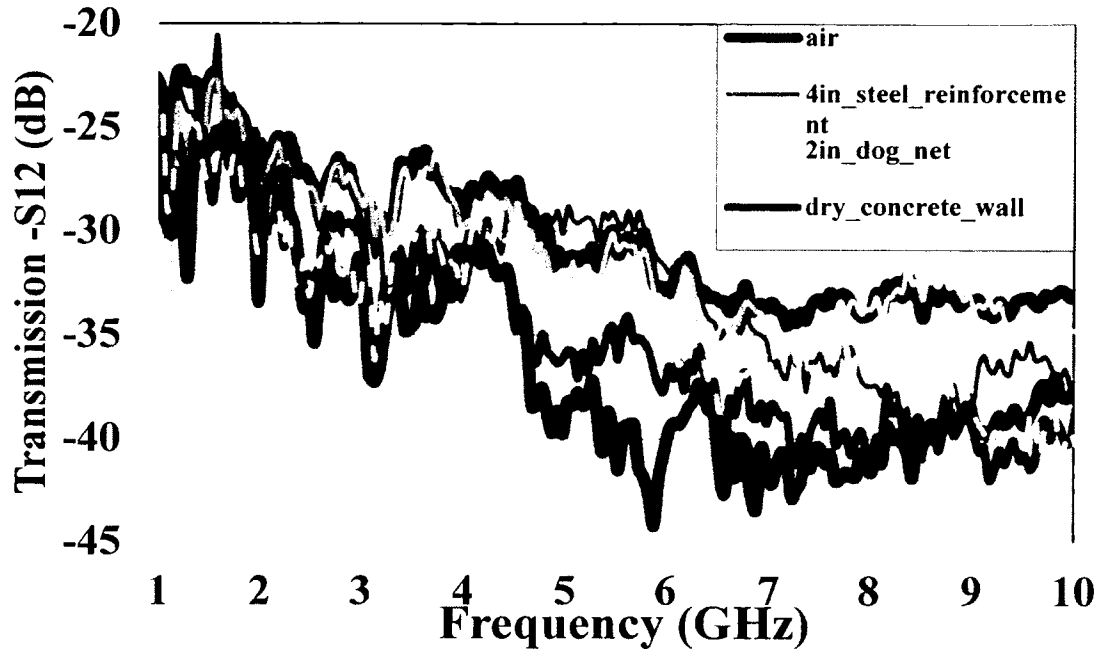


Figure A-8: Transmission loss measurements.

Attenuation/Transmission Loss in Concrete Pipes Using Time Domain Measurements

Ultra wideband systems use precisely timed, extremely short coded pulses transmitted over a wide range of frequencies. Although ultra wideband technology has many old roots, ultra wideband communication is a relatively new technology. In principle ultra wideband technology is the use of short pulses instead of continuous waves to transmit information. The pulse directly generates a very wide instantaneous bandwidth signal according to the time-scaling properties of the Fourier transform relationship between time, t , and frequency, f .

The propagation of electromagnetic waves through a lossy dielectric material can be defined, if we assume a steady-state time-harmonic electromagnetic field. If we assume that then a TEM plane wave propagating in the $+z$ direction can be represented using the phasor expression,

$$E(\omega, z) = E_0 e^{j\omega t} e^{-\gamma z} \quad (\text{A.1})$$

where $\omega = 2\pi f$ is the radian frequency and γ is the complex propagation constant given as

$$\gamma(\omega) = \alpha(\omega) + j\beta(\omega) = j\omega \sqrt{\mu\epsilon} \quad (\text{A.2})$$

where α is the attenuation constant in Np/m, β denotes the phase constant in rad/m, and ϵ and μ are, permittivity and permeability of the material. For non-magnetic materials μ is equal to μ_0 . The conductivity loss can be modeled by an additional imaginary term in the complex permittivity,

$$\epsilon(\omega) = \epsilon' - j(\epsilon'' + \sigma/\omega) \quad (\text{A.3})$$

where $\sigma(\omega)$ is the macroscopic conductivity of the material of interest. The two losses of interest can be combined and represented by an effective loss tangent,

$$p_e(\omega) = \epsilon'' + \sigma/\omega / \epsilon' \quad (\text{A.4})$$

$$p_e(\omega) = \epsilon'' / \epsilon' + \sigma / \omega \epsilon' \quad (\text{A.5})$$

A complex effective relative permittivity can now be written as

$$\epsilon_{re}(\omega) = \epsilon_r(\omega) [1 - jp_e(\omega)]. \quad (\text{A.6})$$

To characterize any subsurface material, the following two parameters should be measured, the dielectric constant and the effective loss tangent, and other directly related parameters. The complex propagation constant is then given by

$$\gamma(\omega) = j\omega/c \sqrt{\epsilon_{re}} \quad (\text{A.7})$$

$$\gamma(\omega) = j\omega/c \sqrt{\epsilon_r(1 - jp_e)} \quad (\text{A.8})$$

where $c \cong 3 \times 10^8$ m/s is the speed of light in a vacuum. For a TEM plane-wave propagating inside the material, the attenuation coefficient and the phase constant can be separated in the exponent

$$E(z, \omega) = E_0 e^{-\gamma(\omega)z} \quad (\text{A.9})$$

$$E(z, \omega) = E_0 e^{-j\beta(\omega)z} e^{-\alpha(\omega)z}. \quad (\text{A.10})$$

The attenuation constant is given by

$$\alpha(\omega) = \omega/c \{ \epsilon_r/2 [\sqrt{1 + p_e^2} - 1] \}^{1/2} \text{ Np/m}, \quad (\text{A.11})$$

while the phase constant becomes

$$\beta(\omega) = \omega/c \{ \epsilon_r/2 [\sqrt{1 + p_e^2} + 1] \}^{1/2} \text{ rad/m}. \quad (\text{A.12})$$

A more widely used unit for the attenuation constant α is dB/m. The conversion to dB/m is simply made using the relationship

$$\alpha \text{ (dB/m)} = 20 \log(e) \alpha \text{ (Np/m)} = 8.686 \alpha \text{ (Np/m)}. \quad (\text{A.13})$$

At low frequencies, the loss due to ionic conductivity is dominant. Radiated transmission measurement is used because it allows us to find both the attenuation constant and dispersion of the material under test. Moreover, it provides direct insight into how critical; a role through-wall propagation plays in UWB communications. The measurement can be performed in time domain or in frequency domain. In the time domain approach, an electromagnetic pulse, $E_i(t, z)$, is applied to a homogenous, isotropic material layer of thickness d . The incident pulse gives rise to a reflected pulse, $E_r(t, z)$, and a transmitted pulse, $E_t(t, z)$. The diagram of the experiments is shown in Figures A-1 and A-2. The transmission scattering parameter is then related to the incident and transmitted signals by,

$$S_{21}(j\omega) = \text{FFT}\{v_t(t)\} / \text{FFT}\{v_i(t)\}, \quad (\text{A.14})$$

where v_t is the voltage at the output terminals of the receiving antenna and is proportional to E_t , while v_i is the voltage at the input terminals of the transmitting antenna and is proportional to E_i and fast Fourier transform (FFT) is used to convert the sampled signal

to the frequency domain data. Therefore, two measurements should be carried out with exactly the same distances and antenna setup. The free-space measurement is used as a reference to account for all the effects that are not due to the material under test; for example, the antennas, the receiver, and the signal generator. So then,

$$E_t^{fs}(j\omega) / E_i(j\omega) = e^{-j\omega\tau}. \quad (\text{A.15})$$

The insertion transfer function is defined as the ratio of two radiation transfer functions,

$$H(j\omega) = E_t(j\omega) / E_i(j\omega) / E_t^{fs}(j\omega) / E_i(j\omega) = E_t(j\omega) / E_t^{fs}(j\omega) \quad (\text{A.16})$$

$$H(j\omega) = \text{FFT}(v_t(t)) / \text{FFT}(v_t^{fs}(t)) = V_t(j\omega) / V_t^{fs}(j\omega). \quad (\text{A.17})$$

In the frequency domain method, the pulse signals are replaced with sinusoidal signals and a vector network analyzer is used to monitor the received waveforms. Otherwise, the measurement procedure is the same as that for the time domain approach. So then, in summary, first the time domain signal $v_t^{fs}(t)$ is measured with a sampling oscilloscope or the frequency domain signal $V_t^{fs}(j\omega)$ is measured with the VNA in the absence of the material layer. Then, the time domain signal $v_t(t)$ or the frequency domain signal $V_t(j\omega)$ is measured with the material layer in place. The insertion transfer function is then calculated by using equations A.16 and A.17. Care must be taken to ensure that the conditions for the free-space measurement are as closely identical as possible to those for the measurement through the material slab.

Experiment 3 (Concrete Pipe)

We recently performed a series of experimental measurements of electromagnetic (EM) propagation through concrete pipes. The concrete pipes were 7.5 m thick, and the pulse width was 150 ps, the experiment was performed with both wet and dry concrete pipes. We will describe the propagation measurements through the pipes, and the

propagation model of a lossy dielectric layer. We will consider the transfer function, dielectric constant, loss tangent, attenuation constant, and time domain impulse response of the concrete pipes. The attenuation increases steadily with frequency, and is a strong function of the moisture of the concrete. The time domain pulse attenuation and dispersion are consistent with the low pass filtering of the attenuation loss us. Frequency and the transmitter portion of the wideband time domain measurement system consisted of a commercial pulse generator and a wideband TEM-horn antenna with dielectric lens. The receiver consisted of an identical Tem-horn antenna and a wideband sampling oscilloscope. We were careful to keep the antenna at the same position for each of our measurements. This will give us more accuracy in our experiment. In this experiment a non-reinforced both dry and wet concrete pipe was used, and we measuring the moisture content with general tools moisture meter. You can see from the graph that the concrete pipe submerged in water for three days had higher moisture content than the dry concrete pipe.

Figure A-9 illustrates magnitude versus frequency for air, metal, and concrete + metal, and demonstrates the same analysis as Experiments 1 and 2. The attenuation of the signal due to the presence of concrete is very low. We had just a small drop in db between one and five GHz). We can expect that the energy within the pulse used in the final prototype will be concentrated within three and five GHz. Figures A-10 (grid) and A-11 illustrate the magnitude of the transmitted signal between two horns antennas dropped about eight db from one and five GHz for the case of 2” concrete pipe. The drop in transmission for all other samples was below six db. Figures A-12 through A-14 show the testing materials.

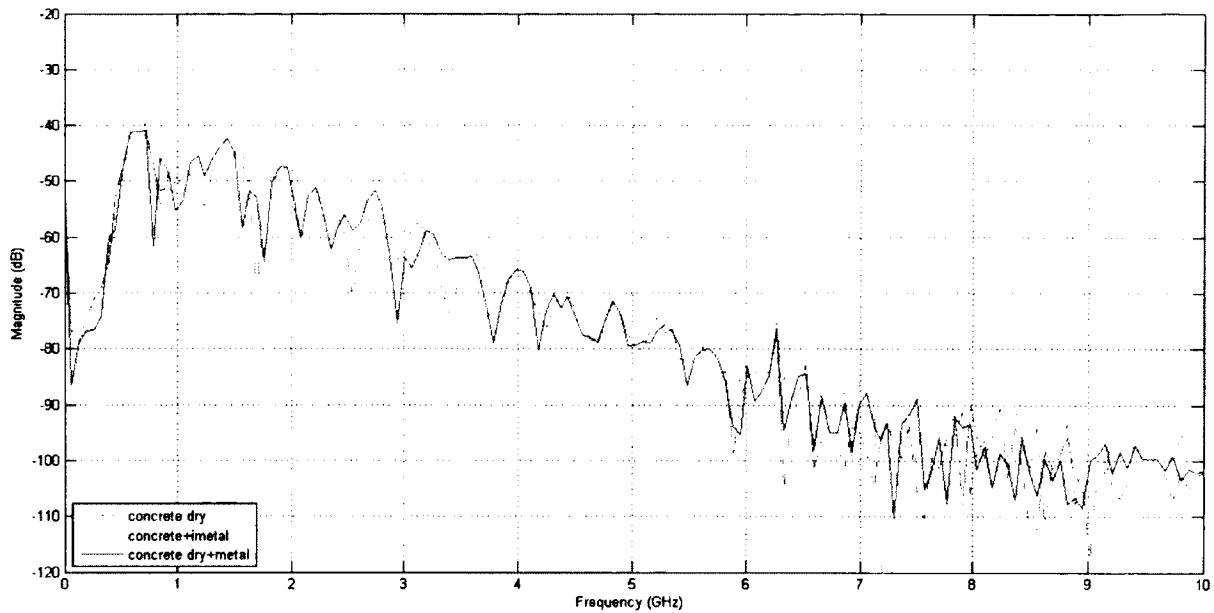


Figure A-9: Magnitude of dry concrete and concrete + metal.

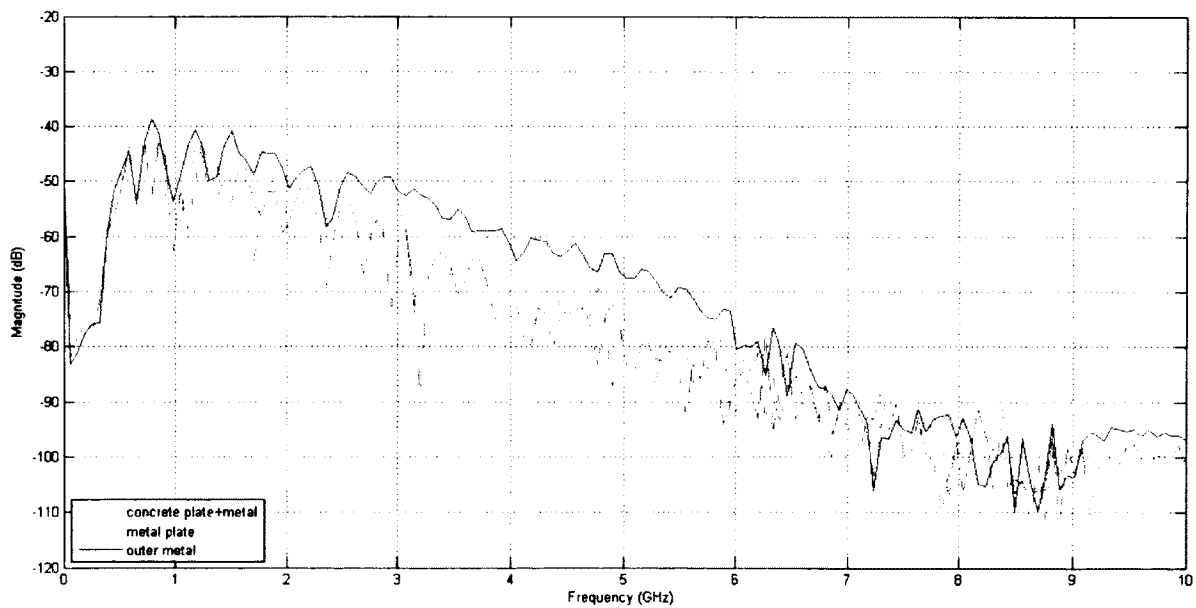


Figure A-10: Magnitude of concrete plate + metal, metal plate, and outer metal.

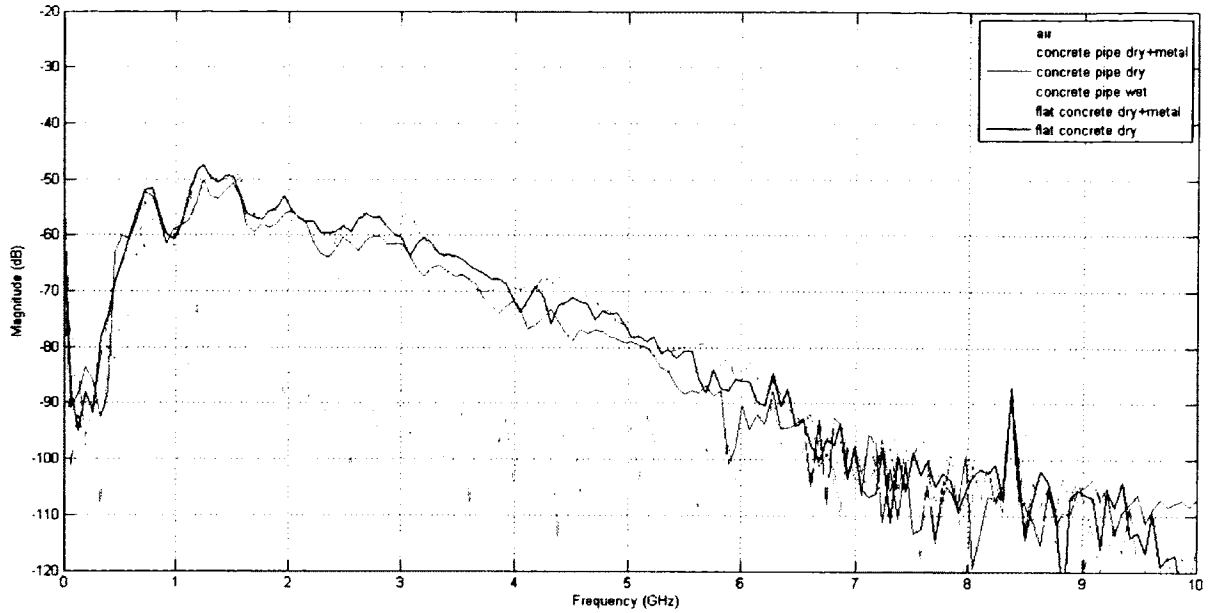


Figure A-11: Magnitude of dry concrete pipe, wet concrete pipe, and flat dry concrete.



Figure A-12: Concrete pipe.

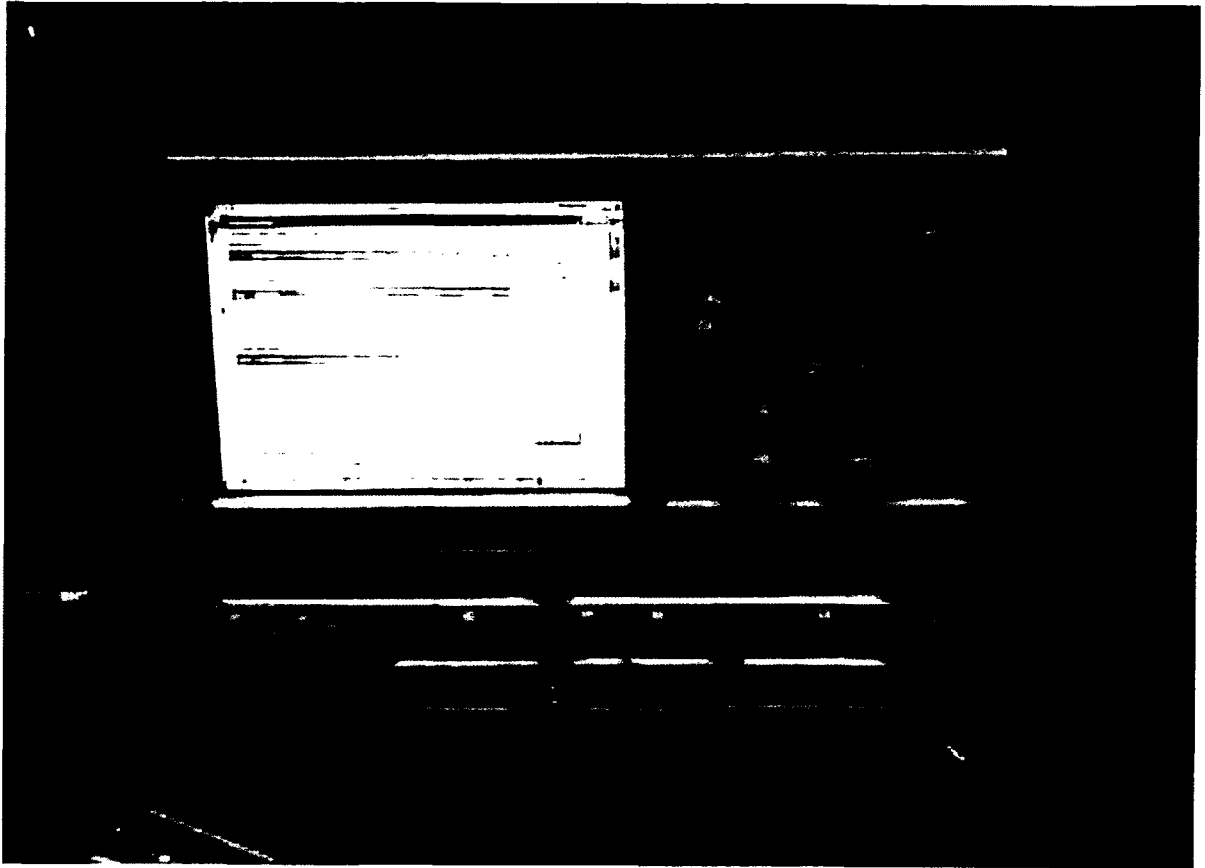


Figure A-13: Oscilloscope.

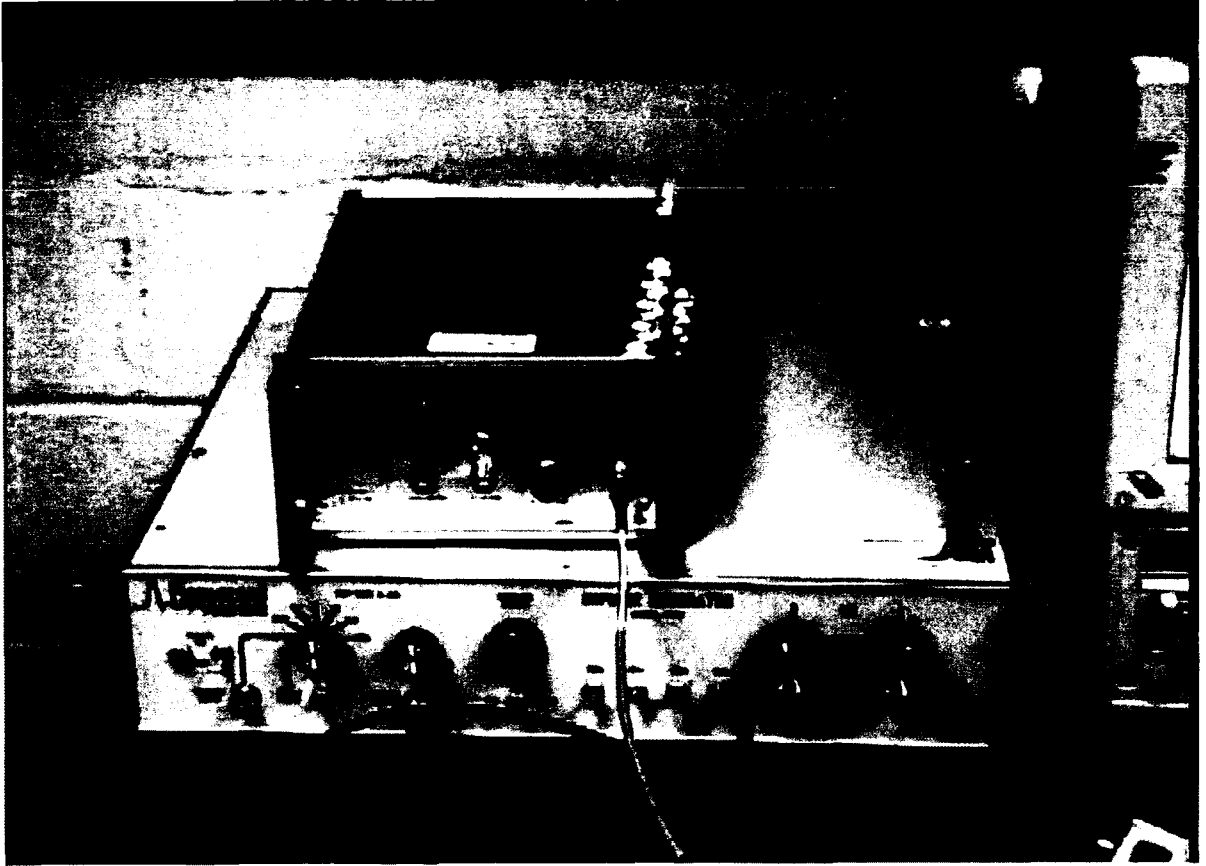


Figure A-14: Impulse generator.

APPENDIX B

GENERAL APPROACHES TO DETERMINE DIELECTRIC PROPERTIES

General Approaches for Determination of Dielectric Properties

Dielectric properties can be determined by various existing approaches depending on the chosen experimental configuration. These approaches include:

1. Approach one uses the total current density J , geometrical capacitance C_0 , electric potential difference V_0 and the phase difference φ .

$$\varepsilon(\omega) = J / C_0 V_0 \omega (\sin \varphi - i \cos \varphi) \quad (\text{B.1})$$

This is the parallel plate capacitor technique which is based on a capacitor model for determining the permittivity of the material. It requires the specimen to have certain shapes with flat surfaces on the two sides contacting the two parallel plates. The constraints on the shape of the specimen and the measurement condition limits the use of the technique, and generally makes it just a laboratory method.

2. Approach two uses the average electric displacement field vector E and the electric field.

$$\varepsilon(\omega) = 1 / \Omega E^2 \int_{\Omega} \varepsilon |\nabla V|^2 d\Omega \quad (\text{B.2})$$

3. Approach three uses the capacitance C , and the equivalent resistance R .

$$\varepsilon'(\omega) / \varepsilon''(\omega) = Q = \omega CR \quad (\text{B.3})$$

where Q is the cavity quality factor or the Q -parameter. This is the resonate cavity technique which is based on a resonator/oscillator model. It provides accurate results rather than a broadband technique. Only results at one frequency are available at a time, suggesting a great amount of time would be needed to collect a wide range of frequency responses. Additionally, it cannot measure sample sizes greater than the cavity volume/ capacity.

4. Approach four uses waveguide wavelengths λ and resonant frequencies ω .

$$\varepsilon'(\omega) = (\lambda / \lambda_g)^2 + (\lambda / \lambda_c)^2 = (\omega_g / \omega)^2 + (\omega_c / \omega)^2 \quad (\text{B.4})$$

This is a waveguide technique based on the transmission line model. Waveguides can only operate in designed frequency bands associated with certain wave propagation modes. Several different samples are needed when the measurement is conducted over a large frequency range. Inaccuracy in the measurements may occur due to the air gaps between the waveguide and the specimen. Waveguide technique can be tedious in terms of sample preparation when the designated frequency band is not available in advance.

5. Approach five uses amplitude and phase measurements of transmitted EM waves through plate specimens (in most cases reflection is needed as well). The amplitude transmission coefficient T_0 is defined by

$$T_0 = \exp [-\pi \sqrt{\varepsilon'} \tan \delta \times d / \lambda_0] \times \exp [i2\pi \sqrt{\varepsilon'} \times d / \lambda_0] \quad (\text{B.5})$$

where d is the thickness of the plate specimen, and λ_0 is the wavelength of the incident wave in free space. For low-loss dielectric ($\tan \delta \leq 10^{-4} \approx 10^{-3}$) the specimen thickness d should be less than the effective wavelength with the dielectric;

$$d < \lambda_e = \lambda_0 / \sqrt{\varepsilon'} \quad (\text{B.6})$$

for the ease of phase estimation. In the case where $d > \lambda_e$, such as the use of high frequencies, the real phase φ of the EM waves transmitted through the specimen is

$$\varphi = s \times 2\pi + \varphi_1 = 2\pi / \lambda_0 \sqrt{\varepsilon'} \times d \quad (\text{B.7})$$

where s is an integer, and $\varphi \in \langle 0, 2\pi \rangle$. For the estimation of the unknown dielectric constant ε'_r , two plate specimens with different thickness are prepared. The phase measurements provide two equations.

$$\sqrt{\varepsilon'_r} = \lambda_0 / 2\pi d_1 (s_1 \times 2\pi + \varphi_1) \quad (\text{B.8})$$

$$\sqrt{\varepsilon'_r} = \lambda_0 / 2\pi d_2 (s_2 \times 2\pi + \varphi_2) \quad (\text{B.9})$$

Solving for the integers s_1 and s_2 leads to the evaluations of ε'_r . With the amplitude Measurement T_{0d_1} and T_{0d_2} , the loss tangent $\tan \delta$ can be determined. Therefore, the complex permittivity is found.